A Three-dimensional Model of Lake Superior with Ice and Biogeochemistry: Investigating Interannual Lake Trends and the Deep Chlorophyll Maximum

A Dissertation
SUBMITTED TO THE FACULTY OF
UNIVERSITY OF MINNESOTA
BY

Brooke White

IN PARTIAL FULFILLMENT OF THE REQUIREMENTS
FOR THE DEGREE OF
DOCTOR OF PHILOSOPHY

Adviser: Katsumi Matsumoto

December 2013

Acknowledgements

I would like to thank my advisor, Katsumi Matsumoto, for his continuous support of my graduate work and his scholarly insights without which I would not have made it to where I am today. I would also like to thank Jay Austin for his time and effort supporting my endeavor to tame ROMS and hosting me in Duluth and on research cruises; Bob Sterner for providing the inspiration for my second chapter through his excellent work with Bridget Seegers and for writing letters in the nick of time; and the rest of my committee, Jim Cotner, Erik Brown, Larry Edwards, and David Fox, for their advice and taking the time to see me through preliminaries and defense.

Thank you to Anna Henderson and Katie Genadek for their friendship that has seen me through grad school and beyond.

Lastly, and most importantly, thank you to my parents, Tom and Julie White, for their never-ending love and for supporting me when I've needed it the most.

Dedication

This dissertation is dedicated to my husband, Jeremy Bellay, for his loving support in both the past and present, and our son, Winston Bellay White, for bringing even more love to my future.

Abstract

The development of a realistically configured three-dimensional model for Lake Superior including prognostic ice and biogeochemistry models is documented. The addition of a prognostic ice model is a significant advance over previous modeling efforts. The hydrodynamic, ice and biogeochemical models are described and behavior of the model during the period 1985 to 2008 and focusing on the annual cycle of 2005 is discussed. The model is found to sufficiently reproduce many observed physical and biological characteristics of Lake Superior. It is also successfully applied in two scientific investigations: interannual trends in lake temperature, ice cover and primary productivity and elucidation of the causal mechanisms of Lake Superior's deep chlorophyll maximum.

The formation of winter ice on Lake Superior has been shown to be important in determining the annual thermal cycle of the lake and long-term trends of surface water temperature increase. However, modeling studies of Lake Superior to date have not included dynamic and thermodynamic ice cover. These physical characteristics of the lake in turn can have significant impacts on biogeochemical cycling within the lake. Modeled long-term interannual trends in increasing water temperature and decreasing ice cover are compared with observed rates. In the model, total annual gross primary productivity is found to correlate positively with mean annual temperature and negatively with mean winter ice cover magnitude.

The deep chlorophyll maximum (DCM) is a near ubiquitous feature in Lake Superior during the summer stratified season. Previous studies have elucidated observable characteristics of the DCM in Lake Superior but the physical and biological

mechanisms controlling the creation and maintenance of the DCM remained unclear. Sensitivity runs are performed to explore the influence of photoadaptation, photoinhibition, zooplankton grazing, and phytoplankton sinking on the vertical distribution of chlorophyll in the water column. The role of a nutricline in determining the presence and nature of the DCM is also explored. The presence of the DCM is dependent upon the presence of thermal stratification in the model. The sensitivity runs reveal that photoadaptation plays a primary role in determining the depth of the DCM in the model while zooplankton grazing and phytoplankton sinking affected the magnitude but not the presence or depth of the DCM. Photoinhibition showed negligible effects on chlorophyll concentration distribution. The presence of a nutricline in the model is also a necessary condition for the formation of the DCM and it influences both the depth and magnitude of the DCM.

Table of Contents

List of tables ..... **vii**

List of figures ..... **viii**

Introduction **1**

Chapter 1: Model development and interannual trends in temperature, ice cover and primary productivity **6**
- **Introduction** **6**
- **Description of model and atmospheric forcing** **8**
  - Hydrodynamic model 8
  - Ice model 9
  - Biogeochemistry and ecosystem model 10
  - Initial conditions and spin-up 13
  - Atmospheric forcing data 14
- **Results and discussion** **16**
  - Physical results 16
  - Biogeochemical results 25
- **Conclusions** **29**

Chapter 2: Causal mechanisms of the deep chlorophyll maximum in lake superior **57**
- **Introduction** **57**
- **Description of model and experimental set up** **62**
  - Physical model 62
  - Biological model 63
  - Atmospheric forcing and initialization 70
  - Experimental set up 71
- **Results and discussion** **73**
  - Comparison of model output and observations 73
  - Contribution of processes to deep chlorophyll maximum 76
  - The role of the nutricline 80
- **Conclusions** **82**

Conclusions **99**

References **106**

Appendix **120**

List of Tables

TABLE 1: Biological parameters **.....31**

TABLE 2: Biological initialization values**.....32**

TABLE 3: RMSE values for surface water temperatures**.....33**

TABLE 4: RMSE values for ice cover **.....34**

TABLE 5: Ice thickness histograms **.....35**

TABLE 6: Biological parameters **.....85**

TABLE 7: Sensitivity model runs**.....86**

TABLE 8: Chlorophyll model-data comparison r-values**.....87**

List of Figures

Figure 1: Lake Superior model bathymetry in meters with EPA station locations and NDBC buoy locations **39**

Figure 2: Ecosystem and ice module schematics **40**

Figure 3: Surface water temperatures at three NDBC buoy locations (west, central, east) for 2005 ..... **41**

Figure 4: Surface water temperatures at three NDBC buoy locations (west, central, east) for 1985-2008 ..... **42**

Figure 5: Maximum summer surface water temperatures (°C) at three NDBC buoy locations across the lake for 1985-2008 ..... **43**

Figure 6: Panels A and C show water column temperatures (°C) at 19 offshore EPA sites in the early spring and summer from the model (black lines) and observed data (gray dots). Panels B and D show modeled surface water temperatures (°C) in the early spring and summer. **44**

Figure 7: Average surface water temperature (C) during the stratified season (July-September) for 1985-2008 for western, central, and eastern NDBC buoys. Model values (asterisks) and observed values (diamonds) and linear fits to the modeled (solid line) and observed (dashed line) values are shown. Spatially averaged: an average of temperatures at the three locations is shown for model output (asterisks) and NDBC buoy data (diamonds) as well as an average of model temperatures over the entire lake surface (dots). Fits to the model output (solid line) and buoy data (dashed line) and for the entire model lake surface averaged temperature (dot-dash line) are shown **45**

Figure 8: A: Model (solid line) and observations from the IMS (asterisks) and Great Lakes Ice Atlas (dots) of percentage of lake surface area covered by ice during 2005. B: Domain-averaged ice-cover thickness in meters during 2005 ..... **46**

Figure 9: Modeled ice thickness (cm, red), percent ice cover (green), and air temperature (°C, blue) for January through April during 2005. Cold 'outbreaks', when ice cover spatial coverage and thickness increases, are noted along with the

springtime warming trend when major ice cover melt occurs and ice cover thickness decreases.....47

Figure 10: Left: Observed ice cover from the IMS (black) on 12 January, 24 February, and 21 March, 2005. Modeled ice cover (black) on 12 January, 24 February, and 21 March, 2005 48

Figure 11: A: The percentage of lake surface area covered by ice for 1985-2008. Model output is shown as a solid line and observations from the NOAA Great Lakes Ice Atlas (1985-2004) and the Multisensor Snow and Ice Mapping System Daily Northern Hemisphere Snow and Ice Analysis at 4km (2005-2008) are shown as dotted lines. B: Domain-averaged ice thickness in meters for 1985-2008 49

Figure 12: A: An IMS observational map of ice cover for January 26, 2005, B: model map of ice cover for same date with ice momentum vectors, C: Modeled Surface water temperatures, D: Atmospheric boundary condition wind directions.....50

Figure 13: Ice-cover season (Jan–May) averaged percentage of lake surface area covered by ice from 1985 to 2008 for model output (asterisks) and observations (diamonds). Linear fits to model output (solid line) and observations (dashed line)51

Figure 14: Direction and relative magnitude of annually averaged horizontal currents for 2005 near the surface (<20m, A) and at depth (>75m, B).....52

Figure 15: Surface water temperature (A, °C), phosphate concentration (B, nmol/kg), and chlorophyll concentration (C, mg/m^3) from model output, July 23, 2005.....53

Figure 16: Summertime water column chlorophyll concentrations (mg/m^3) at the 19 EPA station locations from model output (lines) and EPA observations (circles).54

Figure 17: Total annual gross primary production (Tg C/yr) for 1985 to 2008 from model output (circles) with linear fit (solid line) 55

Figure 18: Total annual gross primary productivity (TG C/yr) versus annual average temperature (C) from model output for 1985-2008 (asterisks) and linear fit to the values (line). B: Total annual gross primary productivity versus winter season (Jan-May) average percentage of lake surface area covered by ice (asterisks) and linear fit (line).....56

Figure 19: Lake Superior model bathymetry (every 50m) with EPA monitoring site locations (white squares) **.....88**

Figure 20: Biological module schematic. State variables are shown as shaded boxes and tracked via phosphorus in the model. Fluxes between state variables are shown as arrows**.....89**

Figure 21: Observed (crosses) and modeled (solid lines) chlorophyll concentrations (mgChl m-3) and observed (dots) and modeled (dashed lines) temperatures versus depth (m) at EPA monitoring sites 4, 11, and 16 in late summer **.....90**

Figure 22: Panel A: Depth of maximum zooplankton concentration (m) and depth of the DCM (m), solid line is one-to-one. Panel B: Concentration of zooplankton in epilimnion (μg l^{-1}) and concentration of zooplankton in hypolimnion (μg l^{-1}) **.....91**

Figure 23: Chlorophyll concentration (mgChl m^{-3}) depth profiles (meters) at locations corresponding to sites 1, 6, 14 for the five sensitivity model runs (solid line=control run, dots=no density dependent phytoplankton sinking, dotted line=no photoinhibition, crosses=constant chlorophyll to carbon ratio, dashed line=constant zooplankton grazing) **.....92**

Figure 24: Depth of maximum phytoplankton concentration (m) and DCM depth (m) for control run (dots) and constant Chl:C ratio run (circles) **.....93**

Figure 25: Spatially-averaged root mean square error of vertical chlorophyll profiles for sensitivity runs compared to control run for July through September. Dash-dot line: constant chlorophyll to carbon ratio, solid line: no density-dependent phytoplankton sinking, dotted line: no photoinhibition, dashed line: constant zooplankton grazing**.....94**

Figure 26: Panel A: The spatial dimension of the magnitude of the DCM (maximum chlorophyll concentration minus surface chlorophyll concentration, mg Chl m^{-3}), Panel B: The spatial distribution of the magnitude of the nutricline (deep phosphate concentration minus surface phosphate concentration, mmolP m^{-3} **.....95**

Figure 27: Panel A: The magnitude of the nutricline (mmolP m^{-3}) against the magnitude of the deep chlorophyll maximum (mgChl m^{-3}) from the model control run for each of the 19 EPA monitoring site locations at several times during the summer season. Pearson's r for each data set is shown. Panel B: The depth of the nutricline (m) against the depth of the deep chlorophyll maximum (m) from the

model control run for each of the EPA site locations at several times during the summer season. Pearson's r is shown for each data set **96**

Figure 28: Panel A: DCM depth (m) and nutricline depth (m) for three forced nutrient profile experiments. Panel B: DCM depth (m) and thermocline depth (m) for forced nutrient profiles experiments **97**

Figure 29: Average depth of the DCM (m) and average depth of the nutricline (m) for the 20 m nutricline (solid line and circles), 40 m nutricline (dashed line and diamonds) and 60 m nutricline (dotted line and squares) sensitivity runs during the summer stratified season **98**

Introduction

Lake Superior is a minimally disturbed, large aquatic system. It is the world's largest lake by surface area and contains approximately 10% of the Earth's surface freshwater. The lake plays a significant role in influencing regional meteorology, as well as being very important to the surrounding region as a source of clean and abundant water and a medium for inexpensive, waterway transportation. It is unusual, when compared to the other Laurentian Great Lakes, in that human impact has been limited. First, Lake Superior is upstream of the other Laurentian Great Lakes and receives runoff from its own catchment basin only. Lake Superior's catchment basin area is relatively small compared to the lake surface area with a ratio of 1.55 (Cotner et al., 2004). Second, development within its basin is not significant: only 3% of the Superior basin is used for agriculture as compared to 27-67% for the other Great Lake basins; over 90% of its basin is covered with forest, which is far less abundant elsewhere (Sea Grant College Program, 1985). Also, the amount of water withdrawn for consumption from Lake Superior is at most a small fraction of the amounts withdrawn from the other lakes (Great Lakes Commission, 2006).

While the disturbance of Lake Superior has been minor compared to the other Laurentian Great Lakes, recent work by Austin and Colman (2007) demonstrates that the thermal characteristics of Lake Superior have been changing over the past quarter century. Their compilation of available summer surface water temperature measurements shows a warming trend (~0.11°C/yr over the last quarter century) in the lake that is in excess of the regional atmospheric warming rates (~0.06°C/yr). This warming is

hypothesized to be the result, in part, of decreasing winter lake ice cover, as determined from the spatial and temporal average of ice cover between December and May (Assel et al., 2003). The declining annual ice cover leads to earlier ice-out and spring overturn, as lake albedo is reduced and shortwave radiation absorption over the late winter and early spring is increased. An earlier overturn provides a longer warming season and the lake is able to warm significantly more than if the season had been delayed by a strong ice cover. **In Chapter 1**, the ability of the numerical model documented herein to reflect trends in lake temperature and ice cover is examined. Associated changes in primary productivity rates in the model are also noted.

A greater warming of surface lake waters over the ambient surface air yields a reduced air-lake temperature gradient. This may lead to increased instability of the atmospheric boundary layer and thus higher surface wind speeds. Recent analyses of wind speeds over Lake Superior buoys and from satellite scatterometry shows a strong relationship between the air-water temperature difference and wind speed, and a significant upward trend in wind speed (Desai et al. 2009).

It is not entirely clear how these trends will affect the Lake Superior thermal structure in the future. On one hand, warmer air tends to strengthen summertime stratification. However, stronger winds would impart larger kinetic energy to the lake and tend to increase mixing and deepen the mixed layer depth. Austin and Allen (2011) found the impact of recent changes in wind speed and air temperature on summer water temperatures to be opposite and of the same order of magnitude. Their estimates,

however, relies upon an assumption of independence of the effects of air temperature and wind speed.

There is significant uncertainty in our knowledge of Lake Superior's biogeochemistry as well. For one, the carbon budget of Lake Superior as based on observations has not be closed at the present time, though the applicability of point measurements to represent lake-wide conditions is currently in debate. The main sink of organic carbon in Lake Superior is respiration, which has been estimated on the basis of deep-water dissolved oxygen consumption. The main source of organic carbon is primary production, which is estimated by ^{14}C uptake experiments. Compilations of estimates of respiration and production suggest that the Lake Superior is net heterotrophic (Cotner et al., 2004; McManus et al., 2003; Urban et al., 2005); organic carbon consumption by respiration exceeds production by photosynthesis. Presumably, heterotrophy is also fueled by external sources of organic carbon from atmospheric deposition and runoff from the watershed. However, the sum of all known inputs of carbon to the lake from rivers, atmosphere, and photosynthesis (0.4-0.9 Tg C $yr^{-1,}$ 0.02-0.41 Tg C yr^{-1} and 2.0-8.2 Tg C yr^{-1}, respectively, Cotner et al., 2004; Urban et al 2005) is only about half of the sum of all known outputs by outflow, sedimentary burial, and respiration (0.1 Tg C $yr^{-1,}$ 0.06-2.0 Tg C yr^{-1} and 13-81 Tg C yr^{-1}, respectively). Respiration rates have the largest range of uncertainty. Recent modeling work by Bennington et al. (2012), however, suggests that respiration rates in Lake Superior show significant temporal and spatial variability with negative implications for the ability of measurements taken at a single point and time in Lake Superior to be extrapolated lake-

wide. In fact, their model results show up to a two order magnitude difference between near-shore and offshore respiration rates.

There are other unexplained features of nutrient and ecosystem dynamics in Lake Superior. Currently phosphate concentrations are very low in the lake. Typical Lake Superior soluble reactive phosphorus (SRP) concentrations are in the range of <0.1 to 10 nmol kg^{-1} (Anagnostou and Sherrell, 2008), which is two to four orders of magnitude lower than typical values in the ocean (which are commonly reported in μmol kg^{-1}). Until recently, phosphorus levels in Lake Superior have been lower than in the other Great Lakes (e.g. Lake Michigan SRP of 20-330 nmol kg^{-1}, Brooks and Edgington, 1994 and Tarapchak and Rubtischun, 1981 and Lake Erie SRP of 20 to 419 nmol kg^{-1}, Makarewicz et al., 2000 and Holland et al., 1994). However, recent changes in some of the Great Lakes has decreased phosphorus levels and lead to even more severe oligotrophy than in Lake Superior by certain measures (e.g. Lake Superior average total phosphorus (TP) of 2.3 μgP L^{-1} versus Lake Michigan average TP of 3.1 μgP L^{-1} and Lake Huron average TP of 2.0 μgP L^{-1}, Barbiero et al., 2012). Phosphorus appears to limit summer production in Lake Superior, though iron may also play a role (Sterner et al., 2004). Recent measurements of dissolved organic phosphorus (DOP) show the presence of a seasonally highly dynamic pool (Baehr and McManus, 2003), suggesting the possibility that DOP may be fueling production in Lake Superior as in the Sargasso Sea (Lomas et al., 2010). Nitrate limits production in many parts of the world ocean, but it is in constant excess in Lake Superior. In fact, nitrate seems to be on a century-long trend of build-up from anthropogenic sources and from changing biogeochemical cycling

(Bennett, 1986, Sterner et al. 2007). A further puzzle in ecosystem dynamics, explored **in Chapter 2**, is the underlying cause of the formation of a pronounced deep chlorophyll maximum at 25-35 m every year during midsummer (Barbiero and Tuchman, 2004).

In this thesis, I document the development of a realistically configured, 3-dimensional numerical model of Lake Superior including hydrodynamics, ice dynamics and thermodynamics and ecosystem dynamics (Chapter 1); I evaluate the ability of the model to reproduce interannual trends in surface water temperature and ice cover for the period 1985 to 2008 and investigate accompanying trends in annual primary productivity during the same period (Chapter 1); I investigate the causal mechanisms of the deep chlorophyll maximum in Lake Superior via sensitivity experiments (Chapter 2); The final section offers conclusions.

Chapter 1

Model development and application to interannual trends in temperature, ice cover and primary productivity

This chapter appeared in full as White, B., J. Austin, K. Matsumoto (2012). A three-dimensional model of Lake Superior with ice and biogeochemistry, Journal of Great Lakes Research, 38:61-71. Reproduced by permission of the Journal of Great Lakes Research.

The formation of winter ice on Lake Superior has been shown to be important in determining the annual thermal cycle of the lake and long-term trends of surface water temperature increase. Austin and Colman (2007) hypothesize that decreased springtime ice cover on Lake Superior has lead to earlier ice out and increased length of the stably stratified season due to decreasing springtime lake albedo and increased absorption of shortwave radiation. These changes in the physical characteristics of the lake in turn can have significant impacts on biogeochemical cycling within the lake. However, modeling studies of Lake Superior to date have not included dynamic and thermodynamic ice cover.

There have been several numerical modeling studies of Lake Superior circulation. Lam (1978) used a hydrodynamic model with four layers in the vertical and 10 km horizontal resolution to simulate water circulation during the stratified season of 1973. As part of the Keweenaw Interdisciplinary Transport Experiment in Superior, a non-orthogonal coordinate model was created for Lake Superior (Chen et al., 2001, Zhu et al.,

2001, Chen et al., 2004). The main focus of publications based on this model was coastal circulation dynamics in the region of the Keweenaw Peninsula. Most recently, Bennington et al. (2010) use a three-dimensional hydrodynamic model with imposed ice coverage to elucidate climatological circulation structures, the mechanisms that control them and their interannual variability. The Great Lakes Coastal Forecasting System (Schwab and Bedford, 1999) provides modeled now-casts and forecasts of water temperature and circulation in the Great Lakes including Lake Superior. This modeling effort provides important information for lake users but there has been no published analysis of output from the model. Significantly, none of the models listed here includes dynamic and thermodynamic ice. By explicitly modeling water and ice, consistency is achieved between the physical fields of the lake (e.g., simulating ice where subfreezing temperatures predict it) and the power to make future projections and conduct climate sensitivity experiments. The role of ice cover in affecting the air-lake flux of heat and gas as well as biogeochemical cycling makes a dynamic and thermodynamic model of ice a critical component for realistic simulation of Lake Superior.

Here I describe a 3-dimensional model of Lake Superior that is based on The Regional Oceanic Modeling System (ROMS, version 3.2). Section 2 describes the model, including the dynamic and thermodynamic ice model and the biogeochemical model, as well as the atmospheric boundary conditions used to force the model. Section 3 presents model results from runs covering 1985-2008 with a specific focus on 2005 and compares them to data where available. Section 4 offers conclusions.

Description of Model and Atmospheric Forcing

Hydrodynamic Model

ROMS is a free-surface primitive equation ocean model that utilizes a terrain-following vertical coordinate and a split-explicit time stepping scheme. The algorithms of the ROMS computational kernel are described in detail in Shchepetkin and McWilliams (2005). ROMS has been successfully applied in many regions around the globe, some including biogeochemical and sea-ice studies (e.g. Fennel et al., 2006, Budgell, 2005, Dinniman et al., 2003, Gruber et al., 2006). The Lake Superior model is implemented using realistic lateral and bottom boundaries (Figure 1). The rectilinear horizontal grid has a resolution of 5 km and there are 20 sigma levels in the vertical, resulting in vertical resolution between less than one and 40 meters. The level 2.5 closure turbulence model presented in Mellor and Yamada (1982) is used to calculate vertical mixing coefficients. A closed basin model is used with no input from tributaries and the surrounding watershed or drainage of water to the St. Marys River. As in Bennington et al. (2010), the closed based model is an appropriate first step for modeling Lake Superior, which has a large volume and long residence time of 178 years (Quinn, 1992). Future inclusion of tributary input will likely increase the accuracy of the ecosystem model in near shore regions of riverine input. In our application to Lake Superior, salinity is set to zero and temperature is the only state variable. To improve the behavior of the model in the

vicinity of the 3.98°C density maximum, an equation of state developed expressly for freshwater systems is implemented. (Chen and Millero 1986).

Ice Model

The ice model used for the Lake Superior implementation is demonstrated by Budgell (2005) in an application to the Barents Sea and further described by Hedström (2009). The main features of this ice model are elastic-viscous-plastic (EVP) ice rheology, ice thermodynamics using single ice and snow layers, and a molecular sublayer adjacent to the base of the ice. The ice and hydrodynamic models are coupled using the same grid and time step.

The dynamics of the ice model are based on the work of Hunke and Dukowicz (1997) and Hunke (2001). Ice momentum is determined by stress from air and water, tilt of the water surface, the Coriolis force, and internal ice stress (Hedström, 2009). A split time step is used in calculating ice momentum with the internal ice stress updated more frequently to resolve internal dynamics. The EVP ice rheology follows the rheology of Hibler (1979) but uses Young's Modulus as a modifiable coefficient to minimize the elastic term and allow for efficient solutions. The ice tracers, including internal ice temperature, surface melt ponds, ice thickness and concentration, and snow thickness are advected according to the calculated ice momentum.

The ice thermodynamics follow Mellor and Kantha (1989) and Häkkinen and Mellor (1992). Ice melting and freezing is calculated on all sides of the ice (top, bottom

and sides, Hedström, 2009, Mellor and Kantha, 1989). The factors in changing effective ice volume and ice concentration are the freezing rate at the air-water boundary (W_{ao}), the rate of freezing at the ice-water boundary (W_{io}), the rate of frazil ice growth (W_{fr}), the melt rate at the ice/snow surface ((W_{ai}), and the runoff rate for surface melt water (W_{ro}, Figure 2). Frazil ice formation is modeled after Steele et al. (1989). Energy fluxes in the snow-ice system are calculated using single ice and snow layers (Semtner, 1976). A molecular sub-layer at the ice-ocean interface is used to improve freezing and melting rates. Fluxes of sensible and latent heat and incoming long- and shortwave radiation are based on those of Parkinson and Washington (1979). I modify the ice model for the Lake Superior application by setting the ice salinity to zero.

Biogeochemistry and Ecosystem Model

The biogeochemical model modified for the Lake Superior implementation is described by Fennel et al. (2006). I use phosphorus as the limiting nutrient in Lake Superior, which allows further simplification of the architecture of the Fasham et al. (1990) type model. There are six state variables: phosphate, phytoplankton, chlorophyll, zooplankton, and large and small detritus (Figure 2). Fluxes between the pools are shown as arrows. Modifications are made to parameter values and initial conditions where observational constraints for Lake Superior are available; otherwise and for simplicity, the original Fennel values are retained even though they are from a different environment (Tables 1 and 2). These values will be modified in the future as relevant data become

available. Modifications made to the primary productivity process are described below and given in equation form in the appendix.

The time rate of change of phytoplankton is a function of zooplankton grazing rates, phytoplankton mortality rates, coagulation with small detritus (and subsequent sinking), phytoplankton sinking rates, and phytoplankton growth rate, itself a function of temperature, light, and nutrient limitation (see Supplemental Materials for governing equation). Temperature in general is positively related to the metabolic rates, and our temperature dependence on growth rates follows the Q10 relation (Kishi et al., 2007). Light availability is modified by the amount of light in the photosynthetically active portion of the spectrum, attenuation due to water and attenuation due to chlorophyll presence. The relationship between available light and rates of photosynthesis follows Platt et al. (1980). Phosphorus limitation follows Michaelis-Menten uptake kinetics (Michaelis and Menten, 1913). Phytoplankton sink at a relatively slow rate and may coagulate with small detritus to join the large detritus pool. Zooplankton grazing rates are characterized using a Holling-type s-shaped curve (Holling 1959, 1962, 1965). Zooplankton time rate of change is a function of rates of zooplankton grazing on phytoplankton and efficiency of assimilation of the grazed material, basal metabolism excretion rates, assimilation related excretion rates, and zooplankton mortality.

The amount of chlorophyll associated with a given phytoplankton mass varies nonlinearly. A portion of phytoplankton growth is allotted to chlorophyll synthesis following the formulation of Geider et al. (1996, 1997). The fraction allocated is a function of nutrient and light availability. This takes into account the process of

photoacclimation in which phytoplankton increase or decrease the amount of resources used in synthesis of light-harvesting cellular components depending upon environmental conditions. This is a potentially important process in the deep chlorophyll maximum. Chlorophyll sinks include grazing by zooplankton, mortality of phytoplankton, and coagulation of phytoplankton with small detritus to form large detritus.

Two size classes of detritus are used in the model. The small class sinks at a characteristic slower rate and represents both the dissolved organic phosphorus pool and minute slowly sinking particulates while the large detritus pool sinks at a faster rate. Both classes of detritus are subject to horizontal advection, and so the limited sinking rates, especially for the small detritus, allow for a horizontal transport over the full depth of the water column (Gruber et al., 2006). The small detritus time rate of change receives inputs from zooplankton through excretion and mortality and through phytoplankton via mortality and coagulation. Losses are remineralization and sinking. Large detritus sources are coagulation of small detritus and phytoplankton and losses are remineralization and sinking. Remineralized detritus reenters the phosphate pool. Upon reaching the bottom boundary, detritus and phytoplankton are immediately remineralized.

In the Lake Superior implementation of the biogeochemical model, a number of important modifications have been made. First, the stoichiometric ratio of carbon, nitrogen, and phosphorus in organic matter of phytoplankton is usually assumed to follow the Redfield ratio of 106:16:1. The ratio of carbon to phosphorus (C:P) ratio in Lake Superior seston, however, is consistently elevated and can reach as high as 400 in summer surface waters (Sterner, pers. comm., 2010) with mean values of approximately

200 frequently seen at the depth of greatest biomass in the summer, 20-40m (Barbiero and Tuchman, 2004). A C:P ratio of 200 is therefore used. Second, a relatively low value of 0.05 mmol P m^{-3} is used for the half-saturation concentration of phosphate uptake by phytoplankton, because phosphate concentrations in Lake Superior are low and Lake Superior phytoplankton and primary production are dominated by picoplankton; Sterner (2010) noted that half of measured chlorophyll would pass through a three micron filter. Similarly, Fahnenstiel (1986) found that 50% of total primary production could be attributed to phytoplankton that passed through a 3 micron filter. The half-saturation concentration value used here is also used in models of Lake Michigan (Chen et al., 2002) and Lake Huron (Bierman and Dolan, 1981). Third, rates of remineralization of small and large detritus were increased from base model levels to reflect rapid recycling in the Lake Superior water column though they still reside within rate ranges seen elsewhere (Leonard et al., 1999). Finally, the model is modified to allow light to be blocked by the presence of ice. The amount of light received is decreased proportional to the ice cover concentration within a grid cell. Initialization values for the state variables were chosen to according numbers from the literature where available (Table 2).

Initial Conditions and Spin up

The model is initialized with waters at a uniform temperature of 4°C (close to the temperature of maximum density), no ice, uniform surface topography and no momentum on 1 January 1985. Biogeochemical state variables are initialized at the values given in

Table 2. The model is spun up for two years using the 1985 annual, realistic atmospheric forcing with three hour time resolution (described below) allowing the model to come into equilibrium. The forcing for 1985 to 2008 is then applied with each year being initialized from the end state of the previous year to produce results for analysis.

Atmospheric Forcing Data

The forcing applied to the model was developed by using interpolated data from the National Oceanic and Atmospheric Administration (NOAA) National Data Buoy Center (NDBC) array of open-lake buoys and Coastal Marine Automated Network (CMAN) stations. The number of these stations providing data varied over the course of the 25 year simulation, with the number of stations providing data increasing monotonically from 7 in 1985 to 18 in 2008. As this data exists only on the US portion of the lake, there is no coverage in the far northern portion of the lake. In addition, the open-lake buoys are typically recovered in November and re-deployed the following spring so that they are not on the lake during the ice-cover season, thus there are no direct measurements over the open lake during the winter.

The available data consists of wind speed and direction and air temperature. The wind speed data was adjusted to 5m using a power law adjustment (Hsu et al., 1994) with p=0.11. All available data was used to construct interpolated wind velocity and air temperature fields over the lake, using objective analysis with a correlation length scale

of 100km. The field was relaxed to the mean of available data in regions distant from the available data.

Although there is one site (ROAM4) where a historical record of humidity is available, a uniform, constant relative humidity of 80% is imposed over the entire domain (note that this implies that the specific humidity will vary with air temperature). A separate run, in which humidity from the single available record was applied uniformly, revealed no significant difference from a run otherwise identical but with constant humidity (not shown).

Both shortwave and longwave radiation were determined using climatological average monthly cloud cover without interannual variability. Downward shortwave radiation was determined by combining the monthly cloud cover estimate with an astronomical prediction of clear-sky radiation and a quadratic cloud cover correction (Barry and Chorley 1976):

$$CC = 1 - 0.65C^2 \qquad (1)$$

Where C is the observed cloud fraction and CC is the cloud correction factor so that

$$Q_{SW\_SFC} = (1 - CC)Q_{SW\_CLEARSKY} \qquad (2)$$

Downward longwave radiation was set using a regression of directly measured longwave radiation at one location in Lake Superior (Austin and Allen 2011) to cloud cover and air temperature:

$$Q_{LW\_DOWN} = 323Wm^{-2} + 4.7Wm^{-2}C^{-1}T_{AIR} - 72Wm^{-2}CC \qquad (3)$$

where T_{AIR} is in °C . Upward longwave radiation is determined in the model as a function of the surface water temperature, and a constant albedo of 0.93 (Payne 1972) is used to

determine the upward shortwave term. Surface water temperature restoring to observed values is not used to correct heat fluxes in this model.

Results and Discussion

Physical Results

Lake Superior, similar to other deep temperate lakes, experiences twice annual mixing of the water column during the spring and fall with a period of relatively strong stratification during the summer and weaker, deeper stratification during the winter months. The duration of the periods of mixing and stratification play an important role in lake biogeochemistry, as they affect vertical distribution of nutrients and phytoplankton. Model output is compared to surface water temperature observations and twice annual vertical water column temperature data.

Surface water temperature observations from NDBC moored buoys are compared to modeled surface water temperatures from corresponding locations in the model grid for 2005 (Figure 3A, B and C). The three Lake Superior NDBC buoys are located in the western, central, and eastern portions of the lake (squares, Figure 1). Due to removal of the buoys during the winter season, observational records span from early spring (April or May) to late fall (November), barring absence of data due to technical difficulties. In general, the annual cycle of temperature in the model captures the extent and timing of the summer stratified season. Timing of vernal onset of stratification and fall cool down

are matched well at the western buoy, though late stratified season temperatures at the central and eastern buoys tend to be cooler than those seen in observations. Following Wang et al. (2010), the root mean square error (RMSE) is used, defined as

$$RMSE = \sqrt{\frac{\sum_{i=1}^{N}(x_i - y_i)^2}{N}} \quad (4)$$

where x and y are modeled and observed values, respectively, to assess the absolute error of the modeled time series compared to observed. The RMSEs at the western, central and eastern buoy locations for 2005 are 1.52 °C, 1.33 °C and 1.56 °C, respectively. These values are similar to those obtained for annual cycles of lake surface water temperature in other modeling studies of the Great Lakes, e.g. 0.7-2.5 °C in Lake Michigan (Beletsky and Schwab, 2001), 0.95-1.43 °C in Lake Ontario (Huang et al., 2010) and 1.039 °C in Lake Erie (Wang et al., 2010). The model does a fair job of reproducing surface water temperatures at all three locations for the period of 1985 to 2008 (Figure 4 A, B and C). The mean RMSEs at the western, central and eastern buoy locations for 1985-2008 are 2.12 °C, 1.77 °C, and 1.69 °C, respectively. The minimum and maximum RMSE for these locations during the 1985-2008 period are 0.50/6.32°C, 0.90/3.57°C, and 0.82/2.97°C, respectively. These occur in the years 2007/1996, 1997/2001, and 1997/2001. The RMSE for each year at the three locations is listed in Table 3. Over the 1985 to 2008 period a general trend of warmer maximum surface water temperatures at the western buoy location than the central or eastern is present in both the model and observations (Figure 5). Though the model tends towards higher

maximum water temperatures, a clear spatial trend is seen. In their modeling study, Bennington et al. (2010) also note that western arm of Lake Superior is warmer than the eastern arm. The trend towards higher maximum surface water temperatures in the model is likely due to a shallow mixed layer depth that precludes penetration of heat to greater depth and thus increases the surface water temperature. This issue is noted in a study of Lake Erie by Wang et al. (2010), and its cause is described in greater detail below.

Typical surface water temperature spatial patterns as seen in 2005 are shown in Figure 6B. Early spring surface water temperatures are uniform to within a few degrees Celsius in the model. This homogenous state in the early spring is verified by vertical temperature profiles (Figure 6A, gray dots) taken by the Environmental Protection Agency in spring 2005 at the nineteen stations indicated in Figure 1 (asterisks). Vertical profiles of temperature at the EPA sampling locations from the model (Figure 6A, solid lines) show slightly warmer surface temperatures with a nearly isothermal water column throughout the lake. Upwelling, key to biogeochemical processes, can be seen along the northwest coast in the map of 2005 model summer surface water temperatures (Figure 6D). It shows characteristic Lake Superior thermal patterns, as noted by Bennett (1978), of summertime upwelling along the northwestern shore and warmer waters along the south shore. A comparison of model (Figure 6C, lines) and observed (gray dots) vertical thermal structure during the summer shows good reproduction of summer surface water temperatures with the model. The lesser variability among the modeled temperatures as compared to observations is possibly due to the fact that the observed temperatures

represent measurements taken throughout the day and night unlike the modeled temperatures. The modeled mixed layer depth is shallow in comparison with observations. This issue has been noted in other modeling studies of the Great Lakes (Huang et al., 2010 and Beletsky and Schwab, 2001) and of the Bering Sea (Hu and Wang, 2010). Hu and Wang (2010) note that wind-wave mixing inclusion is necessary to obtain greater upper mixed layer depth and that use of the level 2.5 closure turbulence model, as was done in this study, is not sufficient to remedy the problem. Wind-wave mixing parameterization may be included in the future to increase the accuracy of the mixed layer depth though it is not within the scope of the current study.

Increasing summer surface water temperatures in Lake Superior over the past century and especially the last 30 years have been noted by Austin and Colman (2007, 2008). Figure 7 plots the surface water temperature averaged over the stratified season (July-September) for the model and observations at the three buoy locations for 1985 to 2008 as well as a linear fit to the data. Both the buoy temperature data and model output concur with the positive trend at all three locations. NDBC buoy data shows a rate of increase of surface water temperature of 0.15±0.05, 0.12±0.07, and 0.12±0.08 $°Cy^{-1}$ at the western, central, and eastern buoys, respectively (Figure 7 West, Central and East). An average of temperatures at the three buoys shows a positive trend of 0.14±0.06 °C per year (Figure 7 Spatially Averaged). Model space- and time-averaged surface water temperatures are consistently warmer than in observations for the first ten years, when the number of meteorological data used to create the surface forcing fields was relatively small. Thus model temperatures show slightly slower rates of increase: 0.08±0.06,

0.07±0.06, and 0.05±0.06°C per year at the western, central, and eastern buoys, respectively. The average of the west, central and east modeled rate of temperature increase is 0.07±0.06°C y^{-1}. An average of modeled temperatures from the entire lake surface, which is representative of overall model behavior, gives a value of 0.10±0.05°C y^{-1}. These values are all comparable to the rate of increase for the summer (JAS) period reported for 1979 to 2006 by Austin and Colman (2008) of 0.11±0.06°C y^{-1}.

Model ice cover is compared to two data sets: NOAA's Great Lakes Ice Atlas (Assel, 2003) and the Interactive Multisensor Snow and Ice Mapping System (IMS) Daily Northern Hemisphere Snow and Ice Analysis at four kilometers (National Ice Center, 2008). The Great Lakes Ice Atlas contains composite ice charts for the entire surface area of the Laurentian Great Lakes from 1973 to 2002 with a recent update to 2005 in Assel (2005). Data covers the lake-ice season (December to April/May) and frequency of the data ranges from every three to four days to every week. Comparison with model output is performed using the spatially average daily ice cover time series for Lake Superior, an analysis product in the Great Lakes Ice Atlas. The IMS database is used to provide data from 2005 to 2008. IMS ice cover data has daily resolution and covers the entire northern hemisphere at a spatial resolution of four kilometers (2004 and onwards). Each four kilometer grid cell is evaluated and designated as being land, snow, ice or water. To compare our model output to this binary format of determining ice coverage for a grid cell, I assign ice cover in each model grid cell in a similar binary manner based on an ice cover greater than thirty percent. Though there is no systematic

data set available for thickness of ice cover on Lake Superior, analyses of modeled ice thickness are presented.

The annual cycle of ice cover and spatially averaged ice thickness during 2005 are shown in Figure 8A and B. Observed ice cover from the IMS Daily Northern Hemisphere Snow and Ice Analysis and the Great Lake Ice Atlas are both available for 2005. Figure 8A compares time series of the percent of Lake Superior's surface area covered by ice calculated from the IMS (asterisks) and the Great Lakes Ice Atlas (dots) with modeled percent ice cover (line). The domain-averaged ice thickness is calculated as the average thickness of all ice cover present on a given day. The Great Lakes Ice Atlas and IMS observations are largely consistent with each other as seen in Figure 8A. An early increase in ice cover and thickness occurs from mid-January to the beginning of February in response to a basin-wide cold air outbreak (Figure 9). Ice begins to form in the periphery of the lake (Figure 10). During an extended period of sub-zero air temperatures from early to mid-March ice cover quickly increases to a maximum of 58% lake surface area coverage on March 18. Ice thickness follows a similar though slightly lagging increasing trend to reach a maximum of 7 cm on March 23. Both ice cover and thickness subsequently decrease rapidly from late March through April concurrent with basin-wide steadily increasing air temperatures. Ice melt timing in the model lags the observations. This is discussed further in the following paragraph. The RMSE of the modeled percent ice cover compared to that calculated from the IMS data set is 7.8%. In comparison with the Great Lakes Ice Atlas time series, it is 8.2%.

The percent ice cover of Lake Superior from 1985 to 2008 is presented in Figure 11A. Observational data from 1985 to 2004 is from the Great Lakes Ice Atlas. Observational data from 2005 to 2008 is from the IMS. The variability in the overall magnitude of ice cover from year to year is reproduced well by the model. On this lake-wide scale, the timing of the onset of ice cover compares well between the data and model. Ice cover melting, however, tends to be delayed in the model as compared with observations, especially in years with large percent ice cover. This may be due to a deficiency in near-surface vertical mixing because of the lack of wind-wave mixing parameterization in the model as noted earlier. This would allow surface water temperatures to remain colder than expected, thus delaying ice cover melting. RMSE values for ice cover for each year are given in Table 4. The average RMSE for the 1985 to 2008 period is 16.9%. The maximum RMSE is 41.3 occurring in 1985 and the minimum is 3.8 occurring in 1998. The RMSE tends to be high in years with greater overall ice coverage when the lag in modeled ice melt in comparison with observations is relatively high. Domain-averaged ice thickness in meters is presented in Figure 11B. Increases in ice thickness are strongly correlated with cold air outbreaks, as noted for year 2005 above. Years with high ice thickness (e.g. 1994 and 1996) exhibit extended periods of sub-zero air temperatures and co-occurring ice thickness increase. Histograms of ice thickness for each year are given in Table 5 (after Wang et al., 2010). The fraction of ice cover with thicknesses in the ranges of 0-5 cm, 5-15 cm, 15-30 cm, and greater than 30 cm are given for each month (December to April). Though there are currently efforts to create airborne and satellite ice thickness retrieval algorithms, existing

measurements of ice thickness on Lake Superior are scant and not readily available (pers. comm., George Leshkevich, 2011). Therefore, information on ice thickness from the model will be useful for future comparison with satellite or other observations.

Figure 12 presents a map of observed and model ice cover and environmental conditions for January 26, 2005. The observed ice cover is from the IMS Daily Northern Hemisphere Snow and Ice Analysis. Geographic distribution of the ice cover is similar between observations (Figure 12A) and model (Figure 12B) with ice cover along the southwestern, southeastern shores and in the northern bays, though the model produces more extensive coverage on the southeastern shore. Zero degree waters are present only along the coastal regions with warmer water over the rest of the lake surface (Figure 12C). Ice can, therefore, only form along a thin region near the shore, but the model ice extends into warmer waters. The presence of ice in warmer waters therefore is explained by advection of ice, indicated by a predominantly east-to-west ice velocity (black arrows, Figure 12B) driven by sustained northwesterly winds (Figure 12D). In other words, along the southern and eastern shores the ice moves away from freezing coastal waters, allowing more ice to form along the shoreline and advecting the ice away in a mechanism similar to that of coastal polynya found in polar seas. The size of the ice cover in this situation is determined by the relative rates of new ice formation nearshore and of ice melting along the outward ice edge. The regular presence of coastally formed ice, especially in years with less than complete ice cover, can also be seen in a comparison of the spatial distribution of ice cover as observed (left column, Figure 10) and in the model (right column, Figure 10) for January 12, February 24 and March 21 2005. Ice cover first

forms in the shallow northern bays, then along the relatively shallow and bathymetrically gently sloping southwestern shores and finally in Whitefish Bay (Jan 12 panels, Figure 10). Ice cover begins increasing in extent in reaction to a cold air outbreak (Feb 24 panels, Figure 10, Figure 9). Ice cover reaches a maximum in mid-March due to continued sub-zero air temperatures following the late February cold air outbreak (not shown). Ice cover occupies nearly the entire coastline with no coverage in the central and eastern basin offshore waters. As ice cover decreases in late March in response to warming air temperatures (Mar 21 panels, Figure 10), the width of ice cover along the coastline decreases with ice cover in the central and eastern basins melting first in the offshore waters. By April, ice cover persists mainly in the shallow northern bays (not shown).

Annual ice cover magnitude has been shown to be decreasing over the past several decades (Austin and Colman, 2007). Figure 13 shows the average percent of lake surface area covered by ice for each year's winter season. The model tends towards slightly greater ice coverage and is decreasing at a rate of 1.20±0.29%/yr for 1985-2008. The observations show a rate of decrease of 0.80±0.20%/yr. These values are comparable to the value of 0.42±0.20%/yr reported by Austin and Colman (2007) for the period of 1979-2006.

Mean annual water current magnitudes and directions at the surface (< 20 m) and at depth (> 75 m) from the model for 2005 are presented in Figure 14. Average annual surface current speed and average annual deep current speed are on the order of 0.50 cm s^{-1} and 0.36 cm s^{-1}. Winter currents both at the surface and at depth tend to dominate the

annual average values, because winter surface currents are stronger than summer currents due to greater wind speeds during the fall and winter. Though using different atmospheric boundary conditions I find that, similar to results in Bennington et al. (2010), winter surface currents tend to reflect wind directions that have a strong northerly component. Winter currents at depth are stronger than summer due to the strength of the surface currents and the lack of strong density stratification. Weaker stratification during the winter allows wind momentum to be transferred more readily into deeper waters than during the summer. Topography (see Figure 1) is reflected in the distribution of cyclonic circulation at the surface and at depth above the deep Eastern and Western basins (Bennington et al., 2010). Current directions also are roughly consistent with those presented in Beletsky (1999).

Biogeochemical Results

Surface maps of modeled temperature, phosphate, and chlorophyll concentrations from August 22, 2005 show mechanistically consistent spatial patterns (Figure 15). Upwelling, indicated by cooler water temperatures, is clear along the northwest shore (Figure 15A). The presence of upwelling is also apparent in elevated surface phosphate concentrations (Figure 15B). A similar spatial pattern in chlorophyll concentrations show the response of phytoplankton to waters with relatively higher nutrient concentration being brought to the photic region of the water column through upwelling (Figure 15C). These relationships demonstrate internal consistency within the biogeochemistry and

ecosystem model. They also show that phosphorus exerts primary control on phytoplankton growth in the model.

The EPA measures chlorophyll concentration with depth annually at nineteen sites (asterisks, Figure 1). Figure 16 compares model chlorophyll concentrations at the same locations and summertime sampling dates with the EPA data. The deep chlorophyll maximum (DCM) is a ubiquitous feature in Lake Superior during the summer months. The depth and magnitude of the DCM is reproduced well in modeled chlorophyll values. Chlorophyll in the model displays less spatial heterogeneity than the observed chlorophyll does. This may be due to the horizontal resolution of the model grid (5km by 5km) and the fact that the observed values represent measurements taken at multiple times throughout the day and night. Surface chlorophyll values in the model tend to be slightly higher than those observed. This could be due to the absence of a phytoplankton photoinhibition mechanism in the ecosystem model. The model also displays lower overall chlorophyll values at sub-thermocline depths.

Productivity in Lake Superior has limited seasonal variability. Sterner (2010) notes only small change in algal biomass and chlorophyll levels in measurements spanning April to November which covers conditions from an isothermal less than two degree Celsius water column (April) through fully developed summer stratification with surface temperatures of 18.38°C. Sterner states an annual range of productivity of 200-350 mg C m^{-2} d^{-1}. An earlier study by Munawar and Munawar (1978) on diversity and biomass of phytoplankton throughout Lake Superior also noted a lack of clear seasonal trends in phytoplankton biomass that set it apart from the other Great Lakes. The model

exhibits a seasonal range of productivity from approximately 20 to 700 mg C m^{-2} d^{-1}. That the model has a stronger seasonal variability than indicated by available observations suggests that the dissolved pool of organic matter may be too small vis-à-vis the particulate pool. As noted above, I attempted to implicitly account for the purportedly strong microbial loop by selecting a low half-saturation concentration of phosphate uptake by phytoplankton and high rates of remineralization of detritus. As in most marine ecosystem models, the selection of these poorly constrained biological parameter values is delicate and difficult. A more judicious selection of biological parameters as well as possibly different ecosystem construction are areas of future improvement. It is worth noting that by removing seasonal peaks in surface phosphate concentration, a strong microbial loop and a larger pool of dissolved organic matter would tend to diminish the appearance of phosphate controlling phytoplankton growth. This may explain why temperature and light come out statistically as dominant controls on primary production (Sterner, 2010). Three other factors that may affect the seasonality of productivity in the model are ice cover presence which has been noted to last longer in the spring in the model compared to observations and which affects the amount of light experienced by the ecological model, the use of a single class of phytoplankton in the model which does not allow for species succession throughout the year, and the use of a constant carbon to phosphorus ratio for phytoplankton.

The average annual gross primary productivity from the model for the 1985 to 2008 period is approximately 6.2 Tg C yr^{-1} (Figure 17). This value is within the ranges offered by Cotner et al. (2004, 5.3-8.2 Tg C yr^{-1}) and Urban et al. (2005, 2.0-6.7 Tg C yr^{-}

^{1}). Model results for 2006 to 2008 range from 7.1 to 7.8 Tg C yr^{-1} and are similar to the more recent value of 7.6 to 9.73 Tg C yr^{-1} from Sterner (2010). Much as the annual surface water temperatures and annual ice cover show large variability, so does total annual gross primary production. The interannual range for this period is about 4.1 Tg C with more productivity during warmer years with less ice cover. Years with high ice cover have reduced levels of annual gross primary production possibly owing to, as mentioned above, the tendency in the model to retain ice in the spring past the date of ice out indicated by observations as well as the impact of ice on light experienced by the ecological model. A fit to these values shows gross primary productivity increasing at a rate of 0.07±0.03 Tg C/yr over this time period (Figure 17).

Gross primary production is strongly correlated with annual average surface water temperatures and average percent wintertime ice cover (r^2=0.98, r^2=0.85, respectively, Figure 18). Two key factors in Lake Superior primary productivity are water temperature and light availability according to Sterner (2010). Therefore, increased surface water temperatures may allow for greater rates of primary productivity. At the same time, stronger thermal stratification reduces the depth to which phytoplankton are mixed in the water column, increasing light availability for primary production. A longer stratified season can thus yield greater annual primary productivity by allowing phytoplankton to experience warmer temperatures and greater light intensity for a larger portion of the year, assuming that nutrients do not become the limiting growth factor.

Conclusions

A new realistically configured three-dimensional model for Lake Superior including for the first time prognostic models of ice and biogeochemistry is presented. For the simulation period of 1985 to 2008, the new model is able to reproduce many physical and biological characteristics of Lake Superior as well as long term interannual trends in water temperature and ice cover.

The annual surface water temperature cycle is well represented by the model with average root mean square errors of 2.12 °C, 1.77 °C, and 1.69 °C in comparison with observations at the western, central, and eastern NOAA buoy locations. Large-scale spatial patterns in surface water temperatures, e.g. higher overall water temperatures in the western arm versus the central and eastern basins, are reproduced by the model. The mixed layer depth tends to be shallow in the model in comparison to observations, possibly because the model lacks wind-wave mixing parameterization, which may be included in the future. A repercussion of the shallow thermocline is relatively high summer maximum surface water temperatures. However, the trend of increasing summertime surface water temperatures in the model during the period 1985-2008 is consistent with observations.

Interannual variability of ice cover magnitude simulated by the model is consistent with observations. Focus on the 2005 shows good reproduction of timing of ice formation and the magnitude and timing of peak ice cover as considered against two sets of ice cover observations. Melting of ice cover in the model is delayed in comparison with observations. This is also likely linked to the shallowness of the mixed

later depth and can be improved in the future. The rate of decrease of wintertime ice cover magnitude from 1985-2008 in the model is similar to but greater than observations.

Spatial patterns of biogeochemical variables show internal and therefore mechanistic consistency within the model, although an improved representation of the microbial loop and dissolved phase of organic matter is an area of future model development. Vertical chlorophyll profiles, including the deep chlorophyll maximum in the stratified season, are reasonably well simulated when compared to observations. Average total annual gross primary production for 1985-2008 is comparable to several recent estimations of productivity including that of Sterner (2010). Long-term interannual gross primary productivity rates are highly variable but show an increasing trend for the period 1985-2008 that is strongly correlated with increasing annual average surface water temperatures and decreasing winter ice cover.

This new model is the first to explicitly model the dynamics of water, ice, and biogeochemistry of Lake Superior. The model is internally consistent, responds well to the data-based forcing fields, and overall reproduces lake observations well. These attributes make this model a useful tool for elucidating mechanisms controlling the physical state and biogeochemical cycling of the lake today and how these may change in the future under global climate change.

Table 1. Biological Parameters

Parameter	Units	Value	Reference
Light attenuation by water	m^{-1}	0.10	Jerome et al. 1983
Light attenuation by chlorophyll	m^{-1}	0.02486	Fennel et al. 2006
PAR fraction	nondimensional	0.43	Baker and Frouin 1987
Phytoplankton growth at 0°C	molC $gChl^{-1}$ d^{-1}	0.4	Kishi et al. 2007
Half-saturation conc. for PO_4 uptake	mmol P m^{-3}	0.05	Chen et al. 2002
Half-saturation conc. for phyt. uptake	$(mmol\ P\ m^{-3})^2$	1.4	Fennel et al. 2006
Maximum chlorophyll to phyt. ratio	mgChl mgC^{-1}	0.0535	Fennel et al. 2006
P-I curve initial slope	molC $gChl^{-1}$ $(W\ m^{-2})^{-1}d^{-1}$	0.1	Kishi et al. 2007
Photoinhibition parameter	molC $gChl^{-1}$ $(W\ m^{-2})^{-1}d^{-1}$	0	-
Photosynthetic Temperature coefficient	$°C^{-1}$	0.0693	Kishi et al. 2007
Phytoplankton carbon to phosphorus ratio	molC $molP^{-1}$	200	Barbiero& Tuchman 2004
Phytoplankton mortality rate	d^{-1}	0.15	Fennel et al. 2006
Zooplankton assimilation efficiency	d^{-1}	0.75	Fennel et al. 2006
Zooplankton basal metabolism excretion	d^{-1}	0.1	Fennel et al. 2006
Zooplankton carbon to phosphorus ratio	molC $molP^{-1}$	106	Fennel et al. 2006
Zooplankton maximum grazing rate	$(mmolP\ m^{-3})^{-1}$ d^{-1}	0.6	Fennel et al. 2006
Zooplankton mortality rate	d^{-1}	0.025	Fennel et al. 2006
Large detritus remineralization rate	d^{-1}	0.05	-
Small detritus remineralization rate	d^{-1}	0.01	-
Phytoplankton sinking rate	m d^{-1}	0.1	Fennel et al. 2006
Small detritus sinking rate	m d^{-1}	0.1	Fennel et al. 2006
Large detritus sinking rate	m d^{-1}	1.0	Fennel et al. 2006

Table 2. Biological Initialization Values

State Variable	Initialization Value (mmol P m^{-3})	Reference
Phytoplankton	0.189	Heinen and McManus 2004
Zooplankton	0.0107	Watson and Wilson 1978
Phosphate	0.025	Sterner et al. 2004
Large Detritus	0.002	-
Small Detritus	0.04	-

Table 3. RMSE values for Surface Water Temperature at West, Central and East buoys.

Year	RMSE (°C)		
	West	Central	East
1985	2.32	1.81	1.52
1986	1.41	2.35	2.44
1987	4.02	2.40	1.45
1988	1.65	2.63	1.66
1989	3.06	1.37	2.06
1990	1.00	1.29	1.37
1991	2.07	1.12	1.59
1992	2.29	1.87	1.93
1993	2.43	1.28	1.78
1994	1.22	1.25	0.85
1995	1.19	1.44	1.13
1996	6.32	1.65	1.94
1997	2.47	0.90	0.82
1998	2.29	1.87	1.77
1999	2.55	2.06	1.74
2000	1.39	2.14	1.74
2001	1.36	3.57	2.97
2002	2.49	1.67	1.79
2003	1.56	2.16	1.97
2004	1.60	1.33	1.18
2005	1.52	1.33	1.56
2006	1.79	1.24	2.20
2007	0.50	1.76	1.83
2008	2.43	2.06	1.35

Table 4. RMSE Values for Ice Cover, 1985-2008

RMSE = root mean square error. See main text for definition.

Year	RMSE (percent)
1985	41.3
1986	27.0
1987	5.2
1988	13.3
1989	31.6
1990	15.5
1991	22.0
1992	15.8
1993	15.7
1994	30.2
1995	19.5
1996	27.9
1997	32.5
1998	3.8
1999	3.9
2000	4.1
2001	10.2
2002	3.7
2003	19.1
2004	24.0
2005	7.8
2006	5.4
2007	8.4
2008	17.1

Table 5. Ice Thickness Histograms for 1985-2008 (Fraction of ice present in each thickness range).
*December values are shifted down to show continuous winter season (Dec-Apr)

Year	Ice Thickness Range	December*	January	February	March	April
1985	0-5cm	--	0.77	0.08	0.1	0.42
	5-15cm	--	0.13	0.19	0.17	0.17
	15-30cm	--	0.04	0.24	0.19	0.12
	>30cm	--	0.06	0.49	0.55	0.29
1986	0-5cm	0.95	0.83	0.51	0.43	0.48
	5-15cm	0.04	0.1	0.24	0.24	0.24
	15-30cm	0.01	0.04	0.14	0.13	0.12
	>30cm	0	0.03	0.12	0.21	0.16
1987	0-5cm	0.7	0.69	0.9	0.97	0.99
	5-15cm	0.14	0.21	0.08	0.02	0.01
	15-30cm	0.16	0.07	0.01	0.01	0
	>30cm	0	0.02	0	0	0
1988	0-5cm	0.99	0.88	0.75	0.72	0.74
	5-15cm	0.01	0.1	0.15	0.16	0.14
	15-30cm	0	0.01	0.04	0.05	0.06
	>30cm	0	0	0.06	0.07	0.06
1989	0-5cm	0.97	0.93	0.84	0.38	0.46
	5-15cm	0.02	0.06	0.11	0.33	0.3
	15-30cm	0	0.01	0.03	0.17	0.12
	>30cm	0	0	0.03	0.12	0.12
1990	0-5cm	0.91	0.83	0.79	0.79	0.8

	5-15cm	0.07	0.11	0.13	0.13	0.08
	15-30cm	0.01	0.03	0.04	0.03	0.05
	>30cm	0.01	0.02	0.04	0.05	0.07
1991	0-5cm	0.97	0.89	0.77	0.6	0.73
	5-15cm	0.01	0.08	0.13	0.22	0.13
	15-30cm	0.01	0.02	0.04	0.1	0.06
	>30cm	0.01	0.01	0.06	0.08	0.08
1992	0-5cm	0.96	0.73	0.81	0.82	0.79
	5-15cm	0.03	0.22	0.14	0.09	0.12
	15-30cm	0.01	0.03	0.03	0.04	0.04
	>30cm	0	0.01	0.02	0.04	0.05
1993	0-5cm	0.99	0.93	0.83	0.66	0.75
	5-15cm	0.01	0.05	0.11	0.22	0.16
	15-30cm	0	0.01	0.03	0.07	0.04
	>30cm	0	0	0.03	0.05	0.05
1994	0-5cm	0.99	0.75	0.12	0.1	0.34
	5-15cm	0.01	0.15	0.18	0.19	0.26
	15-30cm	0	0.05	0.24	0.24	0.16
	>30cm	0	0.05	0.46	0.46	0.25
1995	0-5cm	0.54	0.92	0.84	0.76	0.84
	5-15cm	0.44	0.04	0.11	0.15	0.07
	15-30cm	0.01	0.01	0.03	0.05	0.03
	>30cm	0.01	0	0.03	0.05	0.06
1996	0-5cm	0.96	0.84	0.4	0.12	0.24
	5-15cm	0.03	0.11	0.29	0.23	0.25
	15-30cm	0.01	0.03	0.13	0.2	0.15

	>30cm	0	0.03	0.18	0.46	0.35
1997	0-5cm	0.99	0.86	0.56	0.24	0.47
	5-15cm	0.01	0.1	0.26	0.45	0.28
	15-30cm	0	0.02	0.09	0.16	0.12
	>30cm	0	0.02	0.09	0.14	0.14
1998	0-5cm	0.97	0.95	0.93	0.96	0.89
	5-15cm	0.01	0.04	0.06	0.03	0.04
	15-30cm	0.01	0	0.01	0.01	0.03
	>30cm	0.01	0	0	0.01	0.03
1999	0-5cm	1	0.92	0.9	0.89	0.96
	5-15cm	0	0.07	0.06	0.08	0.02
	15-30cm	0	0.01	0.02	0.02	0.01
	>30cm	0	0	0.01	0.01	0.01
2000	0-5cm	0.99	0.88	0.83	0.85	0.93
	5-15cm	0.01	0.09	0.12	0.11	0.05
	15-30cm	0	0.02	0.03	0.03	0.02
	>30cm	0	0.01	0.02	0.02	0.01
2001	0-5cm	0.96	0.93	0.88	0.82	0.73
	5-15cm	0.03	0.07	0.08	0.09	0.15
	15-30cm	0.01	0.01	0.02	0.03	0.06
	>30cm	0	0	0.02	0.05	0.06
2002	0-5cm	1	0.91	0.91	0.9	0.84
	5-15cm	0	0.07	0.08	0.06	0.12
	15-30cm	0	0.01	0.01	0.02	0.03
	>30cm	0	0.01	0	0.02	0.01

2003	0-5cm	0.91	0.72	0.59	0.13	0.53
	5-15cm	0.05	0.14	0.24	0.33	0.22
	15-30cm	0.02	0.11	0.08	0.25	0.08
	>30cm	0.02	0.03	0.08	0.3	0.18
2004	0-5cm	0.86	0.78	0.61	0.66	0.7
	5-15cm	0.1	0.16	0.2	0.19	0.19
	15-30cm	0.03	0.04	0.09	0.08	0.08
	>30cm	0.01	0.02	0.1	0.07	0.03
2005	0-5cm	0.98	0.87	0.81	0.78	0.71
	5-15cm	0.02	0.1	0.14	0.12	0.13
	15-30cm	0	0.03	0.05	0.05	0.07
	>30cm	0	0.01	0.01	0.05	0.09
2006	0-5cm	0.8	0.94	0.95	0.84	0.72
	5-15cm	0.1	0.05	0.04	0.1	0.18
	15-30cm	0.07	0.01	0.01	0.03	0.07
	>30cm	0.03	0.01	0	0.03	0.03
2007	0-5cm	1	0.92	0.83	0.79	0.9
	5-15cm	0	0.06	0.1	0.13	0.05
	15-30cm	0	0.01	0.03	0.05	0.02
	>30cm	0	0.01	0.03	0.03	0.02
2008	0-5cm	0.99	0.93	0.78	0.6	0.71
	5-15cm	0.01	0.06	0.15	0.21	0.16
	15-30cm	0	0.01	0.04	0.09	0.07
	>30cm	0	0	0.03	0.09	0.05

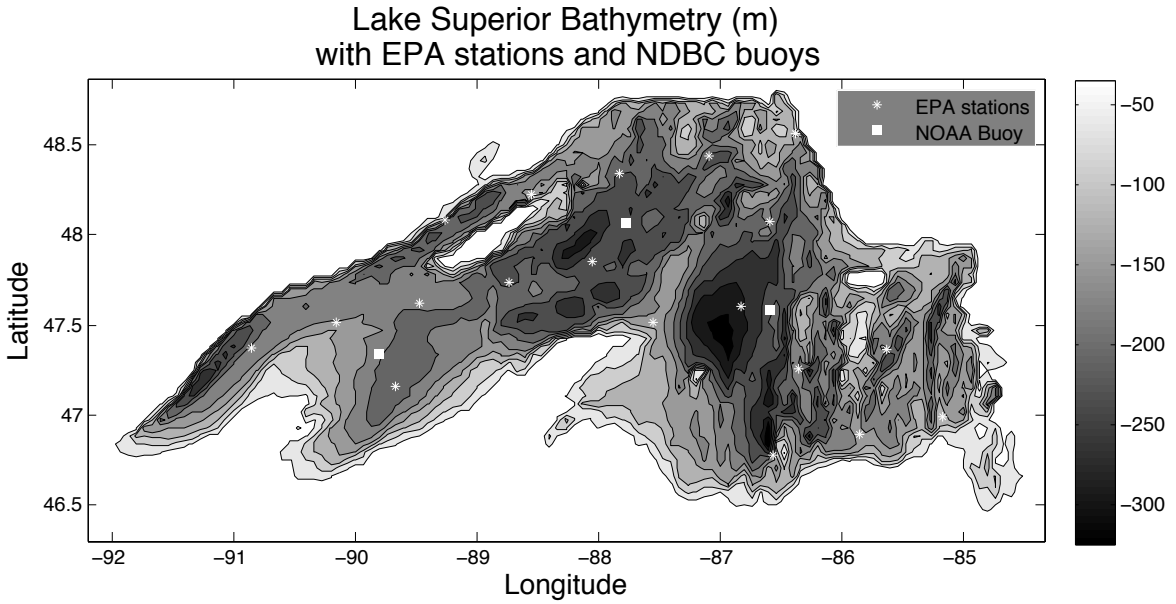

Figure 1. Lake Superior model bathymetry in meters with EPA station locations (asterisks, 19) and NDBC buoy locations (squares, 3). Bathymetry contour lines are every 50 meters.

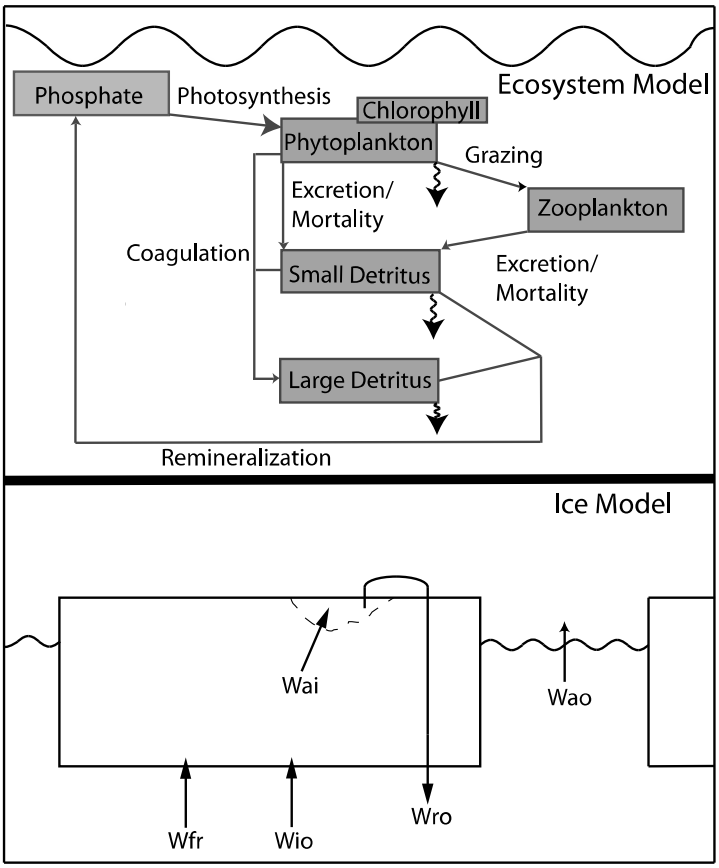

Figure 2. Ecosystem and ice module schematics. Ecosystem: State variables are shown as shaded boxes. Fluxes between he state variables are shown as arrows. Ice: freeze/melt rates contributing to ice volume and concentrations changes are shown with arrows. Wai: melt rate at ice/snow interface, Wao: freeze rate at water/air interface, Wfr: frazil ice formation rate, Wio: freeze rate at ice/water interface, Wro: runoff rate of surface meltwater, after Hedstrom (2009), Fig. 7.

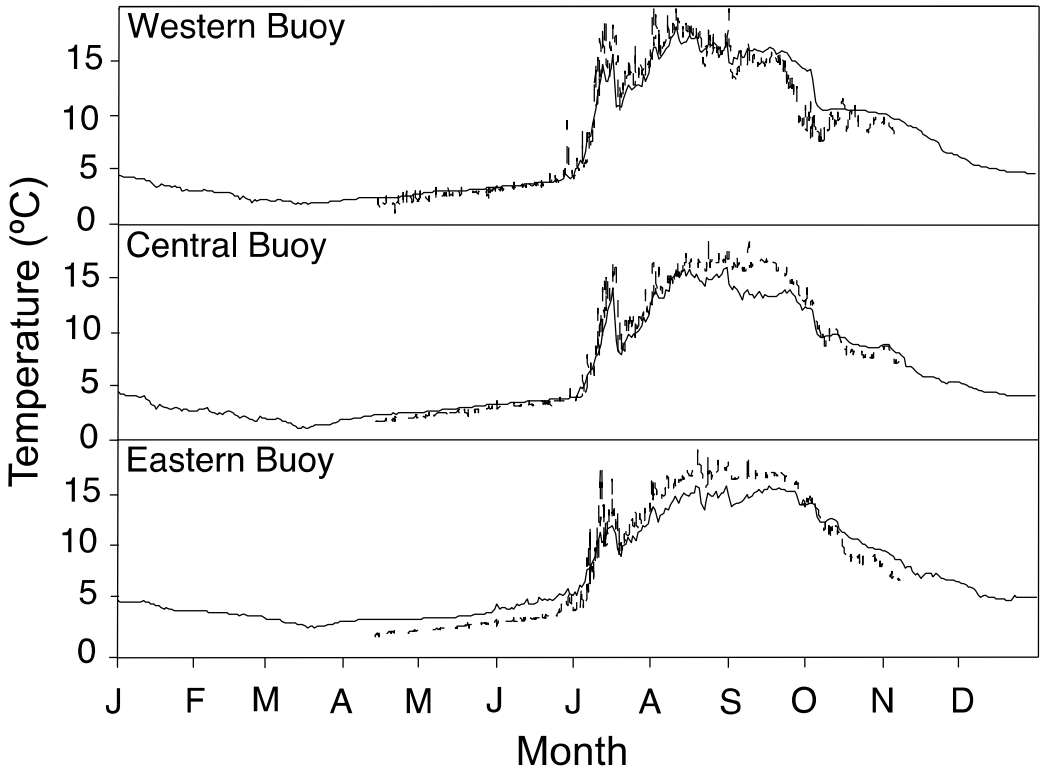

Figure 3. Surface water temperatures at three NDBC buoy locations (west, central, east) for 2005 (°C). Model output is shown as solid lines and NDBC buoy data are shown as dotted lines.

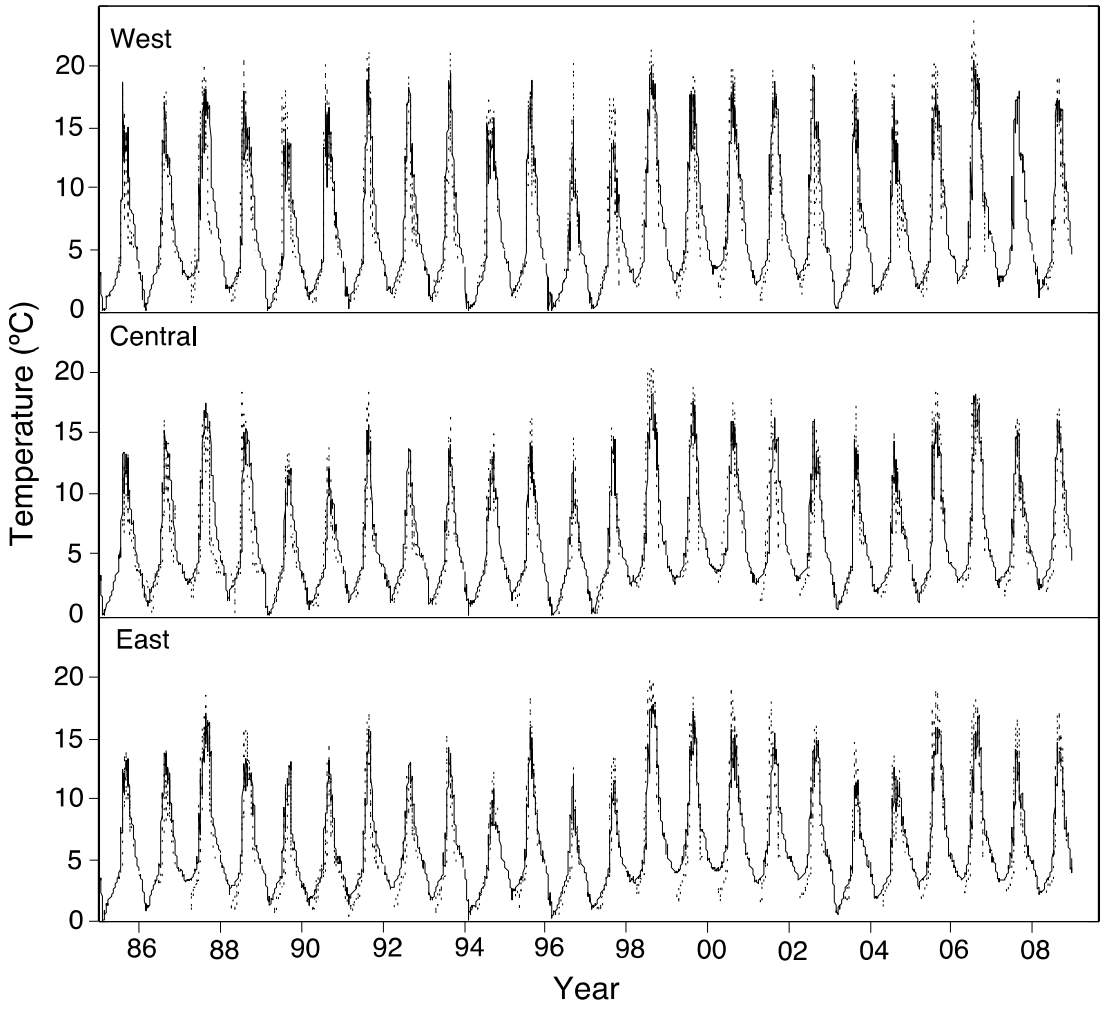

Figure 4. Surface water temperatures at three NDBC buoy locations (west, central, east) for 1985-2008 (°C). Model output is shown as solid lines. Data from NDBC buoys is shown as dotted lines.

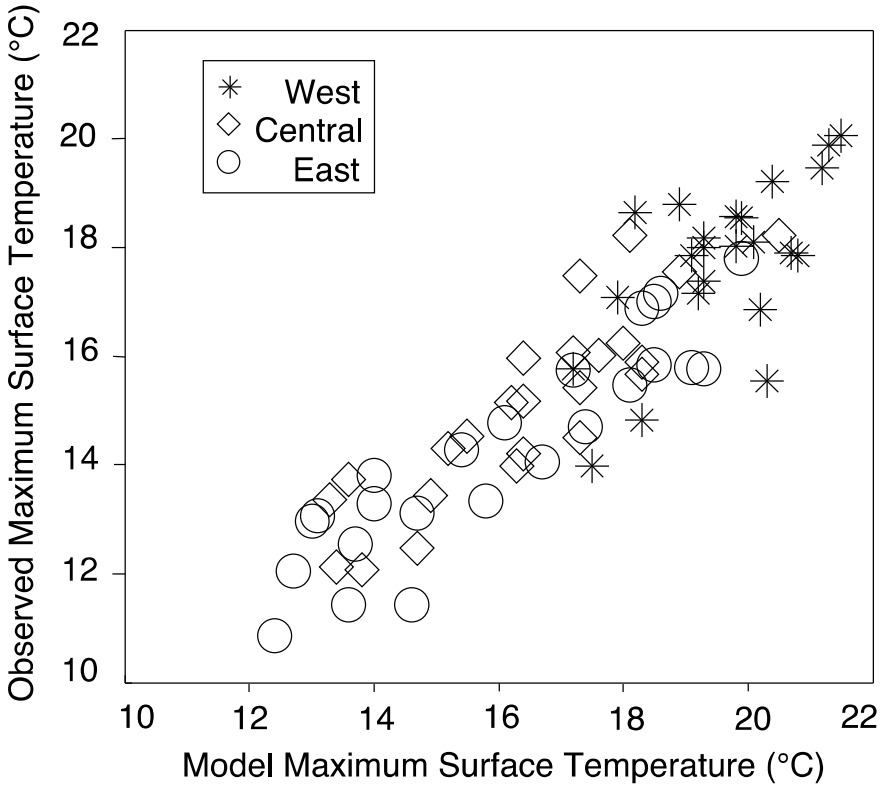

Figure 5. Maximum summer surface water temperatures (°C) at three NDBC buoy locations across the lake for 1985-2008. Buoy observations are plotted against modeled values. Western buoy: asterisks, central buoy: diamonds, eastern buoy: circles.

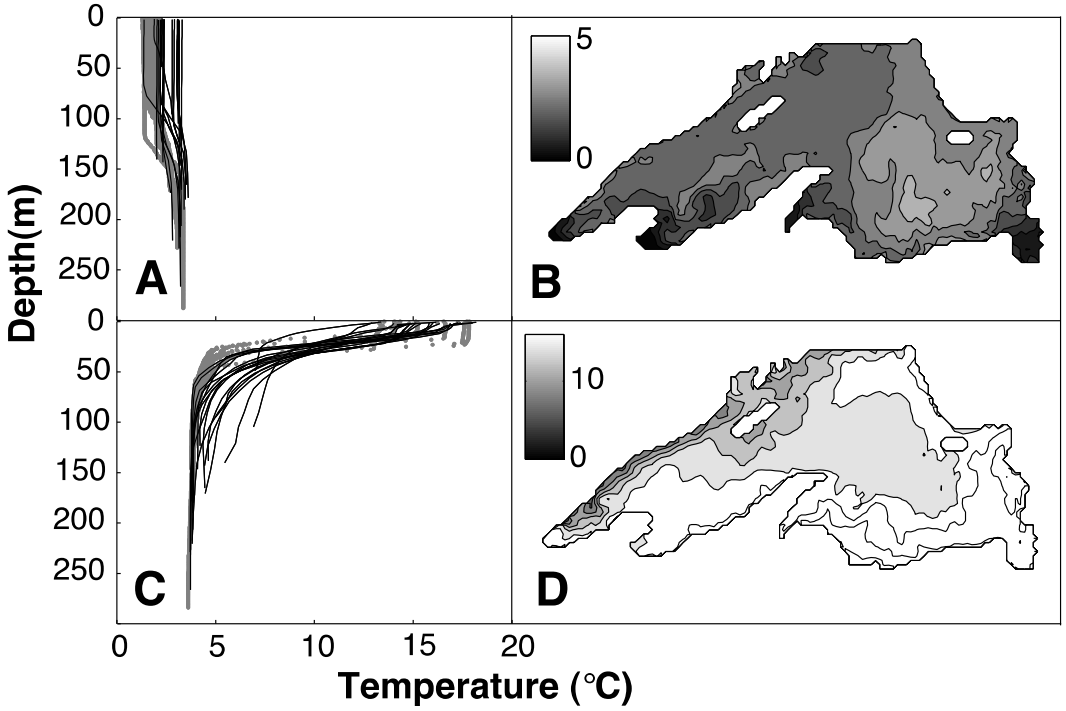

Figure 6. Panels A and C show water column temperatures (°C) at 19 offshore EPA sites in the early spring and summer from the model (black lines) and observed data (gray dots). Panels B and D show modeled surface water temperatures (°C) in the early spring and summer.

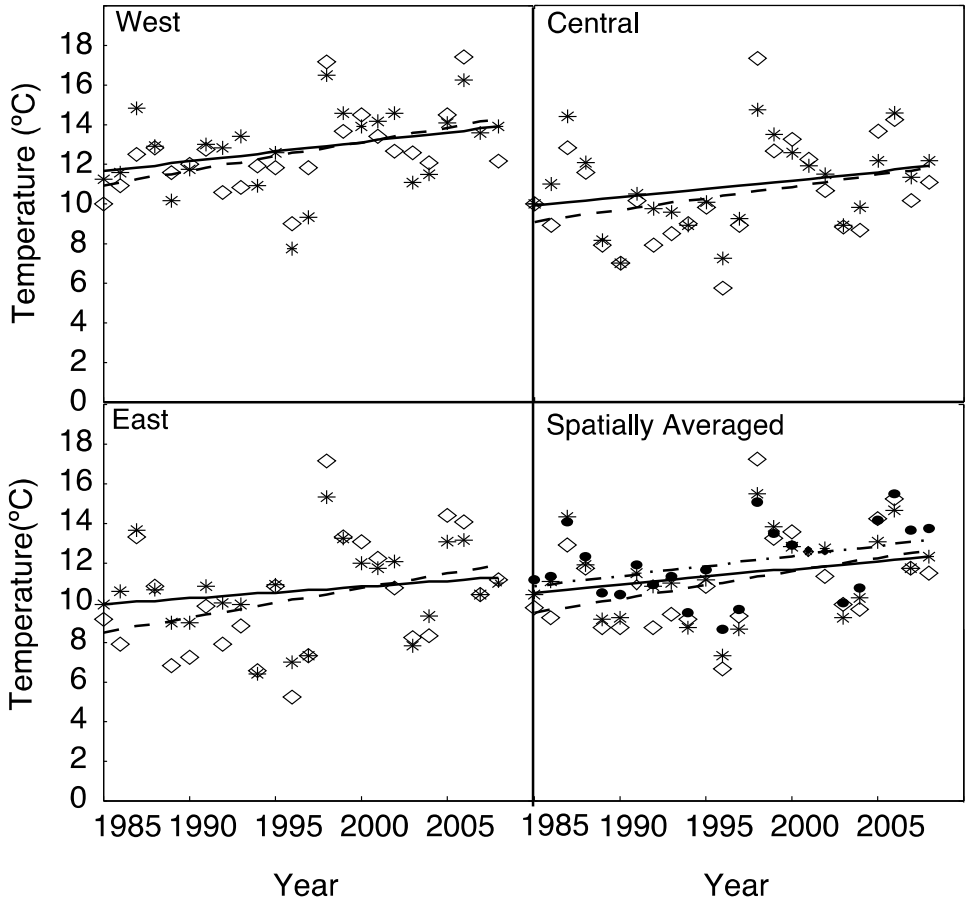

Figure 7. Average surface water temperature (C) during the stratified season (July-September) for 1985-2008 for western, central, and eastern NDBC buoys. Model values (asterisks) and observed values (diamonds) and linear fits to the modeled (solid line) and observed (dashed line) values are shown. Spatially averaged: an average of temperatures at the three locations is shown for model output (asterisks) and NDBC buoy data (diamonds) as well as an average of model temperatures over the entire lake surface (dots). Fits to the model output (solid line) and buoy data (dashed line) and for the entire model lake surface averaged temperature (dot-dash line) are shown.

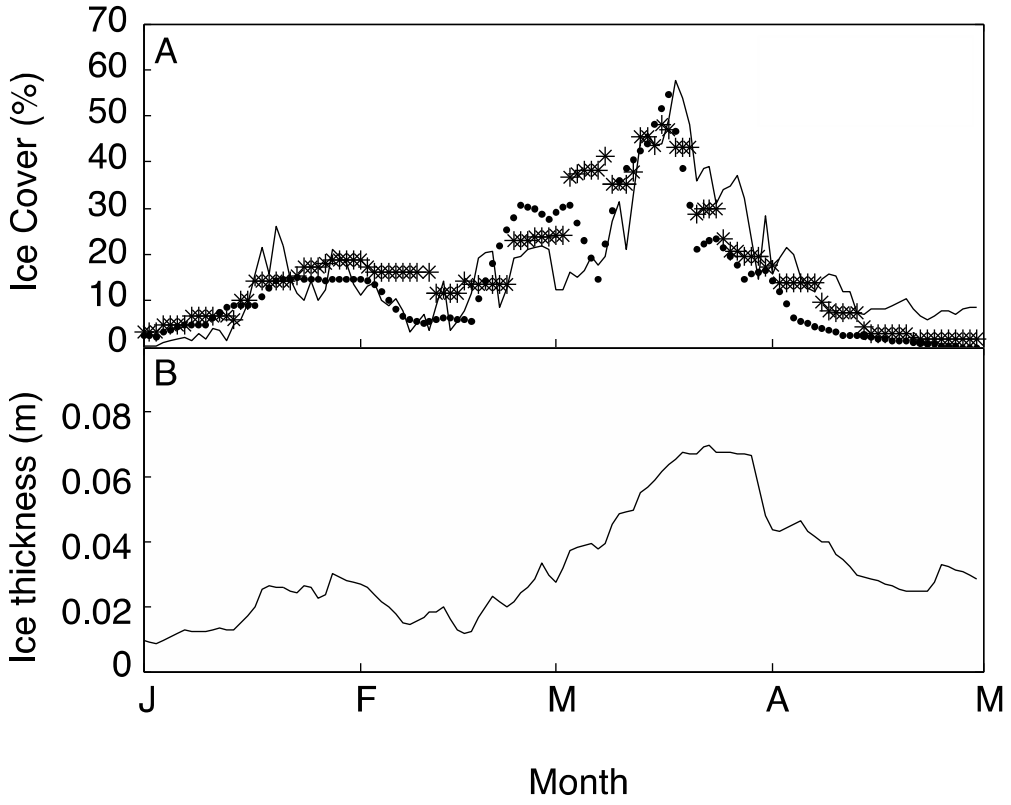

Figure 8 A: Model (solid line) and observations from the IMS (asterisks) and Great Lakes Ice Atlas (dots) of percentage of lake surface area covered by ice during 2005. B: Domain-averaged ice-cover thickness in meters during 2005.

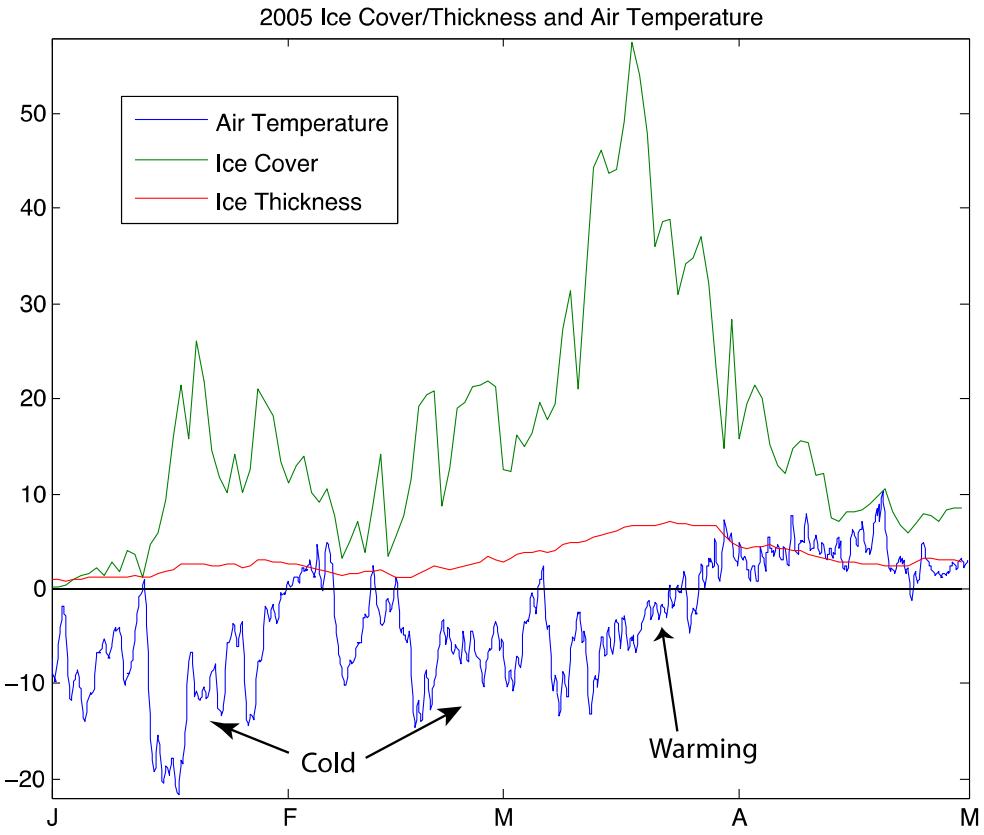

Figure 9. Modeled ice thickness (cm, red), percent ice cover (green), and air temperature (°C, blue) for January through April during 2005. Cold 'outbreaks', when ice cover spatial coverage and thickness increases, are noted along with the springtime warming trend when major ice cover melt occurs and ice cover thickness decreases.

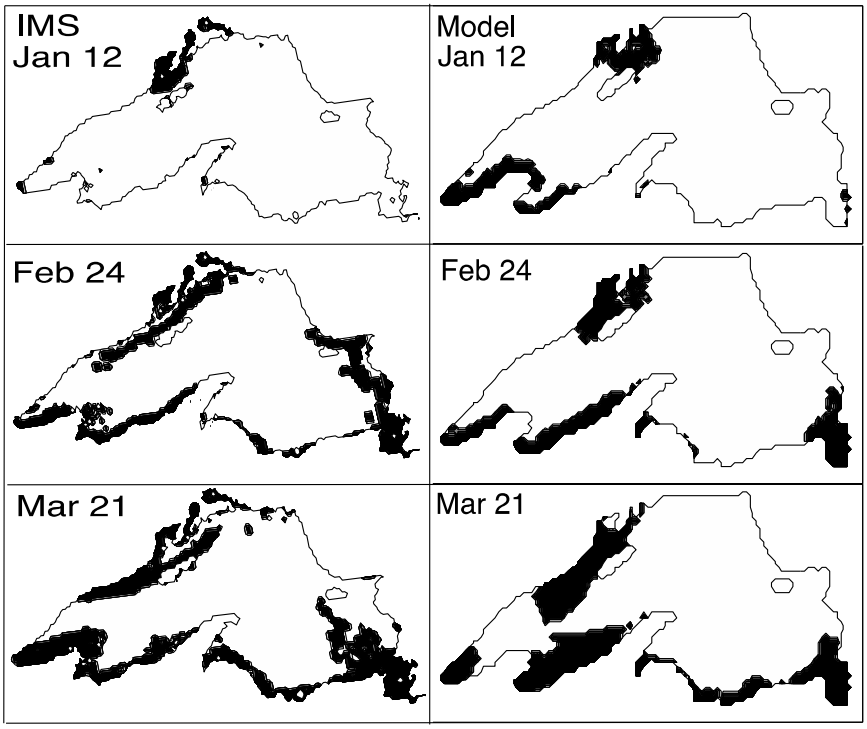

Figure 10. Left: Observed ice cover from the IMS (black) on 12 January, 24 February, and 21 March, 2005. Modeled ice cover (black) on 12 January, 24 February, and 21 March, 2005.

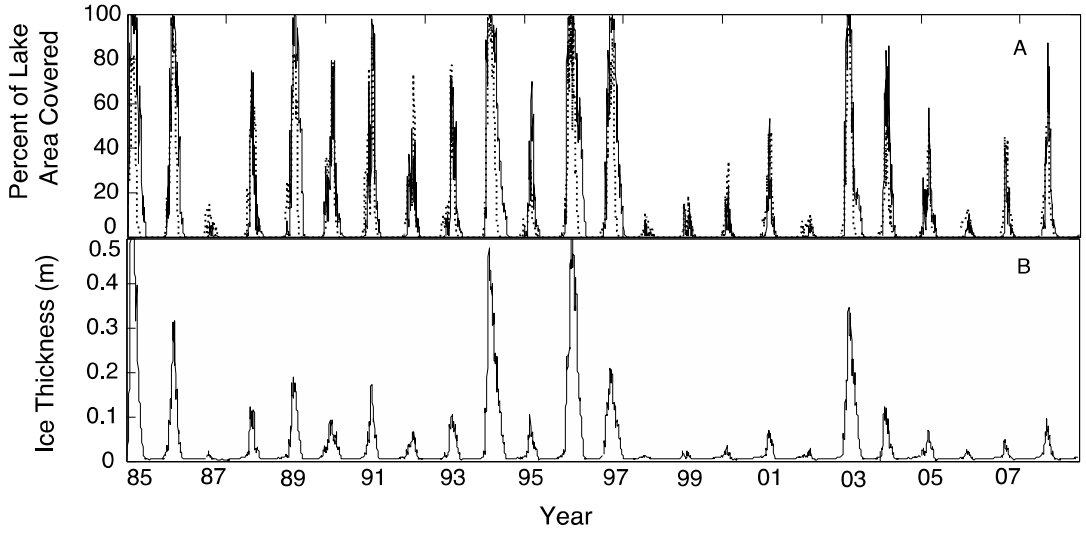

Figure 11. A: The percentage of lake surface area covered by ice for 1985-2008. Model output is shown as a solid line and observations from the NOAA Great Lakes Ice Atlas (1985-2004) and the Multisensor Snow and Ice Mapping System Daily Northern Hemisphere Snow and Ice Analysis at 4km (2005-2008) are shown as dotted lines. B: Domain-averaged ice thickness in meters for 1985-2008.

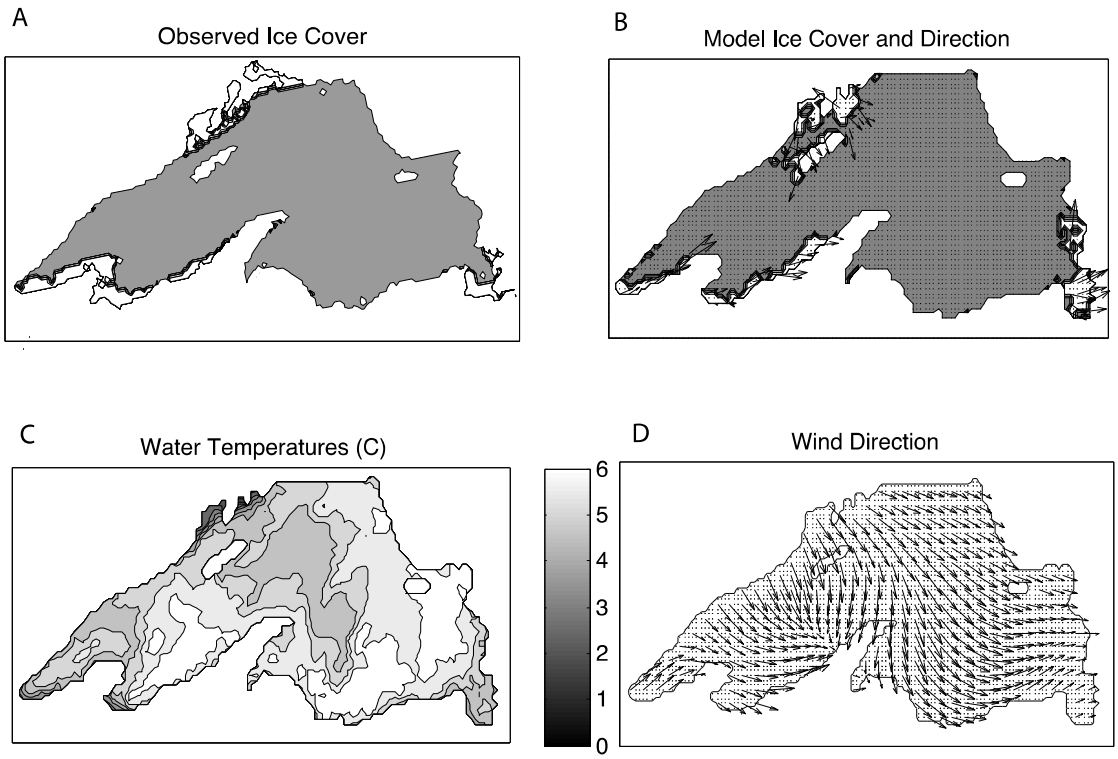

Figure 12. A: An IMS observational map of ice cover for January 26, 2005, B: model map of ice cover for same date with ice momentum vectors, C: Modeled Surface water temperatures, D: Atmospheric boundary condition wind directions.

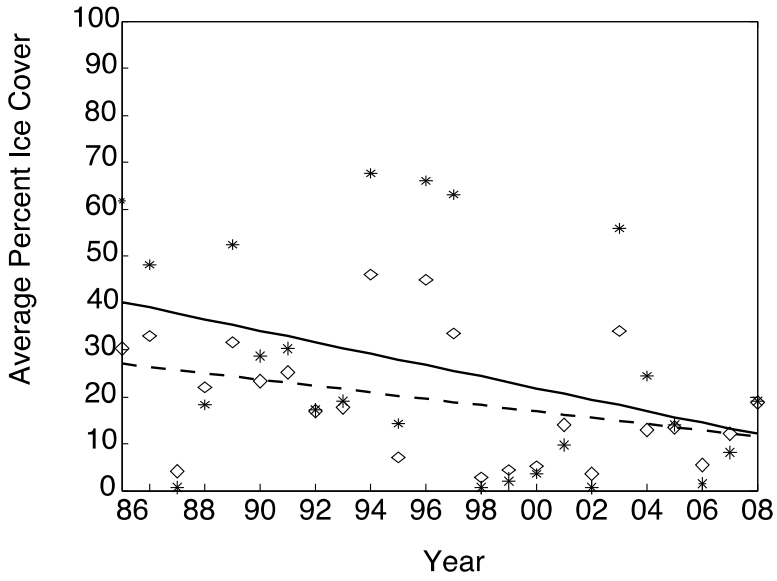

Figure 13. Ice-cover season (Jan–May) averaged percentage of lake surface area covered by ice from 1985 to 2008 for model output (asterisks) and observations (diamonds). Linear fits to model output (solid line) and observations (dashed line).

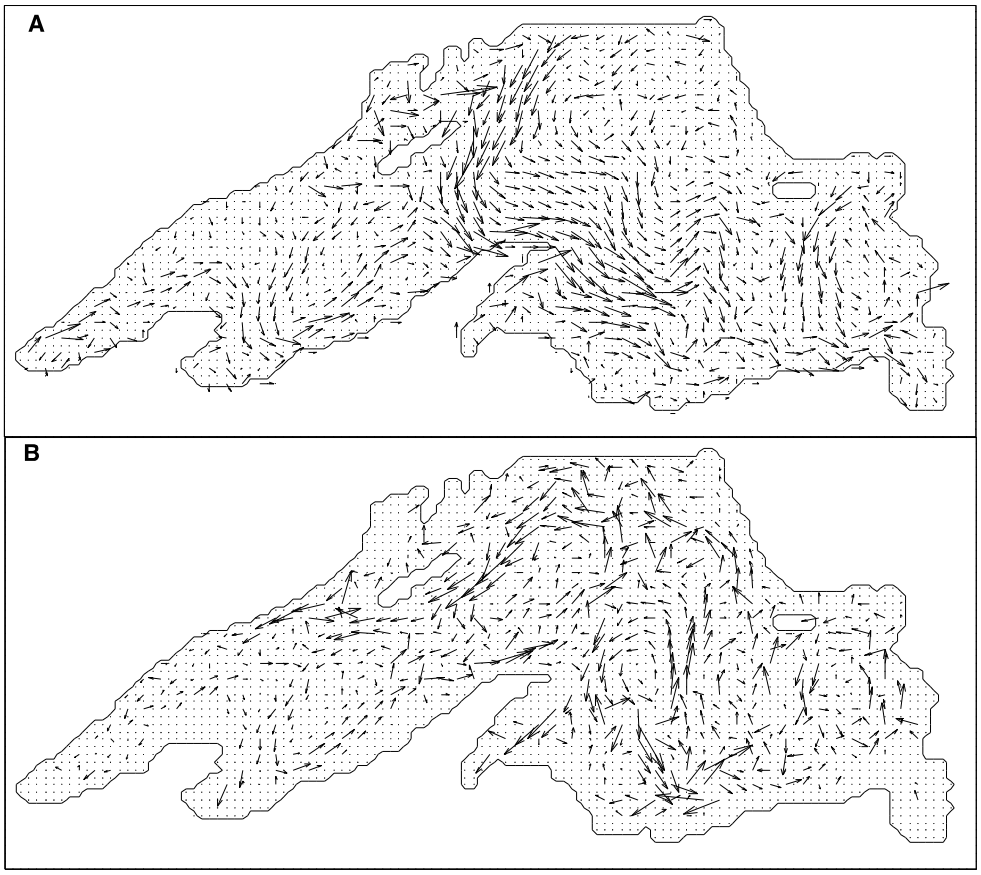

Figure 14. Direction and relative magnitude of annually averaged horizontal currents for 2005 near the surface (<20m, A) and at depth (>75m, B).

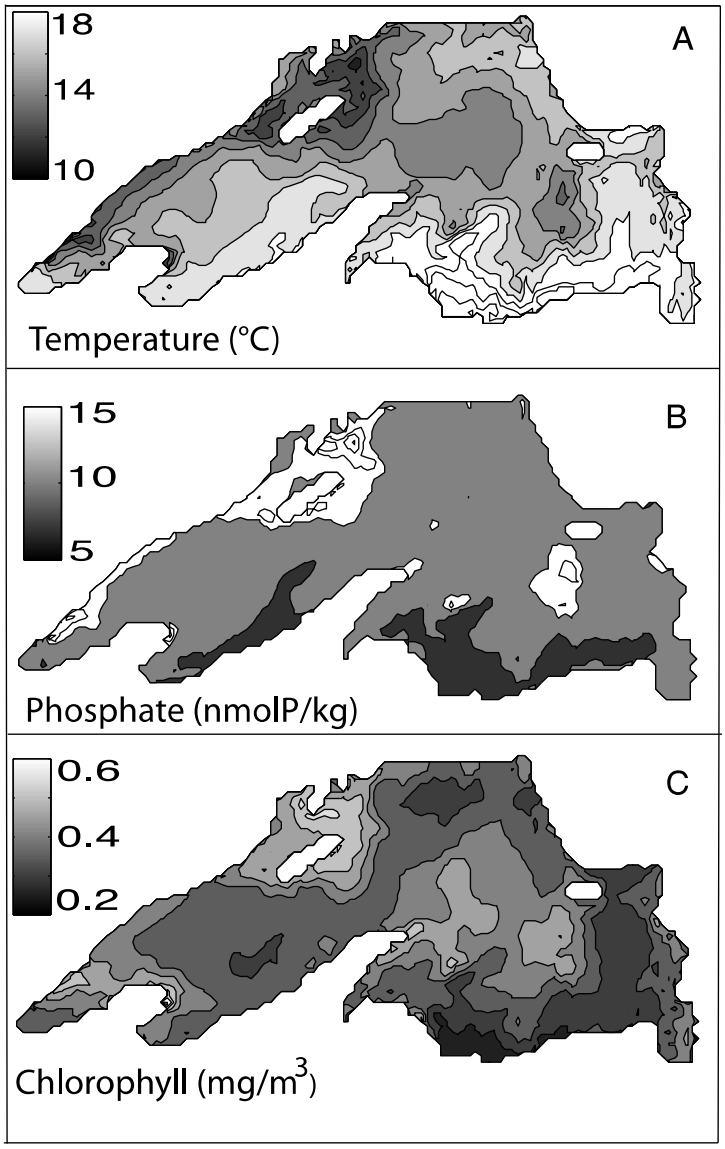

Figure 15. Surface water temperature (A, °C), phosphate concentration (B, nmol/kg), and chlorophyll concentration (C, mg/m^3) from model output, July 23, 2005.

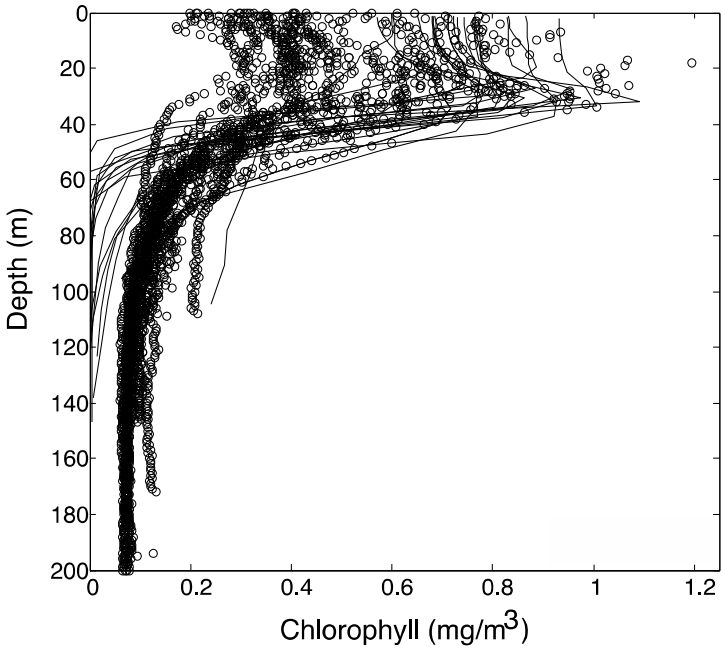

Figure 16. Summertime water column chlorophyll concentrations (mg/m^3) at the 19 EPA station locations from model output (lines) and EPA observations (circles).

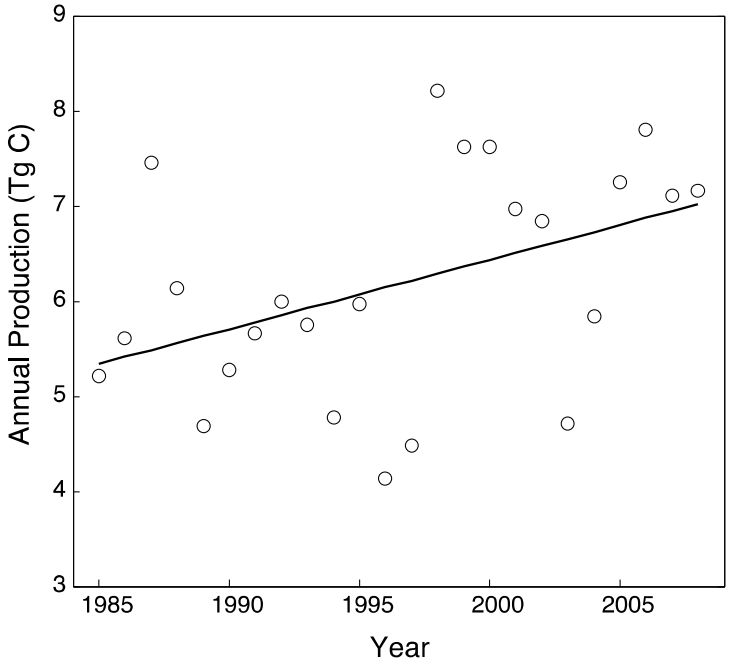

Figure 17. Total annual gross primary production (Tg C/yr) for 1985 to 2008 from model output (circles) with linear fit (solid line).

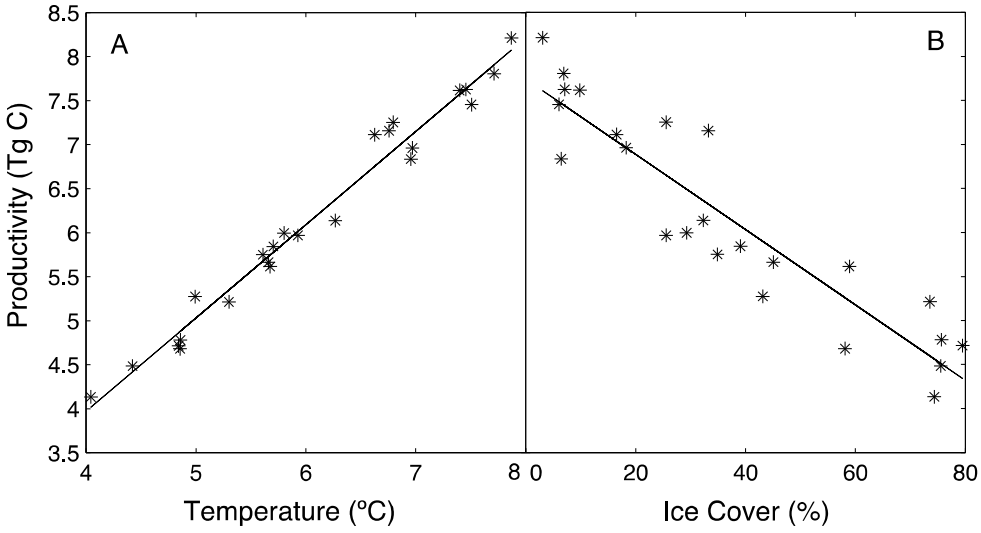

Figure 18. Total annual gross primary productivity (TG C/yr) versus annual average temperature (C) from model output for 1985-2008 (asterisks) and linear fit to the values (line). B: Total annual gross primary productivity versus winter season (Jan-May) average percentage of lake surface area covered by ice (asterisks) and linear fit (line).

Chapter 2

Causal mechanisms of the deep chlorophyll maximum in Lake Superior

This chapter appeared in full as White, B., K. Matsumoto (2012) Causal mechanisms of the deep chlorophyll maximum in Lake Superior: a numerical modeling investigation, Journal of Great Lakes Research, 38:504-513. Reproduced by permission of the Journal of Great Lakes Research.

The presence of a sub-surface chlorophyll maximum is a pervasive phenomenon in both marine and lacustrine waters (Barbiero and Tuchman, 2001, Cullen, 1982, Fennel and Boss, 2003, Riley, 1949). It is frequently present in relatively clear waters in stably stratified regions of the ocean and lakes. Indeed, a 1998 survey by Barbiero and Tuchman (2001) verified the existence of a deep chlorophyll layer in all five of the Great Lakes in August though the deep chlorophyll maximum (DCM) characteristics and spatial distribution varied from lake to lake. The DCM was noted as being the most pronounced and spatially widespread in Lake Superior.

Studies of the summertime DCM in the Great Lakes began more than half a century ago (Putnam and Olson, 1966). Early documentation of the distribution of chlorophyll in Lake Superior include several studies that report the existence of a DCM between 20 and 35 meters depth during the stratified season (Olson and Odlaug, 1966, Watson et al., 1975, Moll and Stoermer, 1982). More recent studies have provided a more thorough (both spatially and temporally) picture of the deep chlorophyll maximum in Lake Superior.

In 1979 Fahnenstiel and Glime (1983) monitored the vertical chlorophyll distribution in Lake Superior. They found that with the onset of thermal stratification (mid-July), the epilimnetic chlorophyll concentration remained near springtime values while a deep chlorophyll maximum developed rapidly near 20 meters depth with chlorophyll levels triple those present in the spring. An increase in subsurface phytoplankton biomass near the depth of the DCM was noted as well as an increase in productivity associated with the DCM.

Barbiero and Tuchman (2004) provide an interannual perspective on the DCM in Lake Superior. In a survey of summertime vertical chlorophyll distribution at 19 offshore sites in Lake Superior from 1996 to 2001, they find a deep chlorophyll maximum in nearly all locations and times further emphasizing the ubiquity of the DCM in summertime Lake Superior. A significant finding of lowered seston carbon to phosphorus ratios in the DCM by Barbiero and Tuchman suggests either greater nutrient availability or possible photoadaptation of the phytoplankton community in the DCM.

Sterner (2010) provides the most recent published information on the phytoplankton community and primary productivity in Lake Superior. In contrast to Fahnenstiel and Glime (1983), Sterner finds peak productivity at a significantly shallower depth than the DCM. Sterner does, however, note a maximum in particulate organic carbon near the DCM depth

Despite the fairly thorough information regarding the characteristics of the DCM in marine and lacustrine environments, the biological and physical mechanisms driving its creation and maintenance are not always well understood. Indeed, a number of

processes have been hypothesized as the causal mechanisms. Cullen (1982) suggests that a deep chlorophyll maximum is caused by different mechanisms in physically differing aquatic environments. Factors affecting the vertical distribution of chlorophyll include depth differential zooplankton grazing, sinking and passive accumulation of phytoplankton due to density-dependent sinking rates, changes in phytoplankton chlorophyll to carbon ratios due to photoadaptation, phytoplankton photoinhibition, supply of nutrients from deep nutrient-rich waters to the photic zone through diffusive processes and sub-surface aggregation of motile phytoplankton to avoid predation (Cullen, 1982, Fasham et al., 1985, Pilati and Wurtsbaugh, 2003, Fennel and Boss, 2003).

In Lake Superior, several of these factors have been hypothesized to contribute to the formation of the DCM. Olson and Odlaug (1966) proposed depth differential grazing of phytoplankton by zooplankton as a factor. They measure zooplankton abundances that are five to ten times greater in the epilimnion than at depth. Based upon this measurement, they conclude that depth differential zooplankton grazing pressure drives the formation of the DCM. Fahnenstiel and Glime (1983) and Sterner (2010) also suggest that it's probable that zooplankton grazing is affecting the vertical chlorophyll distribution in Lake Superior though no further direct evidence is offered.

Both *in situ* production and density-dependent phytoplankton sinking have been suggested to play a role in Lake Superior's DCM. Fahnenstiel and Glime (1983) report production to biomass ratios in the DCM that are comparable to epilimnetic values and conclude that *in situ* growth is the primary determinant in DCM formation with zooplankton grazing as a possible secondary factor. Watson et al. (1975) measured

phaeophytin content, ATP and ^{14}C incorporation into the sub-surface biomass and found that the deep-living algae were viable. However, due to the DCM's proximity to the one percent light level, they determined that *in situ* growth was unlikely to cause the creation of the DCM and instead proposed passive sinking and accumulation of phytoplankton to a density gradient at the DCM depth as the likely mechanism of DCM formation.

More recently, photoadaptation has arisen as a possible contributor to DCM formation. The studies of Barbiero and Tuchman (2001, 2004) and Sterner (2010) cite photoadaptation as a possible factor in DCM formation. Barbiero and Tuchman (2004) find carbon to phosphorus (C:P) ratios in the DCM that are consistently lower than in the epilimnion. They speculate that this could be due to either light limitation of the phytoplankton at depth or to increased availability of nutrients to phytoplankton in the DCM. In support of low C:P ratios at depth reflecting increased phytoplankton access to nutrients, Barbiero and Tuchman (2004) note that they did observe an expected correlation in the interannual variability of the magnitude of the DCM and length of the stratified period and surface water temperatures. This may reflect a connection between stronger nutrient limitation in surface waters and differences in biomass near the surface and at depth. Sterner (2010) suggests that while photoadaptation may be at work in the formation of Lake Superior's DCM, an increase in seston POC near the DCM depth belies photoadaptation as the only operating mechanism. The disparate depths of the DCM and maximum primary productivity found in this modern study leads Sterner to suggest grazing and other phytoplankton losses may play an important role.

Finally, photoinhibition may cause a near-surface minimum in production in Lake Superior and hence affect chlorophyll distributions. Nalewajko and Voltolina (1986) found that photoinhibition in Lake Superior phytoplankton occurred at light intensities as low as 100 $\mu E\ m^{-2}\ s^{-1}$. Zhou et al. (2001) estimated that, if photoinhibition begins at 120 $W\ m^{-2}$, it may extend up to 6-13 meters from the surface based on an extinction coefficient of 0.1-0.2 m^{-1}.

As discussed above, four distinct factors have been proposed as affecting the chlorophyll distribution of Lake Superior: 1) depth differential zooplankton grazing pressure on phytoplankton, 2) sinking and passive accumulation of phytoplankton due to density-dependent sinking rates, 3) photoinhibition of phytoplankton, and 4) photoadaptation of phytoplankton via a dynamic chlorophyll to carbon ratio. However, to date, observational studies have been unable to clarify the controlling mechanisms of DCM formation in Lake Superior. Numerical modeling provides the opportunity to more closely examine these four mechanisms. In this study I use a three-dimensional hydrodynamic model of Lake Superior coupled to a biological model. The biological model includes all of the mechanisms. A suite of five model runs is performed. The control run allows all four of the mechanisms to affect the chlorophyll distribution. To understand the effect of each mechanism four sensitivity runs are performed, each controlling for one of the mechanisms as later described. The resulting chlorophyll distributions are compared and the changes caused by controlling for each mechanism are discussed. The role of a nutricline in DCM formation is ascertained by examining the

manifestation of the DCM and nutricline in the control run and through analysis of three model runs with forced nutrient profiles.

Description of model and experimental set up

Physical Model

The model is described and evaluated in White et al. (2012) and consists of a three-dimensional lake circulation model coupled to mechanistic models of ice and biology. The physical model is based on the Regional Oceanic Modeling System (ROMS, Shchepetkin and McWilliams, 2005), a free-surface primitive equation ocean model and is coupled to a dynamic-thermodynamic ice model. ROMS is implemented in Lake Superior using realistic lateral boundaries and bottom topography (Figure 19). I treat Lake Superior as a closed basin without riverine input or output. The horizontal resolution of the model grid is five kilometers. There are twenty vertical levels. ROMS employs a terrain-following vertical coordinate. This allows for increased resolution near the surface of the lake, a highly biologically dynamic region, and yields non-regular vertical spacing. The vertical resolution in the model ranges from less than one meter near the surface to approximately 40 meters at depth. Salinity in the model is set to zero and a freshwater equation of state (Chen and Millero, 1986) is used. The coupled ice model, based on Budgell (2005), is a unique feature of our lake model. The ice model thermodynamics follow Mellor and Kantha (1989) and Häkkinen and Mellor (1992). The

dynamics of the ice model are based on Hunke and Dukowicz (1997) and Hunke (2001). This physical model configuration reproduces the annual thermal cycle of Lake Superior as well as large-scale spatial patterns in water temperature, the annual cycle of ice cover, and interannual trends in both water temperature and ice cover magnitude (White et al., 2012). For the current experiment, I use meteorological forcing data from the year 2005. The 2005 annual cycle is examined in White et al. (2012). The model captures the annual cycle of surface water and the timing of the onset of stratification and the erosion of the thermocline well. The overall thermal structure is well represented by the model though the modeled mixed layer depth tends to be shallower than observed. There was good reproduction of the ice cover magnitude and, because the 2004-2005 ice season was relatively mild, model issues with ice melt timing are avoided. Spatial distribution of ice cover also concurs well with observations.

Biological Model

As described in White et al. (2012), the currency of the biological model is phosphorus, the limiting macronutrient in Lake Superior (Sterner, 2004). The architecture of the model is based on the biological model of Fennel et al. (2006). The six state variables of the biological model are phytoplankton (P) and phytoplankton chlorophyll (Chl), zooplankton (Z), small and large detritus (D_S and D_L) and phosphate (PO_4) all with units of mmolP m^{-3} (boxes, Figure 20). The microbial loop is included implicitly as organic matter remineralization. Sources and sinks for each state variable

are described below (arrows, Figure 20). Biological parameters modified from those given in White et al. (2012) are shown in Table 6.

Phytoplankton varies as a function of phytoplankton growth, phytoplankton mortality, grazing of phytoplankton by zooplankton, coagulation of phytoplankton with small detritus to form large detritus, and sinking of phytoplankton through the water column as

$$\frac{\partial P}{\partial t} = v \cdot P - m_p \cdot P - graz \cdot Z - coag(D_s + P) - s_p \frac{\partial P}{\partial z} \qquad (5)$$

where v is the phytoplankton growth rate, *graz* is the zooplankton grazing rate, m_p is the phytoplankton mortality rate, *coag* is the coagulation parameter for phytoplankton and small detritus, and s_p is the sinking rate for phytoplankton. Phytoplankton originating in the epilimnion sink through the water column and may settle on or experience much slower sinking rates at density gradients causing an accumulation of phytoplankton (Jerlov, 1959, Cullen, 1982). The effect of this phenomenon on DCM formation is included in the ecological model using varying sinking rates. Due to water density being determined largely by temperature in freshwater Lake Superior, density-dependent phytoplankton sinking is accounted for by decreasing the sinking rate of phytoplankton in water with temperatures less than 6°C. The sinking rate of organic matter can be difficult to constrain. Fennel et al. (2006), in a modeling study of the North Atlantic, quote an organic matter sinking rate range of 0.008-25 m d^{-1} based upon values culled from the literature. Chen et al. (2002) use a value of 0.3 m d^{-1} in their model of Lake Michigan and give a possible range of 0.01-3 m d^{-1}. Chai and Urban (2004) use the water column

residence time of lead and polonium radionuclides in Lake Superior to estimate an average sinking rate of 0.5 m d^{-1}. I use a value of 0.3 m d^{-1} for the general sinking rate. I allow the sinking rate to decrease to 0.01 m d^{-1} in waters with temperatures less than six degrees Celsius in order to emphasize the role of density dependent sinking rates in the formation of the DCM. Phytoplankton and small detritus may coagulate and join the large detritus pool, which has a greater sinking rate. The phytoplankton growth rate is itself a function of temperature, nutrient concentration and light given by

$$v = e^{k_T T} \cdot \frac{PO_4}{k_{PO_4} + PO_4} \cdot f(I) \quad (6)$$

where k_T is the phytoplankton temperature coefficient for the photosynthetic rate and T is the water temperature, k_{PO4} is the half-saturation concentration for uptake of phosphate by phytoplankton, and $f(I)$ is the irradiance function and is described below. Temperature is positively related to the phytoplankton metabolic rate and the temperature dependent term follows the Q_{10} relation (Kishi et al., 2007). The nutrient limitation term is in the form of a Michaelis-Menten function (Michaelis and Menten, 1913) for phosphate.

Photoinhibition is the decline of maximum photosynthesis rates in phytoplankton exposed to greater than optimal irradiance levels (Falkowski et al., 1993). Having too much light can tip the balance between beneficial photosynthetic carbon fixation and light-induced physiological damage to the photosynthetic apparatus in favor of the latter. Therefore, the occurrence of photoinhibition in surface waters can lead to enhanced photosynthesis in the subsurface and thus DCM. To account for photoinhibition I use the photosynthesis-irradiance relation from Platt et al. (1980) defined as

$$f(I) = v_{max}\left(1 - e^{-(\frac{\alpha I}{v_{max}})}\right)e^{-(\frac{\beta I}{v_{\max}})} \quad (7)$$

where v_{max} is the maximum possible photosynthetic rate without photoinhibition (d^{-1}), α is the initial slope of the P-I curve (d^{-1} W^{-1} m^2), β is the photoinhibition parameter (same units as α), and I is the irradiance (W m^{-2}). If β is zero, there is no photoinhibition. As it increases in value, the negativity of the slope of the P-I curve at high irradiances increases. Though Platt et al. (1980) originally devised this formulation based on arctic phytoplankton assemblages, it has also been successfully applied to temperate phytoplankton populations (41°N-45°N, Harrison and Platt, 1985). The median light intensity at which these populations began showing effects of photoinhibition is 131 W m^{-2}. The threshold light intensity for photoinhibition effects is defined as $I_m = v_{max}/\alpha \; ln((\alpha+\beta)/\beta)$ where I_m has units of W m^{-2}. I use a photoinhibition parameter value of 5×10^{-4}. This is in the range observed by Platt et al. and yields a threshold light intensity for photoinhibition effects of 106.1 W m^{-2}.

The irradiance and is attenuated by phytoplankton self-shading and water and is given by

$$I = I_0 \cdot par \cdot e\text{^}\left(-z\left(\kappa_w + \kappa_{chl}\int_z^0 Chl(z)dz\right)\right) \quad (8)$$

where I_0 is the radiation incident at the water surface, κ_w is the attenuation coefficient due to water, κ_{chl} is the attenuation coefficient due to chlorophyll, and *par* is the portion of light available for photosynthesis and is equal to 0.43 (Baker and Frouin,1987).

The time rate of change for chlorophyll is determined by multiplying the phytoplankton equation (Eq. 5) by the chlorophyll to carbon ratio as

$$\frac{\partial Chl}{\partial t} = \rho \cdot v \cdot Chl - graz \cdot Z\frac{Chl}{P} - m_p \quad (9)$$

The ratio of chlorophyll to carbon content in phytoplankton biomass is not constant. Rather it may vary over a range of < 0.01 to >0.1 g g^{-1} (Geider 1987) and it does so dependent upon ambient temperature, nutrient concentration and light in a process termed photoadaptation (Geider et al., 1997). The increased chlorophyll to carbon content ratio of phytoplankton at depth due to low light conditions and relatively greater nutrient availability may contribute to the DCM (Fennel and Boss, 2003). Photoadaptation is incorporated in our model following Geider et al. (1996, 1997) and described by Fennel et al. (2006). In this model, the amount of chlorophyll created is determined by the portion of photosynthate allocated to chlorophyll synthesis as

$$\rho = \theta_{max}\left(\frac{vP}{\alpha IChl}\right) \quad (10)$$

where θ is the phytoplankton chlorophyll to carbon ratio (mgChl mgC^{-1}) and θ_{max} is the maximum value of the chlorophyll to carbon ratio (mgChl mgC^{-1}).

Zooplankton varies as a function of rates of zooplankton grazing on phytoplankton and efficiency of assimilation of the grazed material, basal metabolism excretion rates, assimilation related excretion rates, and zooplankton mortality given by

$$\frac{\partial Z}{\partial t} = graz \cdot \phi \cdot Z - E_m \cdot Z - E_{eg}\left(\frac{P^2}{k_p + P^2}\right)\phi \cdot Z - m_z \cdot Z^2 \quad (11)$$

where ϕ is the assimilation efficiency. Zooplankton grazing rates are characterized by a Holling-type s-shaped curve (Holling 1959, 1962, 1965), defined as

$$graz = graz_m \cdot \frac{P^2}{k_p + P^2} \quad (12)$$

where $graz_m$ is the maximum grazing rate and k_p is the zooplankton half saturation for consumption of phytoplankton. It has been proposed that zooplankton grazing may be greatest at the depth of peak primary production (Longhurst, 1976, Herman 1981). If the depth of peak primary production lies above the DCM, as Sterner (2010) reports in Lake Superior, then heavier grazing of phytoplankton by zooplankton near the surface may help maintain the upper margin of the deep chlorophyll maximum by limiting phytoplankton concentrations in the surface waters. Fennel et al. (2006) give a range of values of 0.5-1.0 d^{-1} for this parameter. Chen et al. (2002) give a range of 0.1-0.86 d^{-1} for the maximum zooplankton grazing rate in Lake Michigan. Seegers (2009) found a mean overall grazing rate of 0.19 d^{-1} and a mean summertime epilimnion rate of 0.32 d^{-1} in Lake Superior with a maximum measured value of 0.41 d^{-1}. Based upon these values from the literature a maximum grazing rate, $graz_m$, of 0.6 d^{-1} is used in the model.

Two size classes of detritus are represented in the model. The small detritus sources are material not assimilated by zooplankton during grazing and mortality losses of zooplankton and phytoplankton. Small detritus losses are coagulation with phytoplankton and subsequent inclusion in the large detritus pool, remineralization and sinking given by

$$\frac{\partial D_s}{\partial t} = graz(1-\phi)Z + m_z \cdot Z^2 + m_p \cdot P - coag(D_s + P)D_s - r_s \cdot D_s - s_s \frac{\partial D_s}{\partial z} \quad (13)$$

The small class sinks at a slower rate and represents both the dissolved organic phosphorus pool and minute slowly sinking particulates. Both classes of detritus are subject to horizontal advection, and so the limited sinking rates, especially for the small

detritus, allow for a horizontal transport over the full depth of the water column (Gruber et al., 2006).

Sources of large detritus include coagulation of phytoplankton and small detritus. Losses include remineralization and sinking given by

$$\frac{\partial D_L}{\partial t} = coag(D_s + P)^2 - r_L \cdot D_L - s_L \frac{\partial D_L}{\partial z} \quad (14)$$

Remineralized detritus enters the phosphate pool. Upon reaching the bottom boundary, both detritus and phytoplankton are remineralized.

The phosphate pool varies as a function of uptake by phytoplankton, assimilation- and metabolic-related excretion by zooplankton, and remineralization of detritus given by

$$\frac{\partial PO_4}{\partial t} = -v \cdot P + E_m \cdot Z + E_{eg}\left(\frac{P^2}{k_p + P^2}\right)\phi \cdot Z + r_s \cdot D_s + r_L \cdot D_L \quad (15)$$

Some aspects of Lake Superior biogeochemistry are rather unique and are reflected in our model. The seston carbon to phosphorus ratio (C:P) is consistently much higher in Lake Superior than the typical Redfield ratio of 106:1 (Sterner, pers. comm., 2010, Barbiero and Tuchman, 2004). The seston C:P value is frequently used as an indicator of the nutrient limitation status of phytoplankton (Sterner, 2011). I use a value of 200:1, the mean seston C:P ratio observed at the depth of greatest biomass in the summer (Barbiero and Tuchman, 2004), for the C:P ratio of phytoplankton in our model. This is similar to values used in other models of Lake Superior (Bennington, 2010) and to the C:P uptake ratio given by Urban et al. (2009b). The half saturation concentration of phosphate uptake by phytoplankton used in the model (0.05 mmolP m^{-3}) reflects the very low phosphate concentrations in Lake Superior and the dominance of picoplankton in the Lake Superior phytoplankton community (Fahnenstiel et al., 1986, Sterner, 2010).

Similar values are used in models of Lake Michigan (Chen et al., 2002) and Lake Huron (Bierman and Dolan, 1981). Remineralization rates are set at the high end of ranges in the literature (Leonard et al., 1999) to represent the rapid recycling of nutrients in the Lake Superior water column. These and other initialization and parameter values for the model were chosen in reference to the literature, originally presented in White et al. (2012), and updated values used in this model implementation are given in Table 6.

In previous experiments (White et al., 2012), this biological model configuration simulated annual gross primary production of 4-8 TgC yr^{-1} over the period 1985 to 2008. These are within the range of values estimated from observations of (2.0-9.73 TgC yr^{-1}, Cotner et al., 2004, Urban et al., 2005, and Sterner et al., 2010).

Atmospheric Forcing and Initialization

The model is forced using meteorological data from the Lake Superior basin with a three-hour time resolution. The forcing is based upon interpolated data from National Oceanic and Atmospheric Administration (NOAA) National Data Buoy Center (NDBC) buoys in open-lake locations and Coastal Marine Automated Network (CMAN) stations. Data from these sites includes air temperature and wind speed and direction. Further description of the atmospheric forcing data including calculation of downward and upward shortwave and longwave radiation is given in White et al. (2012).

The physical model is initialized with a water temperature of four degrees Celsius, no water momentum, uniform surface topography, and no ice on 1 January 1985.

The physical model is spun up for 20 years using atmospheric forcing data for the period 1985-2005 to permit the model to achieve a steady annual cycle. The biological state variables are initialized at the beginning of 2005 to values given in White et al. (2012). The same 2005 annual forcing is then applied again to complete the model run for analysis.

Experimental Set-Up

I use a suite of eight model runs to explore the influence of several processes on the vertical distribution of chlorophyll in Lake Superior (Table 7). The first run is the 'control' run, which has all four potential processes of photoinhibition, density-dependent phytoplankton sinking, photoadaptation, and differential grazing of phytoplankton by zooplankton.

The next four runs are sensitivity experiments, which include three of the processes in their fully functional, time and space varying forms while the influence of the fourth process is eliminated. In the 'constant sinking' sensitivity experiment, the effects of density-dependent phytoplankton sinking are controlled for. Whereas phytoplankton sinking depends on the water density and becomes slower in waters with temperatures less than 6° C in the control run, the rate of sinking is maintained at a fixed rate in the sensitivity run. In the 'no photoinhibition' sensitivity experiment, the effects of photoinhibition are controlled by setting the photoinhibition parameter β to zero (Eq. 7).

In the ‘constant Chl:C’ sensitivity experiment, the effects of photoadaptation are controlled for. Whereas the chlorophyll to carbon (Chl:C) ratio of phytoplankton depends on nutrient concentration, light availability, and temperature (Eqs. 10 and 6) in the control run, the Chl:C ratio is held constant at a value of 0.0283 mgChl mgC^{-1} in the sensitivity run. This value is within Chl:C ratio ranges given in the literature. For example, Geider et al. (1997), using observations of fifteen algal and cyanobacterial species, estimate a maximum Chl:C ratio range of 0.005-0.072 mgChl mgC^{-1}. Chen et al. (2002), in a modeling study of Lake Michigan, give a range of 0.0127-0.0435 mgChl mgC^{-1} for the Chl:C ratio of phytoplankton and use a value of 0.0286 mgChl mgC^{-1}.

In the ‘constant zooplankton’ sensitivity experiment, the effects of depth-differential zooplankton grazing are controlled for. In the control run, the zooplankton concentration can vary with time and space, allowing for the development of spatially variable zooplankton concentrations and thus the possibility of depth differential zooplankton grazing pressure. In this sensitivity run, I hold the zooplankton concentration constant to the initialization value in time and space. Zooplankton grazing pressure is maintained as a sink of phytoplankton but this material is immediately sent to the dissolved phosphate and small detritus pools rather than being added to the zooplankton pool. The processes that normally serve as sinks from the zooplankton pool (mortality and excretion) are disabled as well thus holding the zooplankton concentration constant.

In the next three model runs, I nudge or restore the internal phosphate concentration to target vertical profiles in order to decouple the nutricline from the

thermocline and to examine just the influence of the nutricline on the DCM. The three target profiles have nutricline at depths of 20 m, 40 m, and 60 m (Table 7, 20m Nutricline, 40m Nutricline, 60m Nutricline). In the absence of such targets, the model will simulate the location of the nutricline based on nutrient transport and biogeochemical source and sink terms. Internal restoring essentially creates artificial sources and sinks of phosphate so that the simulated phosphate concentration approaches the target profiles. I use a nudging time scale of 5 days. Because the restoring is not instantaneous, the resulting nutricline does not coincide exactly with the targeted profiles but represents a balance between the target profile and where the model nutricline would exist without restoring.

Results and discussion

Comparison of Model Output and Observations

The resulting chlorophyll and temperature distributions from the control run are compared with observed vertical chlorophyll concentration and temperature profiles from the EPA. Figure 21 illustrates the typical comparison. The observed chlorophyll concentrations were measured using a Seabird SBE-911 CTD with fluorometer at 16 offshore sites (hereafter, 'sites') spread throughout Lake Superior (site locations in Figure 19) as part of the Environmental Protection Agency's (EPA) Great Lakes National Program Office (GLNPO) monitoring program. Nineteen sites are usually monitored in

this program but chlorophyll data from sites 6, 9 and 11 were unavailable for the summer of 2005. Temperature was also measured using the CTD unit. The data were accessed from the Great Lakes Environmental Database (GLENDA). Measurements were taken between 23 September 2005 and 2 October 2005. The vertical sampling frequency for the data is one meter. The model chlorophyll concentration and temperature profiles were taken at the model grid point closest to each corresponding measurement site. The model output profiles, therefore, represent a 5 km^2 grid cell rather than the exact location of the EPA measurement. The vertical resolution of the model at the site locations ranges from one to five meters in the upper 15 meters of the water column (encompassing the surface mixed layer) and from one to seven meters in the upper 40 meters of the water column (encompassing typical depths of the DCM).

The overall magnitude of the DCM in the model compares well with observations (Figure 21). A deep chlorophyll maximum is present in 12 of 16 sites for the observations and in 14 in the model. A DCM is not present in the model in locations where thermal stratification is lacking. The maximum observed chlorophyll concentration is 1.20 mgChl m^{-3} and the equivalent model value is 1.36 mgChl m^{-3}. The mean observed maximum chlorophyll concentration among the sites is 0.78 mgChl m^{-3} compared to the equivalent model value of 0.85 mgChl m^{-3}. The model shows similar variability of maximum chlorophyll concentration among the sites with a standard deviation of 0.18 mgChl m^{-3} compared to a standard deviation of 0.19 mgChl m^{-3} for the observations. The mean depth of the DCM is 28.4 meters in the observations and 31.9 meters in the model. The depth of the DCM in both model and observations displayed a

wide range with standard deviations of 9.3 and 9.9 meters, respectively. The root mean square error (RMSE), defined as

$$RMSE = \sqrt{\frac{\sum_{i=1}^{N}(x_i - y_i)^2}{N}}, \quad (16)$$

where x is the modeled value, y is the observed value and N is the number of values, is used to assess the absolute error of the modeled chlorophyll concentration and temperature profiles compared to the observed for each of the 16 sites with data. The average RMSE for chlorophyll concentration is 0.15 mgChl m^{-3} and for temperature is 2.87°C. The RMSE values are given for each site in Table 8. Much of the temperature error is due to the relative shallowness of the modeled mixed layer depth. This model issue has been noted in other Great Lakes and ocean modeling studies and is likely due to the lack of inclusion of wind-wave mixing in the model as discussed in White et al. (2012). A portion of the chlorophyll error is due to the relatively low modeled chlorophyll concentrations at depths greater than 80 meters, well below the depth of the DCM. This is largely because of the necessity of remineralizing all sinking organic matter that reaches the lowest grid level in the model due to a lack of use of a sediment model and should not have a consequential impact on the DCM.

Zooplankton concentrations and grazing pressure of zooplankton on phytoplankton in the control run are greatest above the DCM throughout the stratified season and across the lake. Maximum modeled zooplankton concentrations are located above the DCM and frequently coincident with the upper margin of the DCM (Figure 22). Zooplankton concentrations on 23 September 2005 at the 19 EPA sites range from

2.66-25.8 μgC l^{-1}. The zooplankton concentration range in the epilimnion is 4.68-25.8 μgC l^{-1} with a mean concentration of 8.87 μgC l^{-1} (Figure 22). In the hypolimnion the range is 2.66-5.71 μgC l^{-1} with a mean of 3.24. The ratio of zooplankton concentration above the DCM to below the DCM varies from 1.76-9.70 with an average of 2.74. The upper end of the modeled range concurs with reports by Olson and Odlaug (1966) and Fahnenstiel and Glime (1983) that zooplankton abundances in the epilimnion were 5-10 times greater in the epilimnion than at depth though the average model value is smaller. Zooplankton grazing rates in the model range from 0.19-0.59 d^{-1} with a mean of 0.25 d^{-1} above the DCM. At depth they are 0.03-0.1 d^{-1} (mean, 0.06 d^{-1}) and the ratio of above DCM to at depth grazing rates is 3.49-18.2 (mean, 6.46). These zooplankton grazing rates compare well with those measured in a recent survey by Seegers (2009), who reports average summertime epilimnion and hypolimnion grazing rates of 0.32 d^{-1} and 0.13 d^{-1}, respectively. A factor not included in the model is diurnal vertical migration by zooplankton. This may be an important behavior among deep-dwelling calanoid communities (Barbiero and Tuchman, 2004) and nocturnal predation at the depth of the DCM by these populations may play an important role in ecosystem dynamics. Further modeling studies including a class of zooplankton with migratory behavior can help to elucidate the role of these zooplankton in determining vertical chlorophyll distributions.

Contribution of Processes to Deep Chlorophyll Maximum

In order to evaluate the impact of density-dependent phytoplankton sinking, photoinhibition, photoadaptation and depth-differential zooplankton grazing, I compare the resulting vertical chlorophyll concentration distribution from the four sensitivity runs to that of the control run both across the lake and over the summertime stratified period.

Figure 23 shows vertical chlorophyll concentration profiles at three sites from eastern, central and western Lake Superior on 23 September 2005 for each of the five model runs. These locations (sites 1, 6, 14) are widely distributed throughout the lake and chose to show typical characteristics of the sensitivity runs. A deep chlorophyll maximum is evident at nearly every site in the control run (solid line). The most interesting sensitivity run is that which controls for photoadaptation (Figure 23, crosses). The resulting vertical chlorophyll distribution is distinctly different from that of the control run in terms of both the depth and magnitude of the DCM. The magnitude of the DCM is decreased, on average, by a factor of approximately 3.5 in the constant Chl:C run. Without photoadaptation, peak chlorophyll concentrations are significantly closer to the surface in the constant Chl:C run. In the control run the DCM and the depth of greatest phytoplankton biomass are vertically separated. However, in the constant Chl:C run, they are located at the same depth, and the shallower DCM is simply a reflection of an increase in phytoplankton biomass (Figure 24). Photoadaptation of phytoplankton thus plays in important role in dictating the depth of the DCM in the model Lake Superior. Fennel et al. (2007), similarly, found that vertical separation of deep chlorophyll and deep carbon maxima in a lake was a sign of phytoplankton photoadaptation and that this process determined the depth of the DCM in the water column. Seegers (2009) measured

a difference in the depths of the chlorophyll and carbon maxima in Lake Superior and noted this as a likely indicator of the role of photoadaptation in the formation of the DCM. Likewise, Barbiero and Tuchman (2004) named photoadaptation as a likely mechanism of DCM formation in Lake Superior based, in part, on their observation of relatively higher chlorophyll to carbon ratios at the DCM depth compared to the epilimnion.

In order to illustrate the average difference in vertical chlorophyll distribution between the sensitivity experiments and the control run over the summer stratified period, spatially averaged RMSE is calculated (Figure 25). First, the RMSE is calculated for the sensitivity run chlorophyll profile compared to the control run chlorophyll profile at the 19 sites for the months of July through September 2005. These are then averaged to obtain the average RMSE shown in Figure 25. The error is greatest (i.e., the expected DCM is least realized) in the constant Chl:C run. This means that photoadaptation, out of the four biological processes tested, has the strongest impact on the vertical chlorophyll distribution and that this impact varies little over the summer.

The other two sensitivity model runs showing a significant change in vertical chlorophyll distribution are the run in which zooplankton grazing was controlled for by holding the zooplankton population constant (Figure 23, dashed line) and the run in which density-dependent particle sinking is controlled for (Figure 23, dots). In the constant sinking run results, a DCM remains in all locations where one was present in the control run. However, in 12 of the 16 locations the magnitude of the DCM is decreased. The maximum decrease seen in DCM amplitude is 0.3 mgChl m^{-3} though the average is

only 0.07 mgChl m^{-3}. This decrease in the DCM magnitude is associated with a decrease in the actual phytoplankton biomass at the DCM depth, indicating that density-dependent phytoplankton sinking may help maintain the DCM via an increase in phytoplankton biomass at the depth of the DCM but that it is not a key factor in the formation of the DCM.

In the constant zooplankton run chlorophyll concentrations in the DCM tend to be lower in comparison with the control run (Figure 23, dashed line). However, in locations where a DCM was present in the control run, there is still a DCM in the constant zooplankton run. This suggests that zooplankton grazing rates in the control run were lower near the DCM than in the constant zooplankton run and that lower zooplankton grazing rates at the depth of the DCM may contribute to maintenance of the DCM. The impact of zooplankton grazing in the model, however, is likely underestimated. Actual impacts of zooplankton grazing may be greater considering that zooplankton concentrations in the model are similar to reported average summertime non-crustacean zooplankton concentrations (6-10 μgC $l^{-1,}$ Fahnenstiel et al. [1998]) but lower than the combined concentrations of non-crustacean and crustacean average summertime zooplankton (28 μgC l^{-1}, Fahnenstiel [1998]) in Lake Superior. Also, diurnal vertical migration of zooplankton such as the deep-dwelling calanoid population is not accounted for in model and may affect chlorophyll concentrations in Lake Superior and thus the DCM. The sensitivity run in which photoinhibition is controlled for shows minimum impact on the DCM. The vertical chlorophyll concentration profile for the no

photoinhibition run is virtually indistinguishable from the control run profile (Fig. 23, dotted line).

Our results thus indicate that density dependent sinking and depth differential zooplankton grazing affect the chlorophyll distribution but that neither they nor photoinhibition play primary roles in the formation of the DCM. This is consistent with Zhou et al. (2001), who measured temperature, chlorophyll fluorescence, and zooplankton concentrations along a transect in the eastern arm of Lake Superior, and noted that while zooplankton grazing and photoinhibition may affect chlorophyll distributions, they were insufficient as factors to completely explain the large scale patterns of chlorophyll concentration.

The Role of the Nutricline

Unlike the sensitivity experiments shown in figure 23, there is no simple way in the model to isolate the impact of just the nutrient distribution on the DCM, as it is intimately tied to stratification and circulation, which obviously significantly affect chlorophyll distribution. Therefore, I assess the role of the nutricline by examining how it manifests in relation to other properties in the control run and by analyzing model runs with forced nutrient profiles. Figure 26 shows the spatial distribution of the magnitude of the DCM and of the nutricline in the control run on 4 August 2005. The magnitude of the DCM is calculated as the maximum chlorophyll concentration in the water column minus the surface chlorophyll concentration. The magnitude of the nutricline is calculated as

the phosphate concentration at depth minus the phosphate concentration at the surface. There is large scale spatial coherence between the strength of the DCM and the nutricline. The distribution of the nutricline also closely mirrors the surface water temperature distribution (not shown) with greater nutricline magnitude in regions of warmer temperatures. Figure 26 demonstrates that the lateral distribution of the DCM magnitude resembles that of the nutricline though it shows greater spatial variability at smaller scales. This suggests that the nutricline and DCM are associated but that the nutricline alone does not entirely dictate the presence and characteristics of the DCM.

The correlation of the magnitudes of the DCM and nutricline remains across the lake and throughout the stratified season. Figure 27a plots the magnitude of the DCM against the magnitude of the nutricline at the nineteen EPA monitoring sites every week from 25 July 2005 to 22 August 2005. The correlation (given in Figure 27a) increases over time. The DCM and nutricline depths are also correlated (Figure 27B, solid line is one to one). Based upon a p-value of < 0.05, the correlations of the magnitude and depth of the DCM and nutricline are statistically significant across the lake and over the summer stratified period.

Model runs with forced nutrient profiles show that the DCM depth is, in part, controlled by the depth of the nutricline. Figure 28, panel A, presents the depth of the DCM compared with the depth of the nutricline on 4 August 2005 for the three forced nutrient profile runs. The DCM depth in the 20m and 40m Nutricline runs lie mostly under the one-to-one line showing that the DCM is located slightly deeper than the nutricline. The tight clustering indicates a strong relationship between the nutricline and

DCM depths. In the 60m Nutricline run the average depth of the DCM still tracks the nutricline depth though the spread of the DCM depths is markedly greater than in the 20m or 40m Nutricline runs. Here, the DCM is occupying a depth where light limitation strongly effects the manifestation of the DCM. At the onset of stratification in July, the average depth of DCM and nutricline coincide in the 60m Nutricline run. As light levels decrease in August and September, the DCM shoals, becoming significantly shallower than the forced depth of the nutricline (Figure 29). Figure 28, panel B, shows that there is not a similar relationship between the depth of the thermocline and the DCM depth in the forced nutrient profile runs. However, as a nutricline is only present with thermal stratification in the model, thermal stratification is clearly a necessary condition for the existence of the DCM.

Conclusions

A deep chlorophyll maximum is a near-ubiquitous biological phenomenon in the summertime stratified waters of Lake Superior. The DCM in Lake Superior has been studied for over a half century but the mechanisms driving its formation and maintenance have remained unclear. Proposed mechanisms affecting the vertical distribution of chlorophyll in Lake Superior include depth differential zooplankton grazing pressure on phytoplankton, sinking and passive accumulation of phytoplankton due to density-dependent sinking rates, photoinhibition of phytoplankton, and photoadaptation of phytoplankton via a dynamic chlorophyll to carbon ratio I use a 3-dimensional

hydrodynamic model of Lake Superior coupled to an ecological model to examine the role of these mechanisms.

Using a set of eight model runs, I determine that the three primary factors contributing to the presence, depth, and magnitude of the DCM in the model are photoadaptation, the presence and characteristics of a nutricline and the presence of thermal stratification. Zooplankton grazing and phytoplankton sinking are found to be secondary contributing factors in the model. Sensitivity runs reveal that photoadaptation plays an important role in determining the depth and magnitude of the DCM. In the control run, the DCM and phytoplankton biomass peak are vertically separated. Controlling for photoadaptation caused the DCM to shift to the shallower depth of the phytoplankton biomass peak. This is consistent with the observations of Barbiero and Tuchman (2004) who proposed photoadaptation as a likely key process in DCM formation based on measurements of increased chlorophyll with little co-occurring increase in particulate organic carbon at the DCM depth.

Density dependent phytoplankton sinking and depth differential zooplankton grazing were of secondary importance and mainly affected the magnitude of the DCM and not its location or presence. Effects of zooplankton grazing in the model may be underestimated due to low zooplankton concentrations compared to observations and due to lack of inclusion of diurnal vertical migration behavior in the model. Similarly, Seegers (2009) found in a focused study on zooplankton grazing in Lake Superior that DCM formation could not be fully explained by grazing pressure despite grazing comprising a substantial loss of primary productivity in the lake and Olson and Odlaug's

(1966) measurement of significantly greater zooplankton concentrations in the epilimnion than at depth. Though Nalewajko and Voltolina (1986) found photoinhibition in Lake Superior phytoplankton communities, controlling for photoinhibition in the model had minimal effect indicating that it is not an important biological process in determining the vertical distribution of chlorophyll.

The magnitude and depth of the nutricline in the model is correlated with the magnitude and depth of the DCM throughout the lake during the summer stratified period. Model runs with forced nutrient profiles show that the depth of the DCM tracks the depth of the nutricline. Barbiero and Tuchman (2004) consistently measured decreased carbon to phosphorus ratios in the DCM as compared to the epilimnion and cite this as evidence of improved nutrient status of the DCM phytoplankton community. They also found a markedly deeper DCM and increased particulate organic carbon concentrations in the DCM in 1998, a very warm year with a significantly extended period of summer stratification. Barbiero and Tuchman note that this may indicate a DCM tracking a deepening nutricline and increased biomass at depth due to increased nutrient supply. Recent studies using increasingly sensitive methods, however, have been unable to measure a distinct vertical nutrient gradient in Lake Superior and very low phosphorus concentrations make these measurements difficult. Consistent presence of thermal stratification in the model prior to the appearance of the DCM indicates that density stratification is a necessary condition for DCM formation.

Table 6. Biological Parameters.

Symbol	Parameter	Units	Value	Reference
κ_w	light attenuation by water	m^{-1}	0.10	Jerome et al. (1983)
κ_{chl}	light attenuation by chlorophyll	$mgChl^{-1}m^{-2}$	0.025	Kirk (1983)
v_{max}	maximum phyt. growth rate	d^{-1}	1.6	Chen et al. (2002)
k_{PO4}	half saturation conc. PO_4 uptake	$mmolP\ m^{-3}$	0.05	Chen et al. (2002)
k_P	half-saturation conc. phyt. uptake	$(mmol\ P\ m^{-3})^2$	0.045	Bennington (2010)
Θ_m	maximum chl. to phyt. ratio	$mgChl\ mgC^{-1}$	0.0535	Geider et al. (1997)
α	P-I curve initial slope	$mgC\ mgChl^{-1}\ (W\ m^{-2})^{-1}d^{-1}$	0.1	Kishi et al. 2007
β	photoinhibition parameter	$mgC\ mgChl^{-1}\ (W\ m^{-2})^{-1}d^{-1}$	5×10^{-4}	Platt (1980)
k_T	photosynthetic temp. coefficient	$°C^{-1}$	0.0693	Kishi et al. (2007)
m_p	phytoplankton mortality rate	d^{-1}	0.15	Taylor et al. (1991)
□	zooplankton assimilation efficiency	-	0.75	Leonard et al. 1999
E_m	zooplankton metabolism excretion	d^{-1}	0.05	Leonard et al. 1999
E_{eg}	zooplankton assimilation excretion	d^{-1}	0.05	Leonard et al. 1999
coag	aggregation rate	$(mmolP\ m^{-3})^{-1}\ d^{-1}$	0.005	Fennel et al. (2006)
$graz_m$	zooplankton maximum grazing rate	d^{-1}	0.6	Fasham (1995)
m_z	zooplankton mortality rate	$(mmolP\ m^{-3})^{-1}\ d^{-1}$	0.025	Fennel et al. (2006)
r_L	large detritus remineralization rate	d^{-1}	0.05	-
r_s	small detritus remineralization rate	d^{-1}	0.01	-
s_p	phytoplankton sinking rate	$m\ d^{-1}$	0.3	Chen et al. (2002)
s_s	small detritus sinking rate	$m\ d^{-1}$	0.3	Chen et al. (2002)
s_L	large detritus sinking rate	$m\ d^{-1}$	1.0	Fennel et al. (2006)

Table 7. Model Runs

Run Name	Type	Run Description
Control	Master run	includes all biological processes
Constant Chl:C	Sensitivity run	constant Chl:C ratio
Constant zooplankton	Sensitivity run	constant zooplankton concentration
Constant sinking	Sensitivity run	density invariable phyt. sinking rate
No photoinhibition	Sensitivity run	no photoinhibition
20m Nutricline	Sensitivity run	forced nutricline at 20m depth
40m Nutricline	Sensitivity run	forced nutricline at 20m depth
60m Nutricline	Sensitivity run	forced nutricline at 20m depth

Table 8. Chlorophyll model-data comparison r-values

Site Number	Chlorophyll RMSE value	Temperature RMSE value
1	0.13	3.61
2	0.09	3.04
3	0.13	2.43
4	0.12	2.29
5	0.13	3.81
7	0.22	3.46
8	0.12	3.21
10	0.13	3.11
12	0.18	2.52
13	0.12	3.30
14	0.07	3.44
15	0.08	0.94
16	0.14	3.67
17	0.11	2.54
18	0.28	2.89
19	0.27	1.67

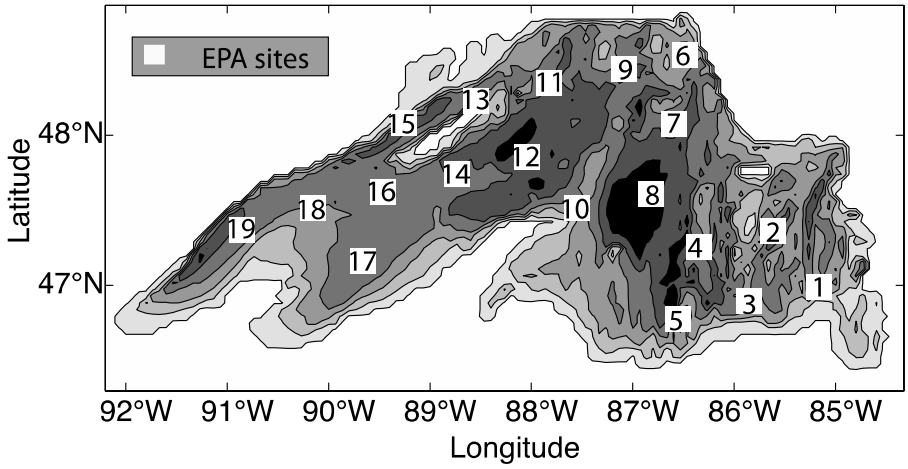

Figure 19. Lake Superior model bathymetry (every 50m) with EPA monitoring site locations (white squares).

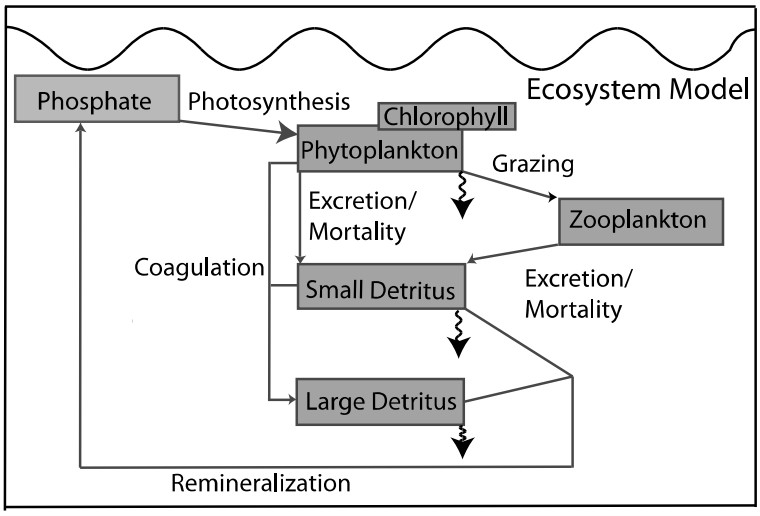

Figure 20. Biological module schematic. State variables are shown as shaded boxes and tracked via phosphorus in the model. Fluxes between state variables are shown as arrows.

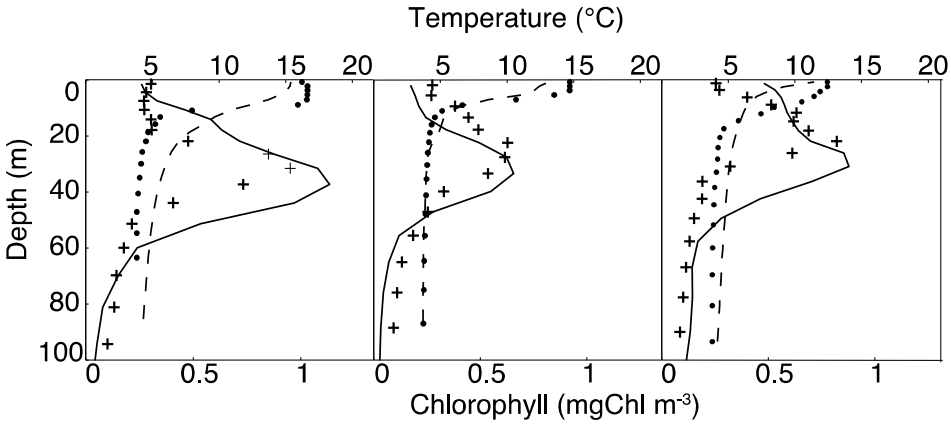

Figure 21. Observed (crosses) and modeled (solid lines) chlorophyll concentrations (mgChl m-3) and observed (dots) and modeled (dashed lines) temperatures versus depth (m) at EPA monitoring sites 4, 11, and 16 in late summer.

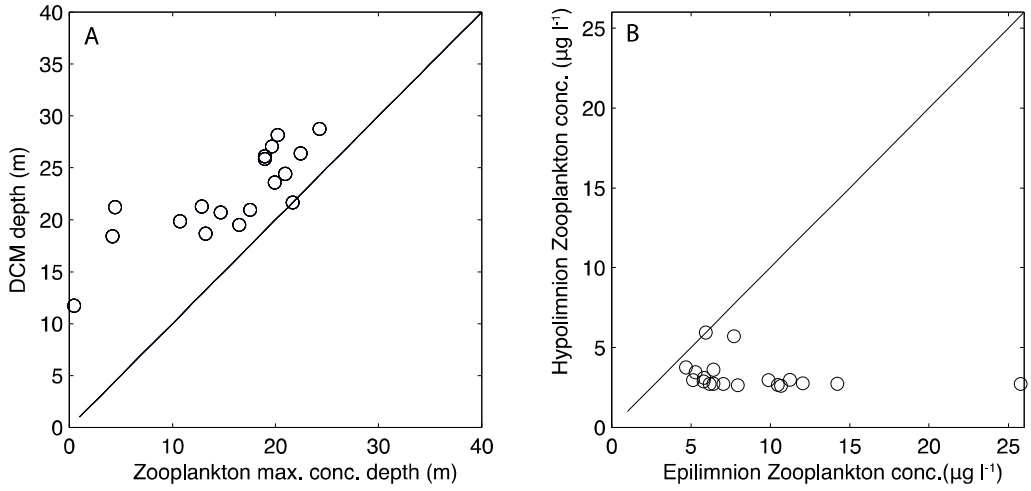

Figure 22. Panel A: Depth of maximum zooplankton concentration (m) and depth of the DCM (m), solid line is one-to-one. Panel B: Concentration of zooplankton in epilimnion (µg l− 1) and concentration of zooplankton in hypolimnion (µg l− 1).

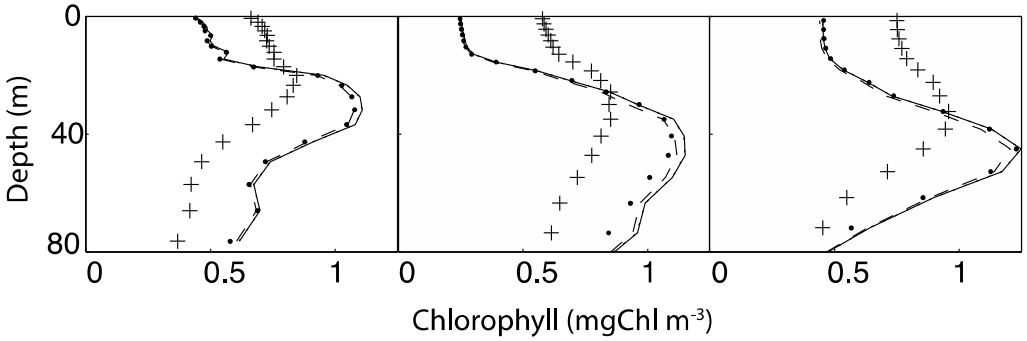

Figure 23. Chlorophyll concentration (mgChl m-3) depth profiles (meters) at locations corresponding to sites 1, 6, 14 for the five sensitivity model runs (solid line=control run, dots=no density dependent phytoplankton sinking, dotted line=no photoinhibition, crosses=constant chlorophyll to carbon ratio, dashed line=constant zooplankton grazing).

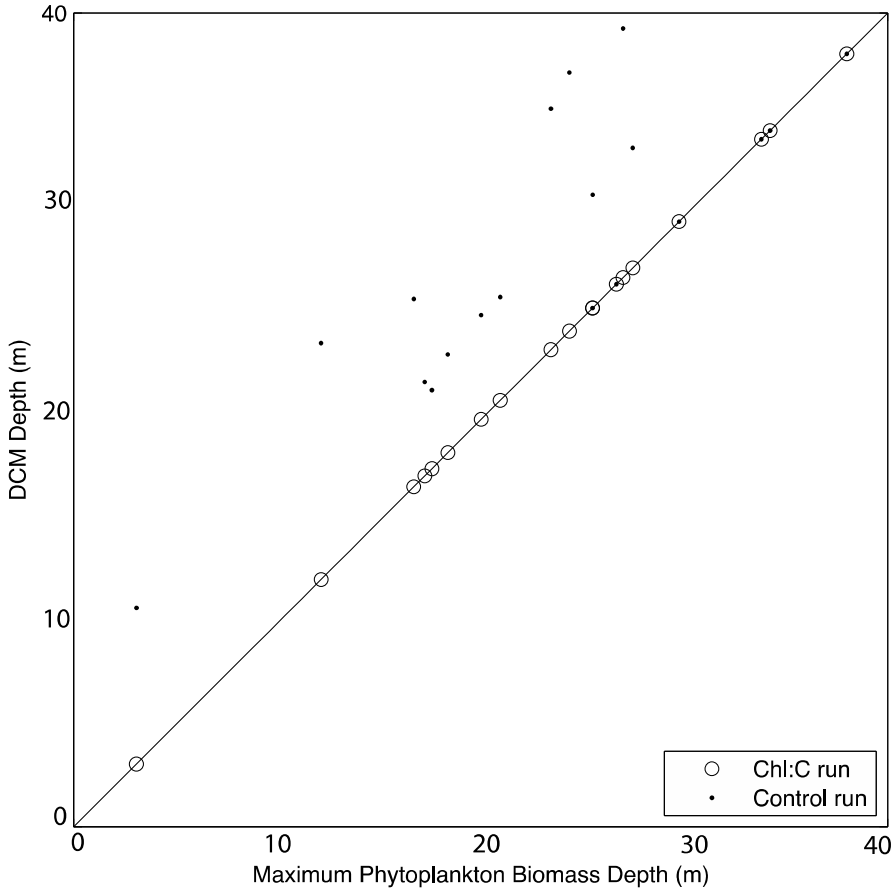

Figure 24. Depth of maximum phytoplankton concentration (m) and DCM depth (m) for control run (dots) and constant Chl:C ratio run (circles).

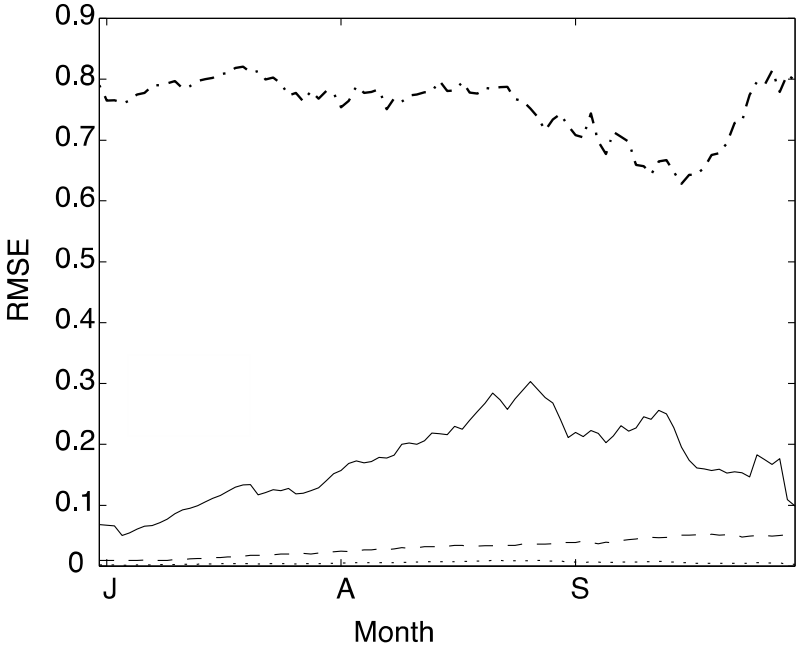

Figure 25. Spatially-averaged root mean square error of vertical chlorophyll profiles for sensitivity runs compared to control run for July through September. Dash-dot line: constant chlorophyll to carbon ratio, solid line: no density-dependent phytoplankton sinking, dotted line: no photoinhibition, dashed line: constant zooplankton grazing.

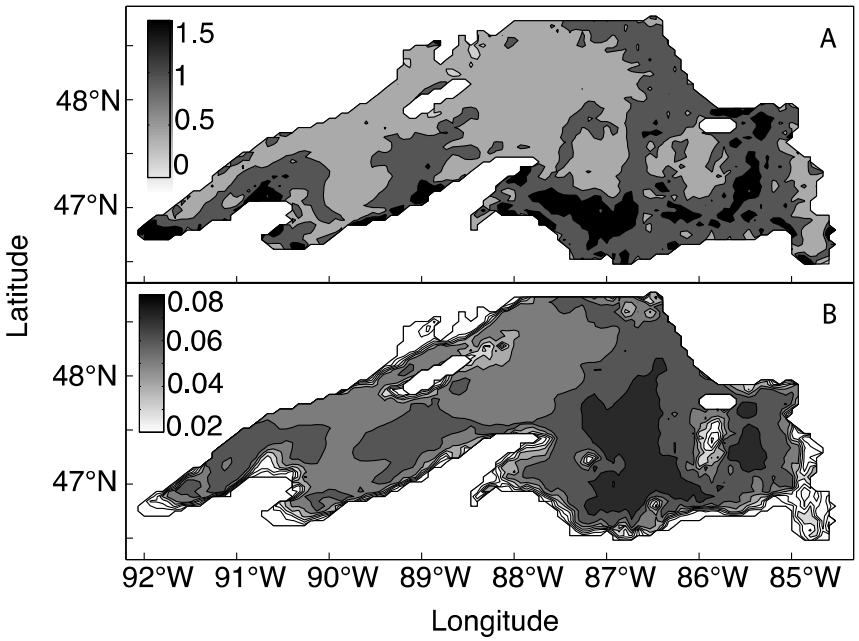

Figure 26. Panel A: The spatial dimension of the magnitude of the DCM (maximum chlorophyll concentration minus surface chlorophyll concentration, mg Chl m-3), Panel B: The spatial distribution of the magnitude of the nutricline (deep phosphate concentration minus surface phosphate concentration, mmolP m-3).

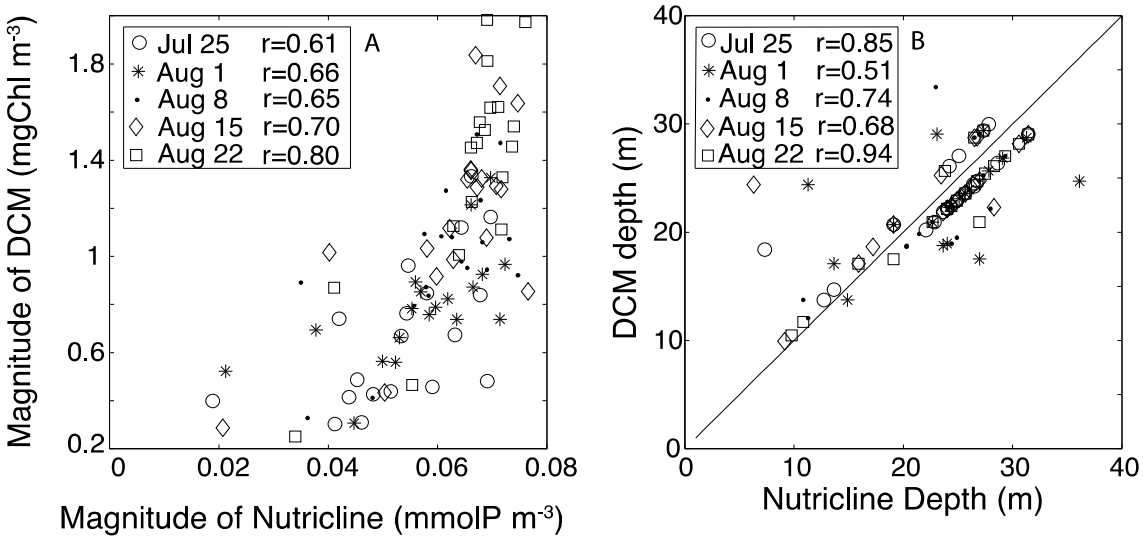

Figure 27. Panel A: The magnitude of the nutricline (mmolP m-3) against the magnitude of the deep chlorophyll maximum (mgChl m-3) from the model control run for each of the 19 EPA monitoring site locations at several times during the summer season. Pearson's r for each data set is shown. Panel B: The depth of the nutricline (m) against the depth of the deep chlorophyll maximum (m) from the model control run for each of the EPA site locations at several times during the summer season. Pearson's r is shown for each data set.

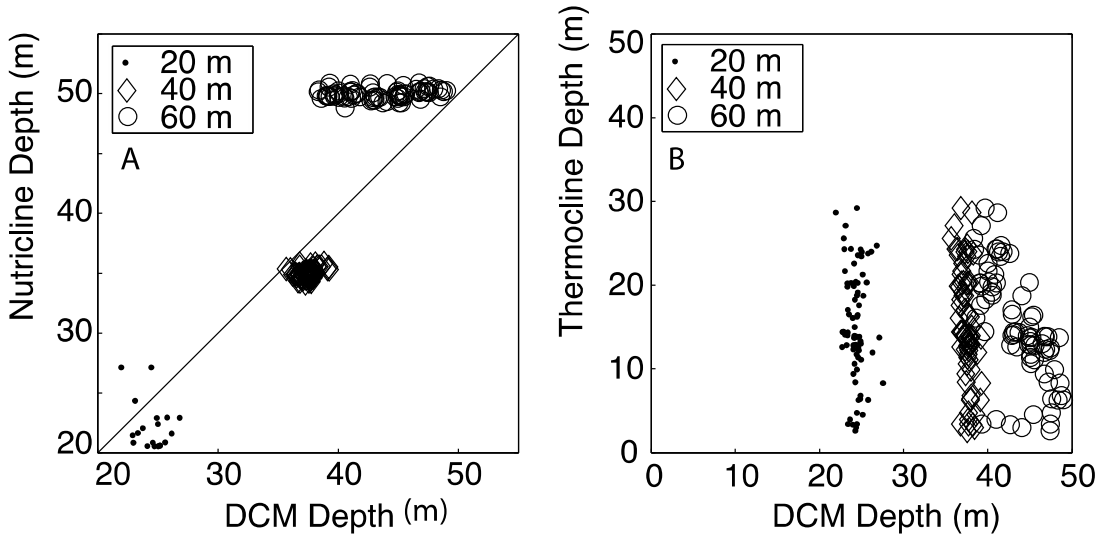

Figure 28. Panel A: DCM depth (m) and nutricline depth (m) for three forced nutrient profile experiments. Panel B: DCM depth (m) and thermocline depth (m) for forced nutrient profiles experiments.

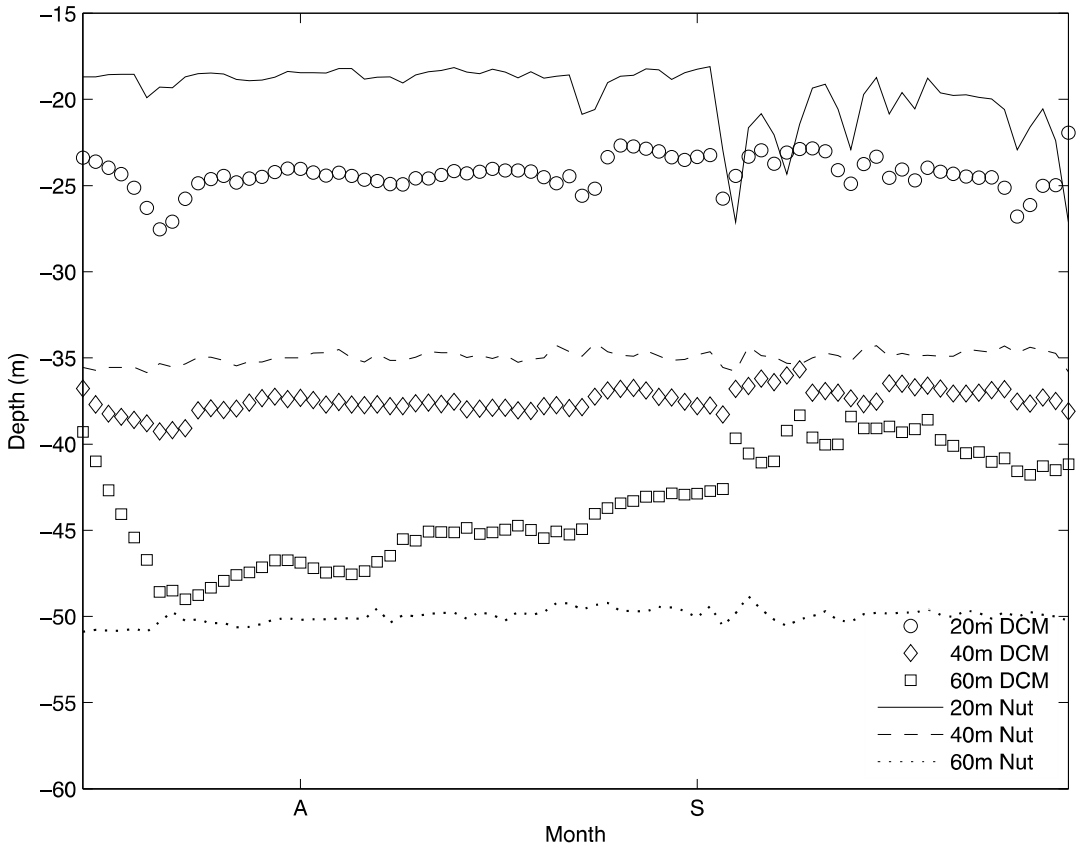

Figure 29. Average depth of the DCM (m) and average depth of the nutricline (m) for the 20 m nutricline (solid line and circles), 40 m nutricline (dashed line and diamonds) and 60 m nutricline (dotted line and squares) sensitivity runs during the summer stratified season.

Conclusions

In this thesis, the development of a realistically configured three-dimensional model for Lake Superior including prognostic ice and biogeochemistry models is documented. The addition of a prognostic ice model is a significant advance over previous modeling efforts that either didn't include ice cover or prescribed it. The hydrodynamic, ice and biogeochemical models are described and behavior of the model during the period 1985 to 2008 and focusing on the annual cycle of 2005 is discussed. The model is found to sufficiently reproduce many observed physical and biological characteristics of Lake Superior. It is also successfully applied in two scientific investigations: interannual trends in lake temperature, ice cover and primary productivity and elucidation of the causal mechanisms of Lake Superior's deep chlorophyll maximum.

The first application of the model to investigate interannual trends in lake temperature, ice cover, and primary productivity is discussed in chapter one. Using a compilation of available summer surface water temperature measurements, Austin and Colman (2007) show a warming trend in Lake Superior over the last quarter century in excess of the regional atmospheric warming rates. The observed annual ice cover magnitude also decreased significantly during the same period and may be driving a feedback that explains the high rate of warming in the lake. Historical meteorological forcing is applied to the model for 1985 to 2008. Analysis of both the modeled average lake surface summertime temperature and wintertime ice cover trends for 1985-2008 show they are consistent with the observed trends. An associated trend in primary productivity is also discussed.

The second application of the model to examine the controlling mechanisms of Lake Superior's deep chlorophyll maximum (DCM) is discussed in chapter two. The three-dimensional hydrodynamic and ice cover models coupled to the ecological model are used to perform sensitivity runs exploring the influence of several mechanisms on the vertical distribution of chlorophyll in the water column. Proposed mechanisms include depth differential zooplankton grazing pressure on phytoplankton, sinking and passive accumulation of phytoplankton due to density-dependent sinking rates, photoinhibition of phytoplankton, and photoadaptation of phytoplankton via a dynamic chlorophyll to carbon ratio. The role of a nutricline in determining the presence and nature of the DCM is also explored using force nutrient profiles to detect correlation of DCM and nutricline depths.

Highlights and key issues for model development and for both applications are discussed in the following sections.

Model Development:
Highlights and Key Issues

Large-scale observed spatial patterns in surface water temperatures, e.g. higher overall water temperatures in the western arm versus the central and eastern basins, are reproduced by the model. The annual surface water temperature cycle is also well represented by the model with average root mean square errors of 2.12 °C, 1.77 °C, and 1.69 °C in comparison with observations at the western, central, and eastern NOAA buoy locations. Simulated interannual variability of ice cover magnitude is consistent with observations. Focus on winter 2005 shows good reproduction of timing of ice formation

and the magnitude and timing of peak ice cover as considered against two different sets of ice cover observations.

Spatial patterns of biogeochemical variables show internal and therefore mechanistic consistency within the model. Vertical chlorophyll profiles, including the deep chlorophyll maximum in the stratified season, are reasonably well simulated when compared to observations. Average total annual gross primary production for 1985-2008 is comparable to several recent estimations of productivity including that of Sterner (2010).

The main issue in the hydrodynamic model is the shallowness of the mixed layer depth as compared to observations. This is possibly due to the model lacking wind-wave mixing parameterization, an improvement to the model that could be included in the future. One repercussion of the overly shallow thermocline is relatively high summer maximum surface water temperatures. Another model discrepancy due to the shallow mixed layer depth is the delay of ice cover melt in the spring.

The microbial loop is currently modeled implicitly through remineralization rates. An improved representation of the microbial loop and dissolved phase of organic matter is an area of future model development. Also, future assessment of physical and biogeochemical model output would benefit from further well-documented, lake-wide interannual observational data sets.

Interannual Trends:
Highlights and Key Issues

The modeled lake wide-average summertime (July-September) surface water temperature increased over the period 1985 to 2008 at a rate of 0.10±0.05°C/yr. This value is consistent with the Austin and Colman (2007) rate of summer time surface water temperature increase of ~0.11±0.06°C/yr. It is similarly also in excess of the regional atmospheric warming rate of ~0.06°C/yr.

The modeled average wintertime ice cover decreased at a rate of 1.20±0.29%/yr over the period 1985 to 2008. This rate is higher than that found by Austin and Colman (2007) of 0.42±0.20%/yr. As stated before, there is a delay in ice cover melt in spring due to the shallowness of the modeled mixed layer depth. This may be related to the rate of decrease of wintertime ice cover magnitude form 1985 to 2008 being greater in model output than in observations. The disparity between modeled and observed average wintertime ice cover is significantly greater during high ice years when longer delays in springtime ice cover melt are also seen. As many of the high ice years occur in the former half of the time period examined (1985-2008) and many of the years during the latter half of the period do not suffer from the issue of delayed ice melt and are much closer to the observed, lower average ice cover magnitude, this bias leads to an apparently higher rate of decrease of ice cover in the model.

Long-term interannual gross primary productivity rates are highly variable but show an increasing trend for the period 1985-2008 that is strongly correlated with increasing annual average surface water temperatures and decreasing winter ice cover.

Causal Mechanisms of the Deep Chlorophyll Maximum: Highlights and Key Issues

Using a set of eight model runs, I determine that the three primary factors contributing to the presence, depth, and magnitude of the DCM in the model are photoadaptation, the presence and characteristics of a nutricline and the presence of thermal stratification. Zooplankton grazing and phytoplankton sinking are found to be secondary contributing factors in the model. Sensitivity runs reveal that photoadaptation plays an important role in determining the depth and magnitude of the DCM. In the control run, the DCM and phytoplankton biomass peak are vertically separated. Controlling for photoadaptation caused the DCM to shift to the shallower depth of the phytoplankton biomass peak, consistent with the observations of Barbiero and Tuchman (2004).

Density dependent phytoplankton sinking and depth differential zooplankton grazing were of secondary importance and mainly affected the magnitude of the DCM and not its location or presence. Seegers (2009) similarly found that Lake Superior DCM formation could not be fully explained by zooplankton pressure despite the high loss of primary productivity due to it. Though Nalewajko and Voltolina (1986) found photoinhibition in Lake Superior phytoplankton communities, controlling for photoinhibition in the model had minimal effect indicating that it is not an important biological process in determining the vertical distribution of chlorophyll.

The magnitude and depth of the nutricline in the model is correlated with the magnitude and depth of the DCM throughout the lake during the summer stratified period. Model runs with forced nutrient profiles show that the depth of the DCM tracks the depth of the nutricline. Barbiero and Tuchman (2004) measured lower carbon to phosphorus phytoplankton ratios in the DCM, consistent with improved nutrient status of DCM phytoplankton. Consistent presence of thermal stratification in the model prior to the appearance of the DCM indicates that density stratification is a necessary condition for DCM formation.

Though zooplankton grazing is concluded to have secondary affects on Lake Superior DCM formation, effects of zooplankton grazing in the model may be underestimated due to low zooplankton concentrations compared to observations. Also, diurnal vertical migration behavior is not included in the model, excluding a dynamic seen in the deep-dwelling calanoid community (Barbiero and Tuchman, 2004) with potential impact to DCM formation.

The magnitude and depth of the nutricline in the model is found to correlate with the magnitude and depth of the DCM in the model. Recent studies using increasingly sensitive methods, however, have been unable to measure a distinct vertical soluble reactive phosphorus gradient in Lake Superior (Anagnostou and Sherrell 2008) and very low phosphorus concentrations make these measurements difficult. A highly dynamic dissolved organic phosphorus pool in Lake Superior (Baehr and McManus, 2003) suggests the possibility that it may be fueling productivity in Lake Superior as in the

Sargasso Sea (Lomas et al., 2010). Iron also plays a role in limiting productivity in Lake Superior (Sterner et al., 2004).

References

Introduction

Anagnostou, E., Sherrell, R.M., 2008. MAGIC method for subnanomolar orthophosphate determination in freshwater, Limnol. Oceanogr. Methods. 6, 64-74.

Assel, R.A. 2003. An Electronic Atlas of Great Lakes Ice Cover. NOAA Great Lakes Ice Atlas. Great Lakes Environmental Research Laboratory, Ann Arbor, Michigan 48105. (http://www.glerl.noaa.gov/data/ice/atlas/)

Austin, J.A., and J. Allen, 2011. Sensitivity of summer Lake Superior thermal structure to meteorological forcing. Limnol. Oceanogr. 56(3), 1141-1154.

Austin, J.A., Colman, S.M., 2007. Lake Superior summer water temperatures are increasing more rapidly than regional air temperatures: A positivity ice-albedo feedback. Geophys. Res. Lett. 34.

Baehr, M.M., McManus, J., 2003. The measurement of phosphorus and its spatial and temporal variability in the Western Arm of Lake Superior. J. Great Lakes Res. 29, 479-487.

Barbiero, R.P., Tuchman, M.L., 2004. The deep chlorophyll maximum in Lake Superior. J. Great Lakes Res. 30, 256-268.

Barbiero, R. P., Lesht, B.M., Warren, G.J., 2012. Convergence of trophic state and the lower food web in Lakes Huron, Michigan and Superior. J. Great Lakes Res. 38, 368-380.

Bennett, E.B., 1986. The nitrifying of Lake Superior. Ambio. 15, 272-275.

Brooks, A.S., Edgington, D.N., 1994. Biogeochemical control of phosphorus cycling and primary production in Lake Michigan. Limnol. Oceanogr. 39, 961-968.

Cotner, J.B., Biddanda, B.A., Makino, W., Stets, E., 2004. Organic carbon biogeochemistry of Lake Superior. Aquat. Ecosyst. Health, 7, 451-464.

Desai, A.R., Austin, J.A., Bennington, V., McKinley, G.A., 2009. Stronger winds over a large lake in response to weakening air-to-lake temperature gradient. Nat. Geosci. 2, 855-858.

The Great Lakes Commission, 2006, Annual Report of the Great Lakes Regional Water Use Database Repository. http://www.glc.org/wateruse/database/.

Holland, R.E., Johengen, T.H., Beeton, A.M., 1995. Trends in nutrient concentrations in Hatchery Bay, western Lake Erie, before and after Dreissena polymorpha. Can. J. Fish. Aquat. Sci. 52, 1202-1209.

Lomas, M.W., Burke, A.L., Lomas, D.A., Bell, D.W., Shen, C., Dyhrman, S.T., Ammerman, J.W., 2010. Sargasso Sea phosphorus biogeochemistry: an important role for dissolved organic phosphorus (DOP). Biogeosciences. 7, 695-710.

Makarewicz, J.C., Bertram, P., Lewis, T.W., 2000. Chemistry of the offshore surface waters of Lake Erie: pre- and post-dreissena introduction (1983-1993). J. Great Lakes Res. 26, 82-93.

McManus, J., Heinen, E.A., Baehr, M.M., 2003. Hypolimnetic oxidation rates in Lake Superior: Role of dissolved organic material on the lake's carbon budget, Limnol. Oceanogr. 48, 1624-1632.

Sea Grant College Program, 1985. Bulletins E-1866-70. Cooperative Extension Service, Michigan State University, E. Lansing, Michigan.

Sterner, R.W., Smutka, T.M., McKay, R.M.L., Xiaoming, Q., Brown, E.T., Sherrell, R.M., 2004. Phosphorus and trace metal limitation of algae and bacteria in Lake Superior. Limnol. Oceanogr. 49, 495-507.

Sterner, R. W., E. Anagnostou, S. Brovold, G. S. Bullerjahn, J. C. Finlay, S. Kumar, R. M. L. McKay, R. M. Sherrell, 2007. Increasing stoichiometric imbalance in North America's largest lake: Nitrification in Lake Superior. Geophys. Res. Lett. 34.

Tarapchak, S.J., Rubitschun, C., 1981. Comparisons of soluble reactive phosphorus and orthophosphorus concentrations at an offshore station in southern Lake Michigan. J. Great Lakes Res. 7, 290-298.

Urban, N.R., Auer, M.T., Green, S.A., Lu, X., Apul, D.S., Powell, K.D., Bub, L., 2005. Carbon cycling in Lake Superior. J. Geophys. Res. 110, C06S90, doi: 10.1029/2003JC002230.

Chapter 1

Anagnostou, E., Sherrell, R.M., 2008. MAGIC method for subnanomolar orthophosphate determination in freshwater, Limnol. Oceanogr. Methods. 6, 64-74.

Assel, R.A. 2003. An Electronic Atlas of Great Lakes Ice Cover. NOAA Great Lakes Ice Atlas. Great Lakes Environmental Research Laboratory, Ann Arbor, Michigan 48105. (http://www.glerl.noaa.gov/data/ice/atlas/)

Assel, R.A., 2005. Great Lakes ice cover climatology update: Winters 2003, 2004, and 2005. NOAA Technical Memorandum GLERL-135.

Austin, J.A., and J. Allen, 2011. Sensitivity of summer Lake Superior thermal structure to meteorological forcing. Limnol. Oceanogr. 56(3), 1141-1154.

Austin, J.A., Colman, S.M., 2007. Lake Superior summer water temperatures are increasing more rapidly than regional air temperatures: A positivity ice-albedo feedback. Geophys. Res. Lett. 34.

Austin, J.A., Colman, S.M., 2008. A century of temperature variability in Lake Superior. Limnol. Oceanogr. 53, 2724-2730.

Baehr, M.M., McManus, J., 2003. The measurement of phosphorus and its spatial and temporal variability in the Western Arm of Lake Superior. J. Great Lakes Res. 29, 479-487.

Baker, K.S., Frouin, R., 1987. Relation between photosynthetically available radiation and total insolation at the ocean surface under clear skies. Limnol. Oceanogr. 32(6), 1370-1377.

Barbiero, R.P., Tuchman, M.L., 2004. The deep chlorophyll maximum in Lake Superior. J. Great Lakes Res. 30, 256-268.

Barry, R.G., R.J. Chorley, 1976. Atmosphere, Weather, and Climate, third ed. ELBS and Methuen, London.

Beletsky, D., Saylor, J.H., Schwab, D.J., 1999. Mean circulation in the Great Lakes. J. Great Lakes Res. 25, 78-93.

Beletsky, D., Schwab, D.J., 2001. Modeling circulation and thermal structure in Lake Michigan: annual cycle and interannual variability. J. Geophys. Res. 106, 19745-19771.

Bennett, E.B., 1978. Characteristics of the thermal regime of Lake Superior. J. Great Lakes Res. 4, 310-319.

Bennett, E.B., 1986. The nitrifying of Lake Superior. Ambio. 15, 272-275.

Bennington, V., McKinley, G.A., Kimura, N., Wu, C.H., 2010. The general circulation of Lake Superior: mean, variability, and trends from 1979-2006. J Geophys Res. 115.

Bierman, V. J., Dolan, D. M., 1981. Modeling of phytoplankton-nutrient dynamics in Saginaw Bay, Lake Huron. J. Great Lake Res. 7, 409-439.

Brooks, A.S., Edgington, D.N., 1994. Biogeochemical control of phosphorus cycling and primary production in Lake Michigan. Limnol. Oceanogr. 39, 961-968.

Budgell, W. P., 2005. Numerical simulation of ice-ocean variability in the Barents Sea region: Towards dynamical downscaling. Ocean Dynamics. 55, 370-387.

Sea Grant College Program, 1985. Bulletins E-1866-70. Cooperative Extension Service, Michigan State University, E. Lansing, Michigan.

Chen, C.A., Millero, F.J., 1986. Precise thermodynamic properties for natural waters covering only the limnological range. Limnol. Oceanogr. 31, 657-662.

Chen, C., Zhu, J., Ralph, E., Green, S.A., Budd, J.W., Zhang, F.Y., 2001. Prognostic modeling studies of the Keweenaw Current in Lake Superior, Part 1: Formation and evolution. J. Phys. Oceangr. 31, 379-395.

Chen, C., Rubao, J., Schwab, D.J., Beletsky, D., Fahnenstiel, G.L., Jiang, M., Johengen, T. H., Vanderploeg, H., Eadie, B., Budd, J. W., Bundy, M. H., Gardner, W., Cotner, J., Lavrentyev, P. J., 2002. A model study of the coupled biological and physical dynamics in Lake Michigan. Ecol. Modell. 152, 145-168.

Chen, C., Xu, Q., Ralph, E., Budd, J.W., Lin, H., 2004. Response of Lake Superior to mesoscale wind forcing: A comparison between currents driven by QuickSCAT and buoy winds. J. Geophys. Res. 109.

Cotner, J.B., Biddanda, B.A., Makino, W., Stets, E., 2004. Organic carbon biogeochemistry of Lake Superior. Aquat. Ecosyst. Health, 7, 451-464.

Desai, A.R., Austin, J.A., Bennington, V., McKinley, G.A., 2009. Stronger winds over a large lake in response to weakening air-to-lake temperature gradient. Nat. Geosci. 2, 855-858.

Dinniman, M.S., Klinck, J.M., Smith, W.O., 2003. Cross-shelf exchange in a model of the Ross Sea circulation and biogeochemistry. Deep Sea Res. Part 2. 50, 3103-3120.

Eppley, R. W., 1972. Temperature and phytoplankton growth in the sea. Fish. Bull. 70, 1063-1085.

Evans, G.T., Parslow, J.S., 1985. A model of annual plankton cycles. Biol. Oceanogr. 3, 327-347.

Fahnenstiel, G.L., Sicko-Goad, L., Scavia, D., Stoermer, E.F., 1986. Importance of picoplankton in Lake Superior. Can. J. Fish. Aquat. Sci. 43, 235-240.

Fasham, M. J. R., H. W. Ducklow, S. M. McKelvie, 1990. A nitrogen-based model of plankton dynamics in the oceanic mixed layer. J. Marine Res. 48, 591-639.

Fennel, K., Wilkin, J., Levin, J., Moisan, J., O'Reilly, J., Haidvogel, D., 2006. Nitrogen cycling in the Middle Atlantic Bight: results from a three-dimensional model and implications for the North Atlantic nitrogen budget. Global Biogeochem. Cycles. 20.

Geider, R.J., MacIntyre, H.L., Kana, T.M., 1996. A dynamic model of photoadaptation in phytoplankton. Limnol. Oceanogr. 41, 1-15.

Geider, R.J., MacIntyre, H.L., Kana, T.M., 1997. Dynamic model of phytoplankton growth and acclimation: responses of the balanced growth rate and the chlorophyll *a:* carbon ratio to light, nutrient-limitation and temperature. Mar. Ecol. Prog. Ser. 148:187-200.

The Great Lakes Commission, 2006, Annual Report of the Great Lakes Regional Water Use Database Repository. http://www.glc.org/wateruse/database/.

Gruber, N., Frenzel, H., Doney, S.C., Marchesiello, P., McWilliams, J.C., Moisan, J.R., Oram, J.J., Plattner, G., Stolzenbach, K.D., 2006. Eddy-resolving simulation of plankton ecosystem dynamics in the California current system. Deep Sea Res. Part 1. 53, 1483-1516.

Häkkinen, S., Mellor, G.L., 1992. Modeling the seasonal variability of a coupled Arctic ice-ocean system, J. Geophys. Res. 97, 20285-20304.

Hedström, K.S., 2009, Technical manual for a coupled sea-ice/ocean circulation model (version 3). OCS Study MMS 2009-062.

Heinen, E.A., McManus, J., 2004. Carbon and nutrient cycling at the sediment-water boundary in western Lake Superior. J. Great Lakes Res. 30, 113-132.

Holland, R.E., Johengen, T.H., Beeton, A.M., 1995. Trends in nutrient concentrations in Hatchery Bay, western Lake Erie, before and after Dreissena polymorpha. Can. J. Fish. Aquat. Sci. 52, 1202-1209.

Holling, C.S., 1959. Some characteristics of simple types of predation and parasitism. Can. Entomol. 91,824-839.

Holling, C.S., 1962. Principles of insect predation. Annu. Rev. Entomol. 6, 163-182.

Holling, C.S., 1965. The functional response of predators to prey density and its role in mimicry and population regulation. Mem. Entomol. Soc. Can. 45, 3-60.

Hsu, S.A., Meindl, E., Gilhousen, D., 1994. Determining the power-law wind-profile exponent under near-neutral stability conditions at sea. J. Appl. Meteorol. 33, 757-765.

Hu, H., Wang, J., 2010. Modeling effects of tidal and wave mixing on circulation and thermohaline structures in the Bering Sea: process studies. J. Geophys. Res., 115, C01006, doi:10.1029/2008JC005175.

Huang, A., Rao, Y.R., Lu, Y., Evaluation of a 3-D hydrodynamic model and atmospheric forecast forcing using observations in Lake Ontario. J. Geophys. Res., 115, C02004, doi:10.1029/2009JC005601.

Hunke, E.C., Dukowicz, J.K., 1997. An elastic-viscous-plastic model for sea ice dynamics. J. Phys. Oceanogr. 27, 1849- 1867.

Hunke, E.C., 2001. Viscous-plastic sea ice dynamics with the EVP model: Linearization issues. J. Comput. Phys. 170, 18-38.

Jerome, J.H., Bukata, R.P., Bruton, J.E., 1983. Spectral attenuation and irradiance in the Laurentian Great Lakes. J. Great Lakes Res. 9(1):60-68.

Kishi, M.J., Kashiwai, M, Ware, D.M., Megrey, B.A., Eslinger, D.L., Werner, F.E., Noguchi-Aita, M., Azumaya, T., Fujii, M., Hashimoto, S., Huang, D., Iizumi, H., Ishida, Y., Kang, S., Kantakov, G.A., Kim, H., Komatsu, K., Navrotsky, V.V., Smith, S.L., Tadokoro, K., Tsuda, A., Yamamura, O., Yamanaka, Y., Yokouchi, K., Yoshie, N., Zhang, J., Zuenko, Y., Zvalinsky, V.I., 2007. NEMURO – a lower trophic level model for the North Pacific marine ecosystem. Ecol. Model. 202, 12-25.

Lam, D.C.L., 1978. Simulation of water circulations and chloride transports in Lake Superior for summer 1973. J. Great Lakes Res. 4, 343-349.

Leonard, C.L., McClain, C.R., Murtugudde, R., Hofmann, E.E., Harding, L.W., 1999. An iron-based ecosystem model of the central equatorial Pacific. J. Geophys. Res. 104, 1325-1341.

Lomas, M.W., Burke, A.L., Lomas, D.A., Bell, D.W., Shen, C., Dyhrman, S.T., Ammerman, J.W., 2010. Sargasso Sea phosphorus biogeochemistry: an important role for dissolved organic phosphorus (DOP). Biogeosciences. 7, 695-710.

Makarewicz, J.C., Bertram, P., Lewis, T.W., 2000. Chemistry of the offshore surface waters of Lake Erie: pre- and post-dreissena introduction (1983-1993). J. Great Lakes Res. 26, 82-93.

McManus, J., Heinen, E.A., Baehr, M.M., 2003. Hypolimnetic oxidation rates in Lake Superior: Role of dissolved organic material on the lake's carbon budget, Limnol. Oceanogr. 48, 1624-1632.

Mellor, G.L, Kantha, L., 1989. An ice-ocean coupled model. J. Geophys. Res. 94, 10937-10954.

Mellor, G.L., Yamada, T., 1982. Development of a turbulence closure model for geophysical fluid problems. Rev. Geophys. Space Phys. 20, 851-875.

Michaelis, L., Menten, M.L., 1913. Die Kinetik der Invertinwirkung. Biochemistry Z 49, 333-369.

Munawar, M., Munawar, I.F., 1978. Phytoplankton of Lake Superior 1973. J. Great Lakes Res. 4, 415-442.

National Ice Center, 2008. *IMS daily Northern Hemisphere snow and ice analysis at 4 km and 24 km resolution*. Boulder, CO: National Snow and Ice Data Center. Digital media. http://nsidc.org/data/g02156.html

Parkinson, C.L., Washington, W.M., 1979. A large-scale numerical model of sea ice. J. Geophys. Res. 84, 6565-6575.

Payne, R.E., 1972. Albedo of the sea surface. J. Atmos. Sci. 29, 959-970.

Platt, T., Gallegos, C.L., Harrison, W.G., 1980. Photoinhibition of photosynthesis in natural assemblages of marine phytoplankton. J. Mar. Res. 38, 687-701.

Quinn, F.H., 1992. Hydraulic residence times of the Laurentian Great Lakes. J. Great Lakes Res. 18, 22-28.

Ralph, E.A., 2002. Scales and structure of large lake eddies, Geophys. Res. Lett. 29, 2177.

Russ, M.E., Ostrom, N.E., Gandhi, H., Ostrom, P.H., 2004. Temporal and spatial variations in R:P ratios in Lake Superior, an oligotrophic freshwater environment, J. Geophys. Res. 109.

Schwab, D.J., Bedford, K.W., 1999. The great lakes forecasting system, in: Moores, C.N.K. (Ed.), Coastal Ocean Prediction. AGU, Washington, D.C., 157-173.

Semtner, A.J., Jr., 1976. A model for the thermodynamic growth of sea ice in numerical investigations of climate. J. Phys. Oceanogr. 6, 379-389.

Shchepetkin, A.F., McWilliams, J.C., 2005. The Regional Ocean Modeling System: A split-explicit, free-surface, topography following coordinates ocean model. Ocean Model. 9, 347-404.

Steele, M., Mellor, G.L., McPhee, M.G., 1989. Role of the molecular sublayer in the melting or freezing of sea ice. J. Phys. Oceanogr. 19, 139-147.

Sterner, R.W., Smutka, T.M., McKay, R.M.L., Xiaoming, Q., Brown, E.T., Sherrell, R.M., 2004. Phosphorus and trace metal limitation of algae and bacteria in Lake Superior. Limnol. Oceanogr. 49, 495-507.

Sterner, R. W., E. Anagnostou, S. Brovold, G. S. Bullerjahn, J. C. Finlay, S. Kumar, R. M. L. McKay, R. M. Sherrell, 2007. Increasing stoichiometric imbalance in North America's largest lake: Nitrification in Lake Superior. Geophys. Res. Lett. 34.

Sterner, R.W., 2010. In situ-measured primary production in Lake Superior. J. Great Lakes Res. 36, 139-149.

Strom, J.D., 2007. Seasonal evolution of dissolved gas concentrations in western Lake Superior: Implications for respiration, primary production and carbon cycling (Master's thesis). University of Minnesota, Duluth, MN.

Sverdrup, H.U., 1953. On conditions for the vernal blooming of phytoplankton. J. Cons. Perm. Int. Explor. Mer. 18, 287-295.

Tarapchak, S.J., Rubitschun, C., 1981. Comparisons of soluble reactive phosphorus and orthophosphorus concentrations at an offshore station in southern Lake Michigan. J. Great Lakes Res. 7, 290-298.

United States Environmental Protection Agency and Government of Canada, 2002. The Great Lakes: An Environmental Atlas and Resource Book, third ed., p. 12.

Urban, N.R., Auer, M.T., Green, S.A., Lu, X., Apul, D.S., Powell, K.D., Bub, L., 2005. Carbon cycling in Lake Superior. J. Geophys. Res. 110, C06S90, doi: 10.1029/2003JC002230.

Wang, J., Ju, H., Schwab, D., Leskevich, G., Beletsky, D., Hawley, N., Clites, A., 2010. Development of the Great Lakes ice-circulation model (GLIM): application to Lake Erie in 2003-2004. J. Great Lakes Res. 36, 425-436.

Watson, N.H.F, Wilson, J.B., 1978. Crustacean Zooplankton of Lake Superior. J. Great Lakes Res. 4, 481-496.

Zhu, J., Chen, C., Ralph, E., Green, S.A., Budd, J.W., Zhang, F.Y., 2001. Prognostic modeling studies of Keweenaw Current in Lake Superior. Part II: Simulation. J. Phys. Oceanogr. 3, 396-410.

Chapter 2

Baker, K.S., Frouin, R., 1987, Relation between photosynthetically available radiation and total insolation at the ocean surface under clear skies. Limnol. Oceanogr. 32(6), 1370-1377.

Barbiero, R.P., Tuchman, M.L., 2001. Results from the U.S. EPA's biological open water surveillance program of the Laurentian Great Lakes: II. Deep chlorophyll maximum. J. Great Lakes Res. 27, 155-166.

Barbiero, R.P., Tuchman, M.L., 2004. The deep chlorophyll maximum in Lake Superior. J. Great Lakes Res. 30(supp. 1), 256-268.

Bennington, V., 2010. Carbon cycle variability of the North Atlantic Ocean and Lake Superior. PhD Dissertation, University of Wisconsin.

Bennington, V., G. A. McKinley, N. R. Urban, and C. P. McDonald (2012), Can spatial heterogeneity explain the perceived imbalance in Lake Superior's carbon budget? A model study, J. Geophys. Res., 117, G03020, doi:10.1029/2011JG001895.

Bierman, V.J., Dolan, D.M., 1981. Modeling of phytoplankton-nutrient dynamics in Saginaw Bay, Lake Huron. J. Great Lakes Res. 7(4), 409-439.

Budgell, W. P., 2005. Numerical simulation of ice-ocean variability in the Barents Sea region: Towards dynamical downscaling. Ocean Dynamics. 55, 370-387.

Chai, Y., Urban, N.R., 2004. ^{210}Po and ^{210}Pb distributions and residence times in the nearshore region of Lake Superior. J. Geophys. Res. 109, C10607, doi:10.1029/2003JC002081.

Chen, C.A., Millero, F.J., 1986. Precise thermodynamic properties for natural waters covering only the limnological range. Limnol. Oceanogr. 31, 657-662.

Chen, C., Ji, R., Schwab, D.J., Beletsky, D., Fahnenstiel, G.L., Jiang, M., Jogengen, T.H., Vanderploeg, H., Eadie, B., Budd, J.W., Bundy, M.H., Gardner, W., Cotner, J., Lavrentyev, P.J., 2002. A model study of the coupled biological and physical dynamics in Lake Michigan. Ecol. Mod. 152, 145-168.

Cullen, J.J., 1982. The deep chlorophyll maximum: Comparing vertical profiles of chlorophyll a,. Can. J. Fish. Aquat. Sci. 39, 791-803.

Fahnenstiel, G.L., Glime, J.M., 1983. Subsurface chlorophyll maximum and associated Cyclotella pulse in Lake Superior. Int. Revue ges. Hydrobiol. 68, 605-618.

Fahnenstiel, G.L., Sicko-Goad, L., Scavia, D., Stoermer, E.F., 1986. Importance of picoplankton in Lake Superior. Can. J. Fish. Aquat. Sci. 43, 235-240.

Fahnenstiel, G.L., Krause, A.E., McCormick, M.J., Carrick, H.J., Schelske, C.L., 1998. The structure of the planktonic food-web in the St. Lawrence Great Lakes. J. Great Lakes Res. 24(3), 531-554.

Falkowski, P.G., Greene, R., Kolber, Z., 1993. Light utilization and photoinhibition of photosynthesis in marine phytoplankton. DOE report number BNL--49821; CONF-9309312--1

Fasham, M.J.R., Platt, T., Irwin, B., Jones, K., 1985. Factors affecting the spatial pattern of the deep chlorophyll maximum in the region of the Azores Front. Prog. Oceanog. 14:129-165.

Fasham, M.J.R., 1995. Variations in the seasonal cycle of biological production in subarctic oceans: A model sensitivity analysis. Deep Sea Res., Part I 42:1111-1149.

Fennel, K., Boss, E., 2003. Subsurface maxima of phytoplankton and chlorophyll: Steady-state solutions from a simple model. Limnol. Oceanogr. 48:1521-1534.

Fennel, K., Wilkin, J., Levin, J., Moisan, J., O'Reilly, J., Haidvogel, D., 2006. Nitrogen cycling in the Middle Atlantic Bight: results from a three-dimensional model and implications for the North Atlantic nitrogen budget. Global Biogeochem. Cycles. 20, GB3007, doi:10.1029/2005GB002456

Fennel, K., Collier, R., Larson, G., Crawford, G., Boss, E., 2007. Seasonal nutrient and plankton dynamics in a physical-biological model of Crater Lake. Hydrobiol. 574:265-280.

Geider, R.J., 1987. Light and temperature dependence of the carbon to chlorophyll ratio in microalgae and cyanobacteria: implications for physiology and growth of phytoplankton. New Phytol. 106, 1-34.

Geider, R.J., MacIntyre, H.L., Kana, T.M., 1996. A dynamic model of photoadaptation in phytoplankton. Limnol. Oceanogr. 41, 1-15.

Geider, R.J., MacIntyre, H.L., Kana, T.M., 1997. Dynamic model of phytoplankton growth and acclimation: responses of the balanced growth rate and the chlorophyll *a:* carbon ratio to light, nutrient-limitation and temperature. Mar. Ecol. Prog. Ser. 148, 187-200.

Gruber, N., Frenzel, H., Doney, S.C., Marchesiello, P., McWilliams, J.C., Moisan, J.R., Oram, J.J., Plattner, G., Stolzenbach, K.D., 2006. Eddy-resolving simulation of plankton ecosystem dynamics in the California Current System. Deep-Sea Res. I 53, 1483-1516.

Häkkinen, S., Mellor, G.L., 1992. Modeling the seasonal variability of a coupled Arctic ice-ocean system, J. Geophys. Res. 97, 20285-20304.

Harrison, W.G., Platt, T., 1985. Photosynthesis-irradiance relationships in polar and temperate phytoplankton populations. Polar Biol. 5, 153-164.

Herman, A.W., Sameoto, D.D., Longhurst, A.R., 1981. Vertical and horizontal distribution patterns of copepods near the shelf break south of Nova Scotia. Can J. Fish. Aquat. Sci. 38, 1065-1076.

Holling, C.S., 1959. Some characteristics of simple types of predation and parasitism. Can. Entomol. 91, 824-839.

Holling, C.S., 1962. Principles of insect predation. Annu. Rev. Entomol. 6, 163-182.

Holling, C.S., 1965. The functional response of predators to prey density and its role in mimicry and population regulation. Mem. Entomol. Soc. Can. 45, 3-60.

Hunke, E.C., Dukowicz, J.K., 1997. An elastic-viscous-plastic model for sea ice dynamics. J. Phys. Oceanogr. 27, 1849- 1867.

Hunke, E.C., 2001. Viscous-plastic sea ice dynamics with the EVP model: Linearization issues. J. Comput. Phys. 170, 18-38.

Jerlov, N.G., 1959. Maxima in the vertical distribution of particles in the sea. Deep-Sea Res. 5, 173-184.

Kirk, J.T.O., 1983. Light and photosynthesis in aquatic ecosystems. Cambridge Univ. Press, New York.

Kishi, M.J., Kashiwai, M, Ware, D.M., Megrey, B.A., Eslinger, D.L., Werner, F.E., Noguchi-Aita, M., Azumaya, T., Fujii, M., Hashimoto, S., Huang, D., Iizumi, H., Ishida, Y., Kang, S., Kantakov, G.A., Kim, H., Komatsu, K., Navrotsky, V.V., Smith, S.L., Tadokoro, K., Tsuda, A., Yamamura, O., Yamanaka, Y., Yokouchi, K., Yoshie, N., Zhang, J., Zuenko, Y., Zvalinsky, V.I., 2007. NEMURO – a lower trophic level model for the North Pacific marine ecosystem. Ecol. Model. 202,12-25.

Leonard, C.L., McClain, C.R., Murtugudde, R., Hofmann, E.E., Harding, L.W., 1999. An iron-based ecosystem model of the central equatorial Pacific. J. Geophys. Res. 104,1325-1341.

Longhurst, A.R., 1976. Interactions between zooplankton and phytoplankton profiles in the eastern tropical Pacific Ocean. Deep-Sea Res. 23, 729-754.

Mellor, G.L, Kantha, L., 1989. An ice-ocean coupled model. J. Geophys. Res. 94, 10937-10954.

Michaelis, L., Menten, M.L., 1913. Die Kinetik der Invertinwirkung. Biochemistry Z 49, 333-369.

Moll, R.A., Stoermer, E.F., 1982. A hypothesis relating trophic status and subsurface chlorophyll maxima of lakes. Arch. Hydrobiol. 94, 425-440.

Nalewajko, C., Voltolina, D., 1986. Effects of environmental variables on growth rates and physiological characteristics of Lake Superior phytoplankton. Can. J. Fish. Aquat. Sci. 43, 1163-1170.

Olson, T.A., Odlaug, T.O., 1966. Limnological observation on western Lake Superior. In Proc. 9th Conf. Great Lakes Res., pp. 109-118. Internat. Assoc. Great Lakes Res.

Pilati, A. Wurtsbaugh, W.A., 2003. Importance of zooplankton for the persistence of a deep chlorophyll layer: a limnocorral experiment. Limnol. Oceanogr. 48, 249-260.

Platt, T., Gallegos, C.L., Harrison, W.G., 1980. Photoinhibition of photosynthesis in natural assemblages of marine phytoplankton. J. Mar. Res. 38, 687-701.

Putnam, H.D., Olson, T.A., 1966. Primary productivity at a fixed station in western Lake Superior. In Proc. 9th Conf. Great Lakes Res., pp. 109-118. Internat. Assoc. Great Lakes Res.

Riley, G.A., Stommel, H., Bumpus, D.F., 1949. Quantitative ecology of the plankton of the western North Atlantic. Bull. Bingham Oceanogr. Coll. 12, 1-169.

Seegers, B.N., 2009. Lake Superior zooplankton community grazing and its implications for the deep chlorophyll maximum. Masters Thesis. University of Minnesota.

Shchepetkin, A.F., McWilliams, J.C., 2005. The Regional Ocean Modeling System: A split-explicit, free-surface, topography following coordinates ocean model. Ocean Model. 9, 347-404.

Sterner, R.W., Smutka, T.M., McKay, R.M.L., Xiaoming, Q., Brown, E.T., Sherrell, R.M., 2004. Phosphorus and trace metal limitation of algae and bacteria in Lake Superior. Limnol. Oceanogr. 49, 495-507.

Sterner, R.W., 2010. In situ-measured primary production in Lake Superior. J. Great Lakes Res. 36, 139-149.

Sterner, R.W., 2011. C:N:P stoichiometry in Lake Superior: Freshwater sea as end member. Inland Waters 1, 29-46

Taylor, A.H., Watson, A.J., Ainsworth, M., Robertson, J.E., Turner, D.R., 1991. A modeling investigation of the role of phytoplankton in the balance of carbon at the surface of the North Atlantic. Global Biogeochem. Cycles 5, 151-171.

Urban, N.R., 2009b. Nutrient cycling in Lake Superior: a retrospective and update. State of Lake Superior. In: Munawar, editor. State of Lake Superior. New Delhi: Goodword Books. P. 83-115.

Watson, N.H.F., Thomson, K.P.B., Elder, F.C., 1975. Sub-thermocline biomass concentration detected by transmissometer in Lake Superior. Verh. Internat. Verein. Limnol. 19:682-688.

White, B., Austin, J., Matsumoto, K., 2012. A three-dimensional model of Lake Superior with ice and biogeochemistry. J. Great Lakes Res. doi:10.1016/j.jglr.2011.12.006

Zhou, M., Zhu, Y., Putnam, S., Peterson, J., 2001. Mesoscale variability of physical and biological fields in southeastern Lake Superior. Limnol. Oceanogr. 46:679-688.

Conclusions

Anagnostou, E., Sherrell, R.M., 2008. MAGIC method for subnanomolar orthophosphate determination in freshwater, Limnol. Oceanogr. Methods. 6, 64-74.

Baehr, M.M., McManus, J., 2003. The measurement of phosphorus and its spatial and temporal variability in the Western Arm of Lake Superior. J. Great Lakes Res. 29, 479-487.

Barbiero, R.P., Tuchman, M.L., 2004. The deep chlorophyll maximum in Lake Superior. J. Great Lakes Res. 30, 256-268.

Lomas, M.W., Burke, A.L., Lomas, D.A., Bell, D.W., Shen, C., Dyhrman, S.T., Ammerman, J.W., 2010. Sargasso Sea phosphorus biogeochemistry: an important role for dissolved organic phosphorus (DOP). Biogeosciences. 7, 695-710.

Nalewajko, C., Voltolina, D., 1986. Effects of environmental variables on growth rates and physiological characteristics of Lake Superior phytoplankton. Can. J. Fish. Aquat. Sci. 43, 1163-1170.

Seegers, B.N., 2009. Lake Superior zooplankton community grazing and its implications for the deep chlorophyll maximum. Masters Thesis. University of Minnesota.

Sterner, R.W., Smutka, T.M., McKay, R.M.L., Xiaoming, Q., Brown, E.T., Sherrell, R.M., 2004. Phosphorus and trace metal limitation of algae and bacteria in Lake Superior. Limnol. Oceanogr. 49, 495-507.

Sterner, R.W., 2010. In situ-measured primary production in Lake Superior. J. Great Lakes Res. 36, 139-149.

Appendix

Biogeochemistry and Ecosystem Model Equations

Modifications have been made to the equations describing the rate of change of phytoplankton concentrations. All other equations are described in Fennel et al. (2006). The equation describing time rate of change of the phytoplankton pool follows from Fennel et al. (2006) as

$$\frac{\partial Phy}{\partial t} = \mu Phy - gZoo - m_p Phy - \tau(SDet + Phy)Phy - w_p \frac{\partial Phy}{\partial z},$$

where *Phy* is phytoplankton, *Zoo* is zooplankton, *SDet* is small detritus, μ is the phytoplankton growth rate, g is the zooplankton grazing rate, m_p is the phytoplankton mortality rate, τ is the aggregation parameter for phytoplankton and small detritus, and w_p is the sinking rate for phytoplankton.

The phytoplankton growth rate is a function of temperature, light, and nutrient concentration given by

$$\mu = v_{\max} \cdot f(T) \cdot f(I) \cdot L_{PO_4},$$

where v_{max} is the phytoplankton growth rate at 0° C. The temperature dependent term follows the Q_{10} relation (Kishi et al., 2007)

$$f(T) = e^{k_{Gpp}T},$$

where k_{Gpp} is the phytoplankton temperature coefficient for the photosynthetic rate and T is the water temperature. The light dependent term (Platt et al., 1980) allows for the inclusion of photoinhibition though the term is held to zero for this experiment and is given by

$$f(I) = \left(1 - \exp\left(-\alpha_{phy} I / v_{\max}\right)\right)\left(\exp\left(-\beta_{phy} I / v_{\max}\right)\right),$$

where α_{phy} is the initial slope of the light saturation curve, and β_{phy} is the photoinhibition parameter. I is limited to the fraction of light within the photosynthetically active wavelengths (par) and is attenuated by water and through phytoplankton self-shading given by

$$I = I_0 \cdot par \cdot \exp\left(-z\left(\kappa_w + \kappa_{chl} \int_z^0 Chl(z)dz\right)\right),$$

where I_0 is the radiation incident at the water surface, κ_w is the attenuation coefficient due to water, and κ_{chl} is the attenuation coefficient due to chlorophyll. Nutrient limitation is in the form of a Michaelis-Menten function for phosphate given by

$$L_{PO_4} = \frac{PO_4}{k_{PO_4} + PO_4},$$

where PO_4 is the phosphate concentration and k_{PO4} is the half-saturation concentration for uptake of phosphate.